

Planetary Caves: A Solar System View of Processes and Products



Special Section:

Exploring planetary caves as windows into subsurface geology, habitability, and astrobiology

Key Points:

- Six speleogenic processes have been identified across the solar system
- Two speleogenic processes were documented—which are driven by different fluids than on Earth—cryovolcanism and methane-based dissolution
- At least 3,545 subsurface access points have been identified on 11 planetary bodies with speleogenic processes observed on an additional four bodies



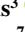
















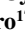









Correspondence to:

J. J. Wynne,
jut.wynne@nau.edu

Citation:

Wynne, J. J., Mylroie, J. E., Titus, T. N., Malaska, M. J., Buczkowski, D. L., Buhler, P. B., et al. (2022). Planetary caves: A solar system view of processes and products. *Journal of Geophysical Research: Planets*, 127, e2022JE007303. <https://doi.org/10.1029/2022JE007303>

Received 17 MAR 2022
Accepted 18 OCT 2022

J. Judson Wynne¹ , John E. Mylroie² , Timothy N. Titus³ , Michael J. Malaska⁴ , Debra L. Buczkowski⁵ , Peter B. Buhler⁶ , Paul K. Byrne⁷ , Glen E. Cushing³ , Ashley Gerard Davies⁴ , Amos Frumkin⁸ , Candice Hansen-Koharcheck⁵ , Victoria Hiatt⁹ , Jason D. Hofgartner¹⁰ , Trudi Hoogenboom⁹ , Ulyana Horodyskyj¹¹ , Kynan Hughson¹² , Laura Kerber⁴ , Margaret Landis¹³ , Erin J. Leonard⁴ , Elodie Lesage⁴ , Alice Lucchetti¹⁴ , Matteo Massironi¹⁵ , Karl L. Mitchell⁴ , Luca Penasa¹⁵, Cynthia B. Phillips⁴ , Riccardo Pozzobon¹⁴ , Jani Radebaugh¹⁶ , Francesco Sauro¹⁷ , Robert V. Wagner¹⁸ , and Thomas R. Watters¹⁹ 

¹Department of Biological Sciences and Center for Adaptable Western Landscapes, Northern Arizona University, Flagstaff, AZ, USA, ²Department of Geosciences, Mississippi State University, Starkville, MS, USA, ³Astrogeology Science Center, U.S. Geological Survey, Flagstaff, AZ, USA, ⁴Jet Propulsion Laboratory, California Institute of Technology, Pasadena, CA, USA, ⁵Johns Hopkins University Applied Physics Laboratory, Planetary Exploration Group, Laurel, MD, USA, ⁶Planetary Science Institute, Tucson, AZ, USA, ⁷Department of Earth and Planetary Sciences, Washington University in St. Louis, St. Louis, MO, USA, ⁸Institute of Earth Sciences, The Hebrew University of Jerusalem, Jerusalem, Israel, ⁹Astra Nova School, Rancho Palos Verdes, CA, USA, ¹⁰Southwest Research Institute, Boulder, CO, USA, ¹¹Cooperative Institute for Research in Environmental Sciences, University of Colorado Boulder, Boulder, CO, USA, ¹²Department of Geological Sciences, University of Alaska Anchorage, Anchorage, AK, USA, ¹³Laboratory for Atmospheric and Space Physics, University of Colorado Boulder, Boulder, CO, USA, ¹⁴INAF-OAPD Astronomical Observatory of Padova, Padova, Italy, ¹⁵Department of Geosciences, University of Padova, Padova, Italy, ¹⁶Department of Geological Sciences, Brigham Young University Provo, Provo, UT, USA, ¹⁷Department of Biological, Geological and Environmental Sciences, University of Bologna, Bologna, Italy, ¹⁸School of Earth and Space Exploration, Arizona State University, Tempe, AZ, USA, ¹⁹Center for Earth and Planetary Studies, National Air and Space Museum, Smithsonian Institution, Washington, DC, USA

Abstract We provide the first solar system wide compendium of speleogenic processes and products. An examination of 15 solar system bodies revealed that six cave-forming processes occur beyond Earth including volcanic (cryo and magmatic), fracturing (tectonic and impact melt), dissolution, sublimation, suffusion, and landslides. Although no caves (i.e., confirmed entrances with associated linear passages) have been confirmed, 3,545 SAPs (subsurface access points) have been identified on 11 planetary bodies and the potential for speleogenic processes (and thus SAPs) was observed on an additional four planetary bodies. The bulk of our knowledge on extraterrestrial SAPs is based on global databases for the Moon and Mars, which are bodies for which high-resolution imagery and other data are available. To further characterize most of the features beyond the Moon and Mars, acquisition (preferably global coverage) and subsequent analysis of high-resolution imagery will be required. The next few decades hold considerable promise for further identifying and characterizing caves across the solar system.

Plain Language Summary Until the last two decades, the potential for caves beyond Earth was principally theoretical. Today, databases of subsurface access points (SAPs) exist for the Moon and Mars. Across the solar system, 3,545 SAPs have been identified on 11 planetary bodies with speleogenic processes identified on another four bodies. Six cave-forming processes beyond Earth have been identified; these include volcanic (cryo and magmatic), fracturing (tectonic and impact melt), dissolution, sublimation, suffusion, and landslides. As more orbiter and fly by platforms with high-resolution instrumentation probe the solar system, our knowledge regarding caves beyond Earth will become more robust—culminating with the robotic and perhaps human exploration of caves on the Moon and Mars.

1. Introduction

In 1966, while examining some of the earliest images of the lunar surface, researchers identified several dark features, which were postulated to be cave entrances (Heacock et al., 1966). Later that year, Halliday (1966) further mused over the existence of lunar caves and briefly discussed their potential importance for future human

© 2022 The Authors.

This is an open access article under the terms of the [Creative Commons Attribution-NonCommercial License](https://creativecommons.org/licenses/by/4.0/), which permits use, distribution and reproduction in any medium, provided the original work is properly cited and is not used for commercial purposes.

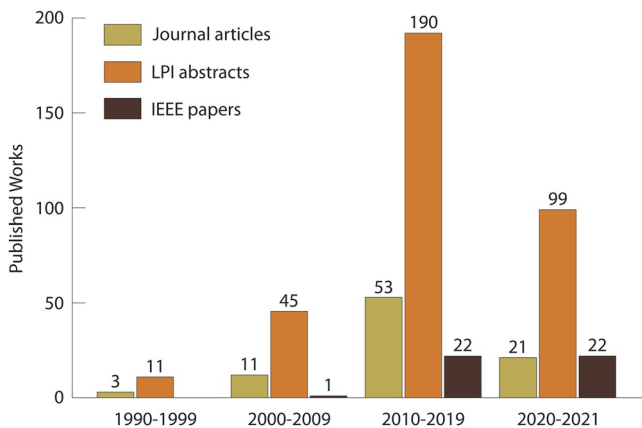


Figure 1. Number of published works (peer-reviewed journal articles, Lunar and Planetary Institute [LPI]-sponsored conference abstracts, and Institute of Electrical and Electronics Engineers [IEEE] papers) presented decadally from 1990 to 2021. From 1966 to 1989, there was one journal article published in 1966, four journal articles between 1970 and 1979, and one journal article and one LPI abstract published in 1985. Note: If the 2020–2021 data were extrapolated to a decade, the numbers would easily exceed the 2010–2019 values. Please refer to Text S1 and Tables S1–S16 Supporting Information, Wynne, Malaska, et al. (2022) for additional information on literature review procedures and associated metadata.

missions. Shortly thereafter, two germinal papers examined the geologic and mathematical rationale for lava tubes in the Oceanus Procellarum region of the Moon using Lunar Orbiter V photographs (Greeley, 1971; Oberbeck et al., 1969); these studies detailed the potential for cave formation processes, which included modeling of cave passage width estimates, roof thicknesses, and lengths of speculated lunar lava tube caves. The potential for lava tubes on Mars has also been discussed. Examining images from Viking Orbiters, Carr et al. (1977) reported the presence of multitudinous tube-fed lava flows and pressure ridges on Alba Mons, Arsia Mons, and Olympus Mons.

Since these inchoative observations, planetary science has witnessed an exponential increase (growing by a factor of ~ 4 per decade) in planetary cave scientific development and technological advancements (with nearly 500 scholarly works published since 1966)—as evidenced by the increasing number of peer-reviewed journal articles, Lunar and Planetary Institute (LPI)-sponsored conference abstracts, and Institute of Electrical and Electronics Engineers (IEEE) papers (Figure 1). Incidentally, the 2023–2032 Decadal Survey emphasized the following: the importance of maturing robotics and instrumentation to access planetary subsurfaces; the need to quantify the environmental covariates driving terrestrial subsurface habitability and diversity (so that this information can be used to gain inference into life potential on other planetary bodies—namely, Mars); and the potential importance of the martian subsurface in the search for life (NASEM, 2022).

Overall, the proliferation in planetary cave related inquiry over the last 20 years coincided with increasingly higher resolution optical platforms onboard orbiting and fly by spacecraft, which drastically improved the resolving capabilities of planetary surfaces. Most notably, the seven pit craters identified on Mars (Cushing et al., 2007) and the first lunar pit (Haruyama et al., 2009) were the first confirmations of cave-like features beyond Earth—ushering in the era of planetary cave identification.

These discoveries shifted the possibility of caves on other planetary bodies from hypothetical to tangible. The accelerated search for additional cave features on the Moon and Mars (refer to Cushing, 2017; Wagner & Robinson, 2021) ultimately expanded into the identification of nearly 3,000 potential subsurface access points (SAPs; this term is applied in lieu of “cave entrance” as we lack any additional evidence to suggest a cave exists) on eight planetary bodies (Titus, Wynne, Malaska, et al., 2021; Wynne, Titus, et al., 2022) and cave-bearing landscapes across the solar system. The prospect of extraterrestrial caves has steadily fueled research efforts to:

- examine microbial life of tellurian caves as Mars analogs (e.g., Boston, 2004; Boston et al., 2006; Léveillé & Datta, 2010; Röling et al., 2015; Selensky et al., 2021; Westall et al., 2015);
- model environments of terrestrial and potential martian cave systems (e.g., Schörghofer et al., 2018; Titus et al., 2010; Williams & McKay, 2015; Williams et al., 2010);
- improve cave detection capabilities (e.g., Cushing et al., 2015; Hong et al., 2015; Pisani & De Waele, 2021; Wynne et al., 2008, 2021);
- develop and expand upon life detection instrumentation and techniques (e.g., Patrick et al., 2012; Preston et al., 2014; Storrie-Lombardi et al., 2011; Uckert et al., 2020);
- expand the number of cave explorer robotic platforms under development (Green & Oh, 2005; Kesner et al., 2007; Morad et al., 2019; Nesnas et al., 2012; Parness et al., 2017; Titus, Wynne, Boston, et al., 2021; Titus, Wynne, Malaska, et al., 2021);
- advance robotic sensing and navigational capabilities (e.g., Agha-Mohammadi et al., 2021; Kalita et al., 2017; Kim et al., 2021; Thakker et al., 2021); and,
- propose mission concepts (e.g., Kerber et al., 2019; Phillips-Lander et al., 2020; Whittaker et al., 2021; Ximenes et al., 2012) and strategies to optimize future planetary cave exploration efforts (e.g., Rummel et al., 2014; Titus, Wynne, Boston, et al., 2021; Titus, Wynne, Malaska, et al., 2021; Wynne et al., 2014; Wynne, Titus, et al., 2022).

Additionally, while the use of lunar lava tube caves as human habitats was proposed over 50 years ago (Halliday, 1966), prototypes for inflatable human habitation modules (e.g., Daga et al., 2010; Krishnan, 2021; Litteken, 2019) have been developed only recently; while not engineered specifically for caves, these habitats could be modified for cave use and thereby gain thermal and radiation protection. These and other efforts concretely demonstrate the sub-discipline of planetary cave science and exploration is on the cusp of a “golden age” of scientific inquiry and technological development.

In the aggregate, these studies and the resultant published works underscored a research need to synthesize planetary cave formation processes and the subsequent subsurface products (i.e., a panoply of prospective cave types) most likely to occur across the solar system (Wynne, Titus, et al., 2022). In this paper, we examine planetary speleogenic processes and/or potential SAPs for 15 planetary bodies (as well as Earth). We also identify gaps in our knowledge, identify landscapes that are consistent with speleogenic processes and where appropriate, discuss currently planned missions that may provide new insights into the potential for caves beyond Earth.

2. Processes and Products

2.1. Earth

The definition of a cave has been primarily influenced by studies focused on terrestrial dissolution processes (e.g., Curl, 1964; Ford & Williams, 2007; Palmer, 2007; White, 1988). Most workers have agreed that an underpinning attribute of a cave is whether it can be entered and examined by humans. Early on, Curl (1964) referred to caves that a human could fit into as a “proper cave” and a subset of all caves; he also included non-dissolution caves in his definition. The dominance of dissolution (or karst caves) in speleology is best demonstrated by the word “pseudokarst,” which has been used as a descriptor of all caves not produced by dissolution—and is still used today (Halliday, 2004). The term pseudokarst will not be used here as it presupposes karst as the dominant speleogenic process both on Earth and elsewhere.

“A cave is a space rather than an object and consequently its definition involves the specification of its boundaries” (Curl, 1964, p. 1). On Earth, caves are either constructional, meaning a void has boundaries added to it, or they are destructional, in which a cave is created by excavating the void within an object (Myrloie, 2019). Examples of constructional caves include: *talus caves*, where the accumulation of blocks of rock subdivides open space into compartments; *tufa caves* form when the precipitation of CaCO_3 at a cliff or steep slope encloses open space; and *reef caves*, where organic precipitation of CaCO_3 encloses an open space by creating boundaries during coral reef formation. Destructional caves consist of: *dissolution caves*, voids produced by removal of material by dissolution; *suffosion caves* (e.g., piping caves), produced by mechanical transport of material; and *volcanic* and *glacial caves*, both of which are produced by a phase transition with the liquid material being removed.

In general, all caves form because of mass transport and therefore are products of erosion and deposition. Constructional caves require that mass be transported “into” a locality to provide the boundaries to enclose a void, while destructional caves must have the mass transported “out of” a locality to leave a void with boundaries. Therefore, constructional caves require that erosion has occurred somewhere beyond the speleogenic site to provide the raw material to construct the boundaries. Destructional caves require that deposition of eroded material occurs away from the speleogenic site. This action is a source and sink dynamic where speleogenesis is not focused on the actual cave site alone, but also on those sources and sinks, without which speleogenesis cannot occur. These sources and sinks operate over a variety of scales; a fracture cave forms when 1 m or less of actual rock motion has occurred, whereas a tufa cave can be precipitated from CaCO_3 as dissolved ions sourced from hundreds of kilometers away.

Speleogenic processes require careful consideration. A cave in limestone results from removal of CaCO_3 by dissolution, a destructional process, whereas a tufa cave results from precipitation of CaCO_3 , a constructional process. Glacier caves are formed due to an H_2O phase change from solid to liquid, with liquid removal behaving as a destructional process. Moreover, the term “erosion cave” has been applied to undercuts in weaker rock units in a cliff face (White, 1988), tafoni (Owen, 2013), and sea caves (Boston, 2004), but White (1988) and Boston (2004) classified suffosion caves as a separate category—yet mechanical erosion as a destructional process includes both categories. To simply define a feature as an “erosion cave” ignores the chemical erosive processes. Incidentally, the term “tectonic caves” by White (1988) and Boston (2004) has been utilized as a descriptor for fracture caves; however, tectonics are not required; any landscape with relief may fail and cause

rock or ice substrate to crack and fracture. Such caves are well known from areas without active tectonics, such as valley walls over-steepened by glacial activity (Cooper & Mylroie, 2015). The occurrence of fracture caves is a transient phenomenon, in that completion of the fracture process means a cliff or hillslope failure and the potential production of talus caves in the residual material. Moreover, the destructional process that produced one type of cave, fracturing, eventually destroys the fracture cave, yet the process may yield another cave type, the talus cave, via constructional processes. Fractures produced by impacts, a one-time tectonic event at a locality, may persist for significant periods of time as they do not require continual gravitational stresses to form. So, for this paper, we will refer to tectonic caves as products of tectonic processes, talus caves as features created by landslides, and impact melt fracture caves as products of a meteoric impact event.

Curl's (1964) concept of a “proper cave” as a structure that humans could enter introduces the problem of exploration bias regarding how researchers view caves. It is not only the size issue, but also a technological one. Mylroie (2019) indicated that a void filled with water was considered a “cave” as it could be explored by scuba divers or remotely operated vehicles, but a lava tube filled with molten lava would by this definition not be a cave as it cannot be directly examined by humans with current technology.

Moreover, this exploration bias extends to whether the subterranean void can be entered. Some voids form without entrances, such as a lava bubbles and blisters (White, 1988) and hypogenic dissolution features at depth (Ford & Williams, 2007; Klimchouk, 2009; Palmer, 2007). Other features contain an entrance from their initial formation by mechanical processes, such as sea caves (via destructional processes) or talus caves (by constructional processes). Epigene dissolution caves commonly have an entry and exit point governed by flowing water—with the formation of entrances being part of the speleogenic process (Ford & Williams, 2007; Palmer, 2007).

Caves of any type can develop initial or additional entrances when the cave is intersected by the surface environment. This commonly occurs when a portion of the ceiling collapses, forming an entrance. Such collapse entrances have been called a “vertical intersection” to differentiate from a “lateral intersection” where slope retreat or valley widening intersects a cave laterally (Mylroie, 1984). Vertical intersection is usually a result of characteristics fundamental to the cave, such as rock strength and chamber width. Collapses can be triggered by other activities such as rock fatigue, surface denudation to thin the roof, fluid infiltration that weakens the host rock, or excessive loading such as glaciation (White, 1988). Lateral intersection is an independent process and results from surface processes alone, which can occur gradually via slope retreat or catastrophically due to landslides.

Because studies on dissolution caves represent the bulk of the speleological scientific literature, cave entrances have been commonly associated with closed contour depressions—including sinkholes or dolines at the local scale and poljes, blind valleys, and uvalas at a landscape scale (Ford & Williams, 2007; Palmer, 2007). These closed contour depressions in karst areas indicate that there has been mass transport of material underground. For limestone areas, mass transport has occurred through conduits involving the solvent, H₂O, the solute, CaCO₃, and the additional mechanical transport of both soluble and insoluble components.

Volcanic processes, and the allied example of geysers, provide a suite of cave types produced by fluid movement from depth to the surface. Volcanic vents and pits are products that form in a variety of volcanic strata, whereas lava tubes require the melt of sufficient low viscosity material to allow extensive lateral flow of lava. Volcanic vents and geysers presuppose a conduit flow system beneath their surficial expression that feeds fluids to the surface. Lava tubes can be considered a type of cave that transitions from constructional, as when a lava flow channel roofs over, to destructional, when lava exits the tube to leave a cave behind. Ice on Earth has a similar broad suite of subsurface features. Crevasses are fracture caves, and moulins feed meltwater caves that traverse the ice body interior—both of which are destructional processes.

For obvious reasons, Earth (and the terrestrial processes therein) has been the model for understanding and characterizing all cave types. The driving question that arises is whether we can use terrestrial speleology to define and understand cave formation processes on other planetary bodies. While Mylroie (2019) initially asserted that using Earth as a frame of reference was fraught with problems, that contention may not apply here. Earth has an active atmosphere and hydrosphere, a large moon, internal heat, and active plate tectonics that completes partial planetary resurfacing while preserving ancient terrains. Importantly, it also possesses most of the surface feature types found on other bodies, due largely to active surface processes including eolian, volcanic, solid-liquid phase transitions, and recent resurfacing, as well as ancient terrains with relict impact structures.

Although we have yet to examine any planetary subsurface beyond Earth and fully recognize there are no perfect analogs, we aver that Earth can be used as a baseline for constructional and destructional processes that will produce extraterrestrial caves. The various bodies in the solar system are made of a suite of materials in a diverse collection of settings, but as they are (or have been) subjected to the same constructional and destructional processes as on Earth, caves will be present. Importantly, applying a terrestrial perspective to cave formation on other planetary surfaces may enable us to predict where caves may occur and how to conclusively identify and characterize them, which have been identified as the initial steps of planetary cave exploration (refer to Titus, Wynne, Malaska, et al., 2021).

2.2. Cave Potential Beyond Earth

From this review, we have identified 3,545 known SAPs on 11 planetary bodies and the potential for speleogenic processes (and thus SAPs) on an additional four planetary bodies (excluding Earth; Figure 2; refer to Supporting Information, Wynne, Malaska, et al., 2022). A SAP is defined as an opening on the surface visible by remote sensing for any planetary body in the solar system. We further intimate that an opening may become characterized as a cave entrance once sufficient data supports the feature connects the surface to the deeper subsurface via a laterally trending void or cave. However, features determined not to represent a subsurface void or cave may still retain high value in planetary research as SAPs could provide much deeper access to the subsurface than current drilling technologies permit (refer to Wynne, Titus, et al., 2022).

The selection of planetary bodies and their accompanying synopses were based upon the availability of high-resolution data to identify SAPs, adequate resolution data to identify and/or infer speleogenic processes, and the research focus by the planetary science community. For all bodies, we framed our level of knowledge using the three research stages proposed by Titus, Wynne, Malaska, et al. (2021)—identification, characterization, and exploration. Identification is the incipient stage whereby a feature is simply identified as a SAP, while characterization involves an indepth examination of the feature whereby a speleogenic process can be determined, the potential for lateral passage more confidently inferred, and thus the ranking of the feature as a potential exploration target. The final stage, exploration, would include entry via robotics to conduct scientific investigations, and perhaps ultimately access by humans. However, the exploration of caves beyond Earth will most likely be constrained to the Moon and Mars—but this is beyond the scope of this paper.

Concerning speleogenic processes beyond Earth, six processes have been identified. These consist of volcanic (cryo and magmatic), fracturing (tectonic and impact melt), sublimation, suffusion, dissolution, and landslides (which could give rise to talus caves). All are known terrestrial speleogenic processes, although fluid composition differs. Specifically, cryo- and magmatic volcanism are the same process but consist of different eruptive materials, while dissolution involves liquid water on Earth and liquid ethane/methane on Titan. Of note, sublimation is probably more common on icy worlds than reported and is somewhat analogous to penitente (see Hopley et al., 2020) and suncup formations on Earth. However, additional observing and modeling will be required to adequately examine the extent of sublimation on other bodies. Tectonic fracturing was documented on 14 extra-terrestrial bodies and is expected to also occur on Titan. Finally, talus cave formation likely occurs on all active worlds (i.e., where slope failure occurs and landslides result). For example, in addition to the information summarized herein, landslides have also been documented on Callisto and Rhea (refer to Beddingfield et al., 2018; Robbins et al., 2019). However, detecting talus caves will be inherently difficult given the comparatively small entrance sizes within a jumbled boulder matrix as observed from terrestrial analogs. Table 1 provides a summary of the information detailed below.

2.2.1. Rocky Bodies

2.2.1.1. Mercury

The best-available surface observations for Mercury are from the NASA MErcury Surface, Space ENvironment, GEOchemistry, and Ranging (MESSENGER) mission, where the narrow angle camera data had an average resolution of 26 m/px (Chabot et al., 2012). Although no SAPs have been confirmed to date, potential cave forming landscapes have been identified and are discussed below.

Much of the surface of Mercury was emplaced originally as volcanic material—either effusively as lava flows, or explosively as pyroclastic deposits (Byrne et al., 2018; Head et al., 2008). Certainly, the planet's smooth plains

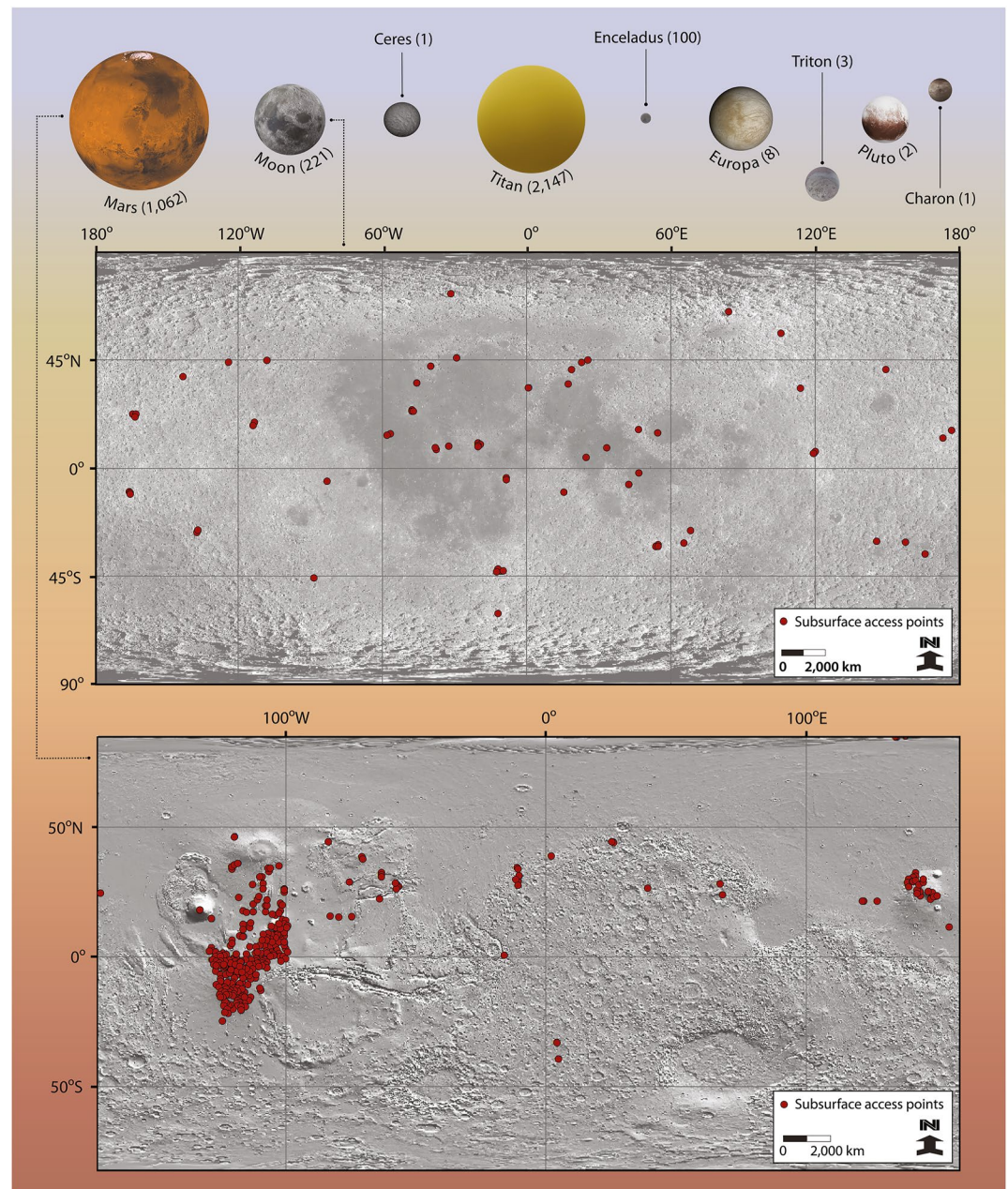


Figure 2. Planetary bodies for which subsurface access points (SAPs) have been identified with number of features per body provided in parentheses (top) with SAP global locations for the Moon (center; modified from Wagner and Robinson [2021]) and Mars (bottom; from Cushing, 2017). All images courtesy NASA.

terrain, which occupies about 27% of the surface (Denevi et al., 2013), is predominantly volcanic, as evidenced by embayment relations, the presence of earlier, buried craters, and spectral contrast with surrounding, older terrain (Byrne et al., 2013; Head et al., 2009, 2011). Given the prevalent planetary process is volcanism (Byrne et al., 2018; Head et al., 2008, 2009, 2011) and that pit craters have been identified from MESSENGER data (Gillis-Davis et al., 2009; see Figure 3a), other volcanic features such as lava tubes, associated collapse pits, and fractures likely exist on Mercury.

Yet the prospect for identifying such features based on existing data is extremely limited. First, almost all presently available global image data for Mercury acquired by the Mercury Dual Imaging System (MDIS) (Hawkins et al., 2007) on the MESSENGER spacecraft were low resolution (150–200 m per pixel (m/px)). Second, higher

Table 1

Research Stage (Identification, Characterization, and Exploration; Refer to Titus, Wynne, Malaska, et al. [2021]), the Six Speleogenic Processes (Volcanic [Cryo and Magmatic], Fracturing [Tectonic and Impact Melt], Dissolution, Sublimation, Suffusion, and Landslides), and the Resultant Processes and Products for All Planetary Bodies Examined Herein

Body	Stage	Processes	Products
Mercury	Identification	Volcanic, tectonic fracturing, sublimation	No SAPs presently documented, but may include volcanic vents, small-scale extensional structures, sublimation pits, and talus caves
Venus	Identification	Volcanic, tectonic fracturing, impact melt fracturing	No SAPs identified to date, but likely number in the thousands; abundant pit crater chains on volcanoes and plains, lava tubes, and small-scale extensional structures are possible
Moon	Characterization	Volcanic, impact melt fracturing, tectonic fracturing	Over 221 SAPs identified (Wagner & Robinson, 2021); mixture of types, although few have clear origins
Mars	Characterization	Volcanic, tectonic (ice and rock), impact melt fracturing, suffusion, dissolution?	1,055 SAPs of volcanic origin and seven SAPs in karst-like terrain identified (Cushing, 2017)
Io	Identification	All volcanic SAP types possible	No SAPs identified to date; most volcanically active body in solar system; dissolution could be possible on frozen SO ₂ plains
Vesta	Identification	Impact melt fracturing, tectonic fracturing	No known SAPs; pitted terrain within Marcia and Cornelia craters and talus caves possible in active terrains
Ceres	Identification	Impact melt fracturing, cryovolcanic, tectonic fracturing, potential dissolution	At least one presumed cryovolcanic caldera identified as a SAP (Crown et al., 2018; Hughson, Russell, Schmidt, Chilton, et al., 2019; Hughson, Russell, Schmidt, Travis, et al., 2019); other features requiring further examination include impact fractures and pitted terrain within at least seven craters and presumed tectonic fractures in at least three regions
Europa	Identification	Tectonic fracturing, cryovolcanic?	Six plumes (i.e., potential geysers), a fracture, and a fracture network detected (Roth et al., 2014, 2016; Sparks et al., 2016; Paganini et al., 2019; this study); an additional undetermined number of large fractures require further study
Titan	Identification/Characterization	Methane-based dissolution with suffusion, sublimation, cryovolcanic, and tectonic fracturing	1,270 SAPs in organic sedimentary deposits identified (Malaska, Schoenfeld, et al., 2022)
Enceladus	Identification/Characterization	Tectonic fracturing, suffusion, cryovolcanic?	100 geysers within the South Polar Terrain identified (Porco et al., 2014)
Ganymede	Identification	Tectonic fracturing, cryovolcanic, sublimation?	One possible cryovolcanic caldera (Sippar Sulcus) and one impact crater chain should be further examined, which are currently the two most promising features
Triton	Identification	Tectonic fracturing, cryovolcanic?	Three plumes identified unambiguously (Croft et al., 1995; Hofgartner et al., 2022); four to 14 additional potential plumes and ≥100 fans (inferred to be cryovolcanic vents and/or phase change caves) in the Southern Hemisphere terrain require further examination
Pluto	Identification	Cryovolcanic	Two possible cryovolcanic vents (Wright and Piccard Montes; Schenk et al., 2018; Singer et al., 2016; Moore et al., 2021); seven possible collapse pits near Virgil Fossae require further examination
Charon	Identification	Cryovolcanic, tectonic fracturing, sublimation/deposition, landslides (i.e., talus cave formation)	One catena (Robbins et al., 2019) and at least 13 lobate aprons that may support talus caves should be further studied
Comet 67P	Identification	Sublimation, fracturing, landslides	18 sublimation pits identified (Vincent, Bodewits, et al., 2015); however, none of these features were considered SAPs; talus caves also possible, but not confirmed

resolution imagery is available for only a small portion of Mercury—all confined to the northern hemisphere. Roughly 4% of the surface imaged at resolutions of ≤50 m/px (Chabot et al., 2012) including a few dozen images acquired during the low-altitude phase of the MESSENGER mission with resolutions as high as 2–3 m/px. Importantly, the average impact velocity at Mercury is around twice that of Earth (Le Feuvre & Wicczorek, 2011). Given that the youngest volcanic flows observed on Mercury are perhaps around a billion years old (Byrne

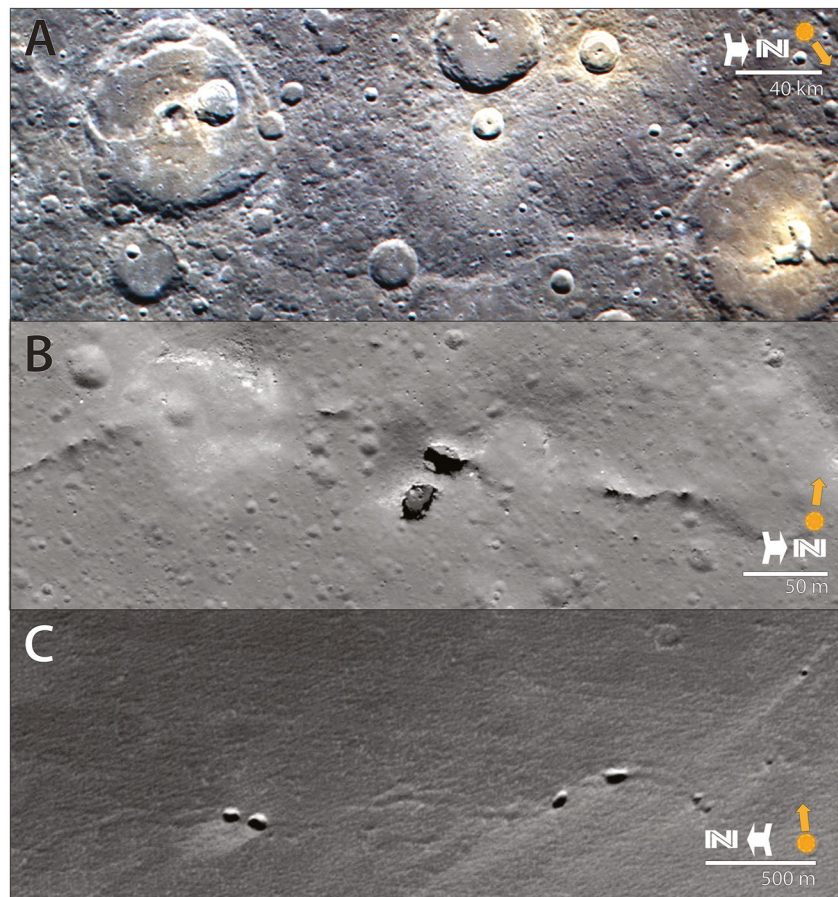


Figure 3. Processes and products for Mercury, the Moon, and Mars. (a) Pit crater formations with Glika Crater (right corner), Mercury. NASA MESSENGER Wide Angle Camera, modified from image # EW1006407109G, credit: NASA/USGS. (b) King crater natural arch, 12 m from floor to top of arch, King Y crater region, the Moon. Lunar Reconnaissance Orbiter NAC, modified from image #M113168034R, credit: NASA/GSFC/DLR/Arizona State University. (c) Presumed lava tube collapse pit chain, northern flank of Arsia Mons, HiRISE, modified from image # ESP_037232_1770, credit: NASA/JPL-Caltech/University of Arizona.

et al., 2016; Prockter et al., 2010), sustained impact bombardment, burial by ejecta deposits, and cave collapse, may have rendered any SAPs that formed undetectable.

There are other depressions on Mercury that are not impact in nature, including: likely sublimation features termed “hollows” (Blewett et al., 2011); irregularly shaped, coalesced depressions interpreted as sites of explosive volcanic activity (Rothery et al., 2014), such as those along the inner perimeter of the Caloris impact basin (e.g., Murchie et al., 2008); and large depressions in expansive lava channels in the planet's northern hemisphere (Byrne et al., 2013). The origin of this third type of depression is unclear, but by all accounts, none of these depressions can be considered SAPs using the currently available data.

Another possible mechanism for the formation of SAPs is the creation of void space from mode-I extensional fracturing of the uppermost portion of the planet's crust. Extension on Mercury is primarily confined to volcanic plains that fill and bury impact basins and craters (e.g., Byrne et al., 2018). To date, none of the available imagery suggests the presence of actual fractures (that could provide access to the subsurface), although we might infer their presence from similar tectonic settings on Earth, the Moon, and Mars.

Although there is evidence of ice in permanently shadowed craters at high latitudes on Mercury (e.g., Chabot et al., 2016; Deutsch et al., 2018; Harmon & Slade, 1992), MDIS images of the crater floors show no reason to suspect cryospeleogenic processes operate there. It is possible, however, that cavities conceptually similar to glacial caves may have at least transiently existed on the innermost planet. Finally, talus and fracture caves are

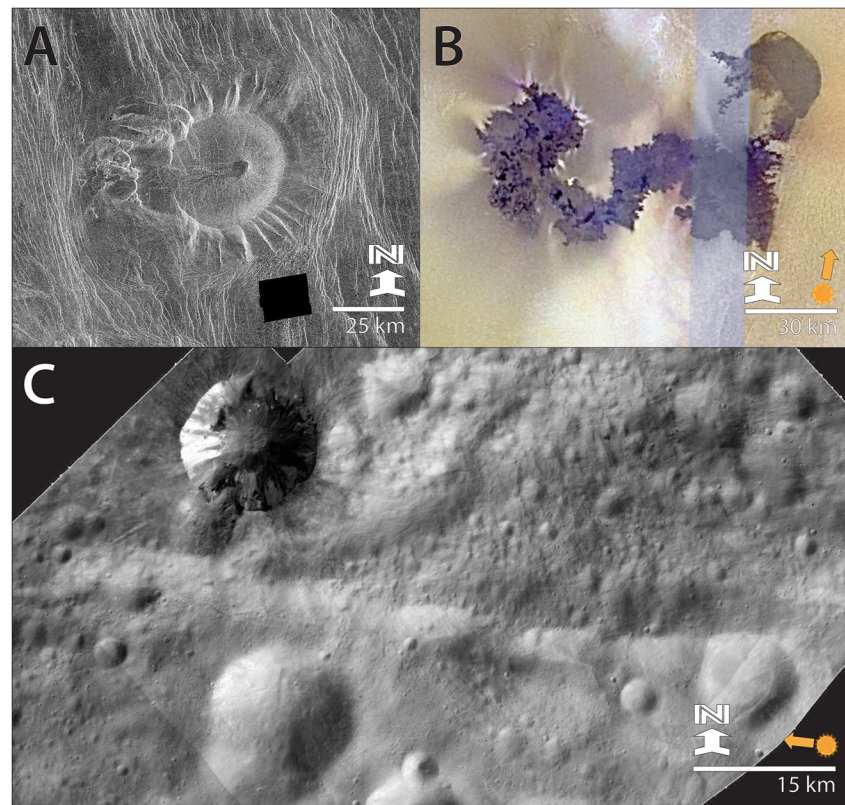


Figure 4. Processes and products for Venus, Io, and Vesta. (a) Pit crater example on Venus (centered on 18.0°S, 5.5°E). Portion of Magellan left-look global radar image mosaic, credit: NASA/JPL-Caltech. (b) Image of the active Prometheus lava flow field and volcanic plume sources on Io. Galileo Solid State Imaging experiment image #PIA02565, credit: NASA/JPL-Caltech/University of Arizona. (c) Robigalia Catena (top left) and surrounding environs on Vesta. NASA Dawn orbiter, mosaic of Framing Camera high altitude mapping orbit images #FC21B0010897_11294002155F1A, FC21B0010898_11294002554F1A, and FC21B0010899_11294002954F1A, credit: NASA/JPL-Caltech/UCLA.

expected to be present on Mercury; however, given the low resolution of imagery presently available, their occurrence on Mercury remains unconfirmed.

SAPs on Mercury may ultimately be confirmed once higher-resolution data from the joint ESA/JAXA BepiColombo mission are acquired and analyzed. BepiColombo has a suite of instruments including a laser altimeter and a high-resolution stereo camera (≥ 5 m/px at perihelion; Cremonese et al., 2009). Orbital insertion is planned for late 2025, with a prospective extended mission lasting until 2028.

2.2.1.2. Venus

Venus is a volcanic world with a surface replete with volcanic landforms and products. The planet hosts vast rift zones, thousands of recognized volcanoes (and likely many more yet to be identified), and as much as 80% of the surface is thought to comprise at least in part extensive lava flows (e.g., Ivanov & Head, 2013). Pit craters have been mapped on several of the largest shield volcanoes on Venus, including on Sif, Maat, Nyx, and Tepev Montes (Mouginis-Mark, 2016; Rogers & Zuber, 1998; Senske et al., 1992). In addition, the longest lava channel (at nearly 7,000 km) in the solar system occurs on Venus (Komatsu et al., 1992); thus, there are almost certainly lava tubes of considerable length, which have yet to be resolved.

Based on the profusion of volcanic features that we observe with radar image data from the Magellan mission, we suggest that lava tubes, associated collapse pits, fractures, and pit craters (e.g., Figure 4b) are widespread on Venus. Locations eminently likely to contain SAPs include extensional structures not only on the flanks of large volcanoes but throughout the plains (possibly the surficial manifestation of dikes), as well as those in association with the planet's major rift zones. Additionally, there are a diminutive number of higher-resolution surface images, returned by a series of Soviet Venera landers, that resolved enigmatic landscapes featuring boulder fields,

finer, and platy-like rocks that may be sedimentary in nature (e.g., Basilevsky et al., 1985) or may represent exfoliation. However, no potential SAPs were identified in this data set.

Three orbital missions to Venus (NASA's VERITAS and DAVINCI, and ESA's EnVision), one of which has a descent probe element (DAVINCI), are planned for the 2020s and 2030s. VERITAS will carry an X-band synthetic aperture radar, nominally capable of imaging the surface at 15–30 m/px resolution (Freeman et al., 2016); EnVision, equipped with SAR (in the S-band), will be able to acquire radar image data at nominal resolutions of 30 m/px with some highly local areas up to 10 m/px resolution (Ghail et al., 2018). These platforms will permit searches for voids and surface changes indicative of volcanic activity. Spectrometers designed to peer through several near-infrared atmospheric spectral windows will also provide compositional information that will be invaluable in the search for cave-bearing landscapes, as well as possibly active calderas, vents, pits, and collapses.

2.2.1.3. The Moon

Lunar Reconnaissance Orbiter (LRO) has imaged most of the lunar surface at a 0.5–2 m/px scale, with more than 55% coverage at higher sun angles (i.e., 45° of zenith). The combination of the spatial resolution and high solar incidence has been favorable for the identification of SAPs (Estes et al., 2019; Robinson et al., 2010; Wagner & Robinson, 2021). To date, hundreds of SAPs have been identified on Earth's Moon. These features fall into three general categories based on the host terrain: impact melt, mare, and highlands (Wagner et al., 2014). The majority of known lunar SAPs occur in impact melts, usually Copernican in age (<~1 Ga) with at least 276 lunar SAPs identified (Wagner & Robinson, 2021). For 221 of these features, it is not possible to clearly resolve the walls of the pits; thus, we cannot rule out the likelihood of lateral passage. Of these, 15 SAPs not associated with impact melts occur in the lunar maria (volcanic plains aged 1.2 to 4.0 Ga; Hiesinger et al., 2011), and five occur in the lunar highlands (>~4 Ga terrain). These latter two types are typically larger than the impact melt type (median diameter of 55 vs. 15 m; Wagner & Robinson, 2021), although it is unclear if this is due to differences in the underlying void spaces.

Most research to date has been focused on the collapse pits (or skylights), due to the possibility that they could connect to extensive lava tube networks. Theoretical modeling indicates that lava tubes from a few hundred meters to over 1 km in diameter could be structurally sound on the Moon (e.g., Oberbeck et al., 1969; Thein et al., 2020); however, the presence of such features has yet to be confirmed. Given the inferred viscosity of mare basalt flows, the Moon should contain lava tubes. Additionally, sinuous rilles or chains of depressions have been identified as potentially collapsed sections of lava tubes up to 500 m in diameter (Coombs & Hawke, 1992; Hörz, 1985).

An alternate formation hypothesis for the SAPs and their resolvable and unresolvable underlying void space is the formation and expansion of a subsurface fracture, driven by either tectonic stresses and/or intrusive volcanism. This process has been proposed as a formation mechanism for the origin of chains of drainage pits observed in lunar grabens (Fielder, 1965; Wilson et al., 2011). This process has also been proposed as the origin of some pit craters in Hawai'i (Okubo & Martel, 1998), which can have similar sizes and morphologies to lunar SAPs. Additionally, tectonic activity and/or volcanism have also been proposed for pit crater formation on Mars (Vijayan, 2020; Wyrick et al., 2004).

The identified SAPs themselves rarely reveal the formation mechanism(s). One mare SAP, in Lacus Mortis, is located 800 m from the edge of a graben, suggesting a potential tectonic origin (Wagner & Robinson, 2014). Two SAPs in the Marius Hills region of Oceanus Procellarum offer circumstantial evidence of roof collapses into lava tubes. One is in the floor of a surface lava flow channel (Haruyama et al., 2009), and the other is aligned with a 45 m deep, 400 m wide (1.2 km long) linear depression that may be a collapsed section of lava tube—although the pit feature itself is only ~16 m deep (Wagner & Robinson, 2021; Yokota et al., 2018). Also, interpretations of gravity and radar data are suggestive of a possible linear void space beneath the Marius Hills pits, although these observations are at the limits of resolution of their respective instruments (e.g., Chappaz et al., 2017; Kaku et al., 2017). The other mare and highland SAPs have no clear surface indications of the formation process, which is likely due to the extreme age of the host terrains. The void spaces may be of a similar age to the host terrains (i.e., billions of years old), while the surface has been heavily modified by impacts since formation. Extant SAPs presumably formed due to seismic activity (perhaps often from nearby impacts), and breached the surface relatively recently compared to the emplacement of the host terrain (Wagner & Robinson, 2014)—as noted for Mercury. These features may be associated with particularly deep and/or stable void spaces.

SAPs in impact melts are likely to have a different set of formation mechanisms, as they form in a material with different mechanical properties than mare basalt or highland regolith. Impact melt ponds form from large masses of molten rock, melted at the moment of impact, that pool in depressions and cool over tens of thousands of years (Melosh, 1989). In most cases, the majority of the impact melt from a crater is within the crater itself, and that is where most impact melt SAPs are found. One notable exception is the 20 km wide external melt pond of King crater, which lies in a pre-existing depression centered 16 km northwest of King crater (Figure 3b). This pond has the highest density of SAPs on the Moon, although it is unclear if the external nature of the pond led to the high density of SAPs (Wagner & Robinson, 2014). The presumed origin of the terrain, cooling in place from a large, ponded mass of molten rock, would not be expected to result in large lava tubes or intrusive magmatic features. Despite this, some impact melt SAPs have similar depth/diameter ratios and elliptical openings to mare SAPs, albeit usually at a much smaller scale. Two hypotheses for the source of many of the underlying void spaces are subsurface cooling fractures, and lava-tube-like structures formed by post-emplacement subsurface melt flow driven by shifts in the underlying terrain in response to the post-impact stress regime (Ashley et al., 2012; Wagner & Robinson, 2014). Importantly, not all impact melt SAPs can be explained by these mechanisms; in particular, there are numerous SAPs that formed in positive relief features that may be inflationary in origin (Wagner & Robinson, 2021). The clearest example of this type is a natural arch in the King crater melt pond, which likely formed by two collapses in the roof forming a single void space that encompasses most of the area under a positive relief feature (Wagner & Robinson, 2014).

There are no planned missions for the Moon that will further enhance our ability to resolve SAPs.

2.2.1.4. Mars

Mars shares similar geochemical composition and geologic history with Earth. However, being approximately one-third in size with a thicker and more stable crust, volcanism was caused primarily by mantle plumes, which formed extensive volcanic provinces (Greeley & Spudis, 1981). For comparison, the Tharsis province on Mars is approximately 2,226 km², while the largest igneous province on Earth (Siberian Traps) covers around 777 km². In these regions, individual lava flows extend hundreds of kilometers in length and tens of meters in thickness—underscoring the vast potential for lava tube networks on Mars (Peters et al., 2021; Sauro et al., 2020).

To date, more than 1,162 SAPs have been identified on Mars (Baioni et al., 2009; Cushing, 2017). The Mars Global Cave Candidate Catalog (MGC³) includes a variety of features including pit craters partially filled with eolian sediments (Cushing, 2017), while more than 100 potential sinkholes and cave entrances have been recently reported in the evaporitic domes within the Tithonium Chasma of Valles Marineris (Baioni et al., 2009). Most of the known features are constructional in origin with the majority occurring in volcanic edifices and surrounding lava fields including Tharsis Montes (Ascraeus, Arsia, and Pavonis), Olympus Mons, Elysium Mons, Alba Patera, Apollinaris Mons, Hadriacus Mon, Tyrrhenus Mons, Cyane Fossae, Daedalia Planum, Syria Planum, Nili Patera, and Syrtis Major Planum.

Of the features documented in the MGC³, the following morphologies were identified: (a) lava tube skylight features (i.e., collapse features) within long rilles, channels, and collapse chains (e.g., Figure 3c), (b) atypical pit craters (APCs) usually isolated with peculiar morphological characteristics, (c) small rimless pits (SRPs) along flow channels, (d) pinholes (likely representing small entrances), (e) lateral entrances on cliffs, and (f) deep extensional fractures (Cushing, 2017). These general classifications were based strictly on individual morphologies and were not intended to express the potential speleogenic origin of each SAP. In a project to identify their respective and potential origins, Sauro et al. (2020) proposed that most of the SAPs along lava channels, or aligned within downward sloping sinuous paths, were suggestive of deflated lava tubes. Also, depending on the presence of specific morphological characteristics (such as channel benches or surface bulges), it may be possible to discern between different lava tube types based upon different speleogenic processes (Kempe, 2019), such as ceiling overcrusting or inflation. The latter process seems to be most common on the flanks of major shield volcanoes and is probably responsible for the expansive lava field of the Tharsis region (Bleacher et al., 2017; Keszthelyi & Self, 1998). In support of this hypothesis, tubular sinuous ridges hundreds of meters wide and hundreds of kilometers in length have been observed on the lava plains of the southwest Tharsis region (Zhao et al., 2017). Compared to terrestrial analogs, these features were interpreted as undrained inflated tubes. Through examining the surface expressions of lava tube collapse candidates, the underlying cavities could range in size from 20 to over 100 m in width and up to hundreds of kilometers in length (Sauro et al., 2020; Zhao et al., 2017).

While the lava tube origin for SAPs within sinuous pit chains is well-accepted, the genesis of isolated atypical pit craters (APC) in volcanic terrains remains vigorously debated. Isolated APCs may be related to void collapses of partially drained dikes—as observed on Kilauea Volcano, Hawai'i (Cushing et al., 2015; Okubo & Martel, 1998; Okubo & Schultz, 2005) and on the basaltic plateaus of Golan between Israel and Syria (Frumkin & Naor, 2019). This idea was supported by the possibility that subjacent caverns (i.e., stopping chambers) and/or tunnels (i.e., evacuated dike tips) may have remained intact and that some APCs could be connected to lateral passage at the crater floor. Conversely, Kempe (2019) proposed these features may have formed due to the presence of permafrost layers at great depths and the subsequent melting due to rising volcanic heat that resulted in the excavation of tremendous void spaces that collapsed and formed APCs.

Other typical SAPs observed in the Martian volcanic terrains are situated along dilatational faults and grabens. Wyrick et al. (2004) showed that most tectonic pits on Mars are infilled by debris but could be related to subsurface voids created by tensional stress. Additionally, several SAPs in the MGC³ are associated with dilatational faults distributed along the flanks of volcanic edifices of the Tharsis region and along flat-lying floors of extensional grabens; these features are strikingly similar to analogs on Iceland (Ferrill et al., 2011) and Hawai'i (Okubo & Martel, 1998). These SAPs probably provide access to limited tectonic cavities, as they are mostly infilled by surrounding lithologies and sediments.

Given the widespread presence of soluble lithologies and the historical abundance of liquid water on the surface (and at least some evidence of water occurring within the subsurface contemporarily), dissolution caves may also occur on Mars. Baioni (2018), Parenti et al. (2020), and references therein suggested the presence of several karst-like features including dolines, sinkholes, karrens, and entrenched channels carved within the evaporitic lithologies (including kieserite) of equatorial regions. In these settings, destructional caves may have formed by draining surface water or acted as pathways for hypogenic fluxes; however, few SAPs have been identified in these areas. Most of the dissolution cave entrances in analog terrains on Earth are mainly situated along canyons and vertical cliffs. Thus, their presence on Mars could be overlooked by the limited observation capabilities of orbiting spacecraft (Baioni et al., 2009; Pisani & De Waele, 2021).

Moreover, several studies have shown that the early Noachian and Hesperian eons of martian history contained expansive surface and subsurface water deposits (Andrews-Hanna & Lewis, 2011). Evaporative processes allowed the deposition of thick deposits of Ca and Mg sulfates throughout much of Mars. Even carbonates have been deposited on the floors of some craters through abiotic processes (Bridges et al., 2019). In some of these regions, such as Arabia Terra, subsequent wet and dry phases, including the rise of hydrothermal fluids, could have facilitated the formation of both epigenic and hypogenic cave-forming processes (Baioni & Sgavetti, 2013; Baioni et al., 2009). Additionally, abundant water and CO₂ ice occurs as permafrost, glaciers, and icecaps in the polar regions—where these deposits are subjected to sublimation. Radar studies suggest the potential presence of subglacial hypersaline water bodies beneath the south polar ice cap (Lauro et al., 2021; Orsei et al., 2018), although alternative interpretations are possible (Biersen et al., 2021; Smith et al., 2021). If subglacial lakes are present, networks of submerged cavities could have developed. In high latitude regions, thermokarst may have also played an important role in the formation of sinkholes and related potential subsurface cavities (Baioni et al., 2014).

In addition to the variety of cave types that could be found on Mars, one of the most intriguing questions is the potential presence of water or CO₂ ice deposits. Water ice could represent important in situ resource for human exploration (refer to Linne et al., 2017), as well as a promising target for astrobiology—especially where volcanic heat once interacted with ice in the subsurface (Williams et al., 2010). Importantly, the predominant cave ice type is expected to be perennial hoarfrost that slowly grows in supersaturated cavities, although its presence may be constrained to certain latitudes where subsurface seasonal temperatures allow for ice preservation (Schörghofer, 2021).

Mars is the only other solar system body that could have experienced the same variety of speleogenic processes as on Earth. Mars has also had the most intensive and sophisticated observation orbiting and ground equipment of any other body in the solar system; thus, the identification and characterization of a large number of SAPs may also be due to positive observational bias. Regardless of the reason, Mars supports the greatest diversity of SAPs in the solar system.

The latest mission to the Martian surface, Mars 2020 (consisting of the Perseverance rover and Ingenuity helicopter), did not land in an area with known SAPs. While the Mars 2020 mission may not be useful in further examining known SAPs, the advent of powered flight on Mars provides an approach that may one day be used to both confirm SAPs as cave entrances and potentially examine the deeper recesses of confirmed caves (e.g., Lee et al., 2019; Santamaria-Navarro et al., 2019; Wiens et al., 2019).

Finally, orbital characterization of Martian SAPs may benefit from the proposed mission, International Mars Ice Mapper (IMIM; Ianson et al., 2021), which would acquire synthetic aperture radar radargrams of the martian surface. IMIM's primary objective would be to identify the presence of ice between 5 and 10 m below the surface. Incidentally, this is a similar depth where lava tubes are expected to occur. If acquired, these data could be used to identify SAPs with extended void space via the return reflections from cave ceilings and floor. Additionally, this platform could determine if those features characterized as caves contain ice deposits, as well as map the extent of those deposits.

2.2.1.5. *Io*

The jovian satellite Io has hundreds of active volcanoes (Veeder et al., 2015) because of intense tidal heating (Peale et al., 1979). This makes Io unique in the solar system. As observed from both spacecraft (most notably Voyager and Galileo) and ground-based telescopes (e.g., Cantrall et al., 2018; de Kleer et al., 2019; de Pater et al., 2016), Io's volcanic activity is dominated by high temperature (>1,100 K) silicate volcanism (Davies, 2007). Volcanic structures' observed modes of eruption, and the resulting geomorphology support the dominant presence of relatively low viscosity silicates, which interact with sulfurous ices in the lithosphere and on the surface.

Images taken by the Galileo Solid State Imaging (SSI) experiment revealed the presence of extensive lava flows with relatively low relief (e.g., Keszthelyi et al., 2001). The highest resolution Galileo Near Infrared Mapping Spectrometer (NIMS) observations mapped the temperature distribution on the surfaces of some of Io's most active lava flow fields, including Prometheus (Leone et al., 2009) and Amirani (Davies et al., 2014). Measurements of thermal emission, temperature derivations, and imagery of newly covered areas revealed that lava was being actively emplaced.

While no SAPs have been detected on Io, the presence of long, active lava flows strongly support the movement of lava under insulating crusts (e.g., Davies, 2007), and within lava tubes (Davies et al., 2016; Keszthelyi et al., 2001; Leone et al., 2009). Davies et al. (2016) examined the likelihood of lava tubes on Io, and their possible use for answering some of the most pressing questions about Io's composition and interior state. They concluded that lava tubes almost certainly exist, where long-lived active lava flow fields with apparently steady eruption rates are common. The composition of Io's dominant lavas is yet to be answered but is most likely in the basalt to ultramafic range (e.g., Davies et al., 2000; Keszthelyi et al., 2007). Regardless of composition, lava tubes can form even with ultramafic lavas, despite their initial low viscosity (Williams et al., 2001). The cooling of ultramafic lava along the edges of a flow channel leads to crystal growth that increases lava yield, strength, and viscosity. In turn, this leads to the same tube formation processes as found with basaltic lava. If eruptions persist, subsequent substrate thermal erosion (Williams et al., 2001) can form a flow channel that can then be roofed over. Substrate thermal erosion is more pronounced with ultramafic lava due to high eruption temperatures and the tendency for high-discharge rate lava flows to be initially turbulent, with increasing heat flow to the substrate. On Earth, some ultramafic lava flows may have been emplaced via lava tubes (e.g., Barnes, 1985; Gràcia et al., 1997; Hill et al., 1995).

Extensive lava flows are common on Io's surface (e.g., Veeder et al., 2009). Some highly active lava flows fields were imaged repeatedly by instruments onboard the Galileo spacecraft. These include the Amirani flows, which are greater than 300 km long, and the Prometheus flows at more than 100 km in length (Keszthelyi et al., 2001). As noted by Davies et al. (2016), these are candidate locations where active lava tubes may still be present. Using Galileo NIMS data of Prometheus (at 1.4 km/px resolution), Leone et al. (2009) reported a few small, isolated areas of elevated thermal emission and higher temperatures than those observed in the other, more expansive areas along the length of the flow field. These apparent lava tube skylights (i.e., collapse features potentially providing access to the tube) were located between the active vent to the east and an area of on-going lava flow emplacement to the west.

Amirani presents similar morphology but is more extensive. As noted by Keszthelyi et al. (2001) and Davies et al. (2014), this lava flow field is marked by breakouts both along and at the distal ends of the flow field.

Thermal mapping of the lava flow surface using Galileo NIMS data revealed discrete thermal anomalies along the lava flows separated by areas of relatively cool lava on the surface (Davies et al., 2014). A caldera-like volcanic depression (i.e., patera) at the southern end of the Amirani flow was also a source of high thermal emission and was connected by a thin, dark lineation. This linear feature was likely a channel or tube that either fed the flow or the flow drained into the patera (Keszthelyi et al., 2001).

At Pele, a Galileo imager observation revealed a sinuous feature >10 km long that had intermittently spaced hot spots. This has been interpreted as being fountaining activity along the edge of a lava lake (McEwen et al., 2000; Radebaugh et al., 2004). Alternatively, these hot spots may be lava tube skylights. It is not possible to definitively determine eruption style at this location from available data.

As summarized by Davies et al. (2016), Galileo visible and infrared data were used to estimate the volumetric fluxes at both Prometheus and Amirani employing two different methods—which showed remarkable convergence—supporting the potential for lava tube formation. Comparison of pairs of observations (see Keszthelyi et al., 2001) obtained at relatively high spatial resolutions showed new areas of low-albedo surface overlaying the older lava flows. With a constant resurfacing of Io from plume fall out and remobilized surface ices, the lava flows at Amirani and Prometheus expressed a range of surface albedo values, which were governed in part by their age—as older flows cooled to the extent that sulfurous compounds could condense, and therefore a strong contrast with newly emplaced, hot, dark lava could be observed. Using reasonable estimates of lava flow thickness of 1–10 m, time-averaged discharge rates (eruption rate) were estimated at 50–500 m³/s at Amirani and ~5–50 m³/s at Prometheus (Keszthelyi et al., 2001). For the second method, lava cooling model fits (Davies, 1996) to Galileo NIMS thermal emission spectra (Davies et al., 2000) were applied. Instantaneous discharge (effusion rate) rates varied between 9 and 125 m³/s at Prometheus with an average of ~50 m³/s (Davies et al., 2006) and from 16 to 140 m³/s at Amirani (Davies, 2003; Davies et al., 2014). Despite the uncertainties of the independent estimates, there was excellent concordance between these two methods (Davies et al., 2016). Nevertheless, given the low spatial resolution of Galileo imager data compared with the dimensions of lava tubes, the presence of lava tubes could not be confirmed using these data.

A comparison of the different planetary environments of Earth, the Moon, and Io suggests similarities and differences in lava tube dimensions and morphology (as reported by Davies et al. (2016)). Accordingly, as the gravity on Io is nearly equivalent to the Moon, kilometer-wide lava tubes may be possible. However, given that estimated lava fluxes were only about an order of magnitude above the fluxes observed in terrestrial lava tubes, this suggests tubes on Io may not be as voluminous as lunar lava tubes. Moreover, as the carrying capacity of a tube is proportional to the fourth power of the tube radius (i.e., Poiseuille's Law), lava tubes only two to three times larger than terrestrial lava tubes are possible on Io. However, for Io, given the lower gravity and potentially lower slopes—as most lava flows appear on relatively flat surfaces between paterae and mountains—would require conduits a few times larger than terrestrial features to support the same flux (Davies et al., 2016). Thus, lava tubes on Io are expected to be roughly an order of magnitude larger than those on Earth. Most terrestrial lava tubes range from a few to tens of meters in diameter (e.g., Sauro et al., 2020). Occasionally exceeding this size by tens of meters, we expect tube passages on Io to be on average 10 to several tens of meters wide (occasionally exceeding this proportionately to the largest tubes on Earth). With such dimensions, lava tubes on Io are expected to have a flow velocity of approximately 1 m/s, which is similar to the flow rates of terrestrial lava tubes. Smaller tubes, once filled with higher and faster flows, may be present, but lava tube passages wider than 100 m seems unlikely (Davies et al., 2016).

Skylights in active lava tubes are of particular interest because of their proposed use to constrain lava eruption temperatures (Davies et al., 2016). When active, a skylight briefly exposes the lava stream. Cooling by radiation is therefore limited. A skylight <30 m in length above a lava flow with a speed of 1–5 m/s would maintain a temperature distribution across the skylight high enough to differentiate between basaltic lava (typically ~1,470 K) and ultramafic lava (typically ~1,900 K). Given that lava tubes are highly insulating, the temperature of the lava can be within a few degrees of the eruption temperature even tens to hundreds of kilometers from the vent (Harris & Rowland, 2009). Measuring the lava eruption temperature therefore immediately confers strong constraints on lava composition, and hence the state and composition of Io's upper mantle. Overall, skylights are highly attractive targets for this purpose as they present a stable thermal source on the timescale of observations and are, as discussed above, likely common on Io. Thus, these features may represent the most important targets for a future mission (e.g., McEwen et al., 2019).

The features described above may not be ideal (at least at the time of imagery acquisition) to evaluate and/or to be considered SAPs as they represent active lava transport systems. If subsequent missions determine these flows are no longer active, these regions (i.e., Amirani and Prometheus) will warrant further examination—as they will likely represent regions supporting relatively recently developed lava tubes. Otherwise, efforts should be focused on regions that are no longer volcanically active but have been in the recent past. Given that the surface of Io is dominated by active volcanism, this will be an easy task. However, the surface ultimately becomes blanketed by SO₂ frost, which may hamper identification of SAPs on Io.

2.2.1.6. Vesta

The proto-planet, Vesta, is the second largest asteroid in the main asteroid belt (Russell et al., 2012). Although no SAPs have been identified, imagery from the Dawn spacecraft (Russell & Raymond, 2011) Framing Camera (Sierks et al., 2011) found several features indicative of speleogenic processes (Titus, Wynne, Boston, et al., 2021; Yingst et al., 2014). These processes include tectonic, phase transition (Boston, 2004), and landslides.

Tectonic processes on Vesta were evident while completing the geologic mapping of the asteroid (Yingst et al., 2014). Most noticeably, the equatorial region contains wide, long flat-floored troughs that have been interpreted as faults that formed due to the Rheasilvia impact (Buczkowski et al., 2012). Pit crater chains (i.e., linear assemblages of rimless pits) are ubiquitous across Vesta. While many are associated with equatorial graben-like features, the largest, including Albalonga and Robigalia Catenae (see Figure 4c), occur on the Vestalia Terra plateau, where the equatorial troughs do not deform (Buczkowski et al., 2014). These features are typically associated with subsurface void spaces, where surface material collapses and partially infills the void (Wyrick et al., 2004). Caves associated with pit crater chains have been confirmed on Earth (Ferrill et al., 2011; Okubo & Martel, 1998) and SAPs have been identified within these features on Mars (Cushing, 2012, 2017; Cushing et al., 2015; Wyrick et al., 2004). Thus, the pit crater chains on Vesta, especially the three large features on Vestalia Terra, could support tectonic caves like those found under pit crater chains in Iceland (Ferrill et al., 2011).

With steep slopes often near the angle of repose, the topographic relief on Vesta is similar to the Moon and Mars (Jaumann et al., 2012; Russell et al., 2012), where slope failure is a common resurfacing process (Jaumann et al., 2012). While this geologic process could result in the infilling of existing speleogenic features, talus caves would likely be created within the jumbled rock matrix.

Overall, post-impact tectonic processes that formed grabens and pit crater chains, the sublimation of volatiles (that likely gave rise to pitted terrains), and slope failures lend credence to the possibility of SAPs on Vesta. Based on the ages of these landscape features, tectonic and sublimation caves are likely ancient—consistent with the early impact history of this proto-planet (1.77–3.13 Ga; Schmedermann et al., 2014), while talus caves, if they exist, could be younger.

2.2.2. Icy Bodies

2.2.2.1. Ceres

Ceres is the innermost dwarf planet in the solar system and the most massive object in the main asteroid belt between Mars and Jupiter (Russell et al., 2016). Observations by NASA's Dawn spacecraft determined Ceres to be a partially differentiated world with a low density (~1,300 kg/m³) ice-rich crust with an average thickness of 40 km (Ermakov et al., 2017).

The ice-rich nature of the near surface of Ceres is supported by the observation of abundant landforms and surface features suggestive of ground ice, including lobate landslides (in icy areas may represent solifluction), pitted terrain, salt deposits, fluidized ejecta, and floor fractured craters (e.g., Buczkowski et al., 2019; Hughson et al., 2018; Hughson, Russell, Schmidt, Chilton, et al., 2019; Raponi et al., 2019; Schmidt et al., 2017; Sizemore et al., 2019). Additionally, hydrologic, cryovolcanic, and tectonic processes are hypothesized to have recently occurred (e.g., ~9 to 22 Ma for Occator crater; Nathues et al., 2020; Schmidt et al., 2020), and it is likely presently losing water vapor from currently exposed water ice patches (Combe et al., 2019; Landis et al., 2019). These processes may be relevant to the formation of near-surface voids and may provide access to the subsurface; subsequently, subsurface voids that also support icy and potentially briny environments are of astrobiological interest (Castillo-Rogez et al., 2020).

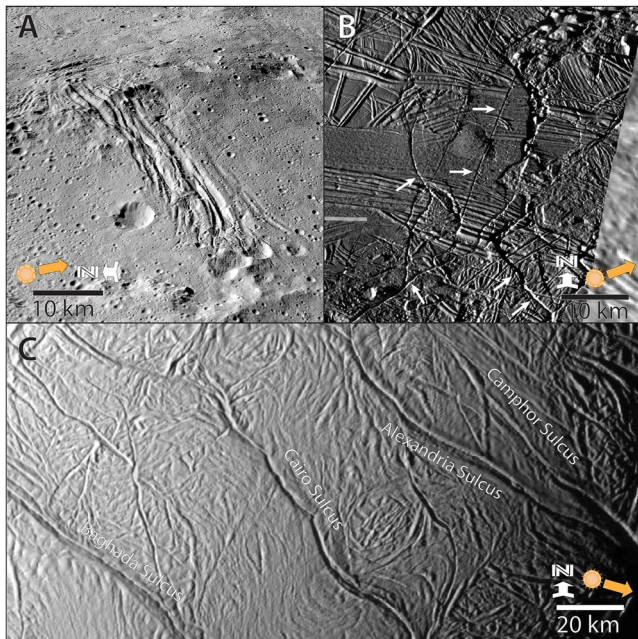


Figure 5. Processes and products for Ceres, Europa, and Enceladus. (a) Oblique view of the Nar Sulcus fractures within Yalode crater on the southern hemisphere of Ceres. Vertical exaggeration is a factor of 1.5. Image adapted from Dawn's Framing Camera Global LAMO mosaic, credit Roatsch et al. (2016). (b) Fracture network, Europa (centered at 35.5°N, 273.7°E). White arrows denote fractures. NASA Galileo, Solid-State Imaging image #11E0024, credit: NASA/JPL-Caltech/USGS. (c) Tiger Stripes, South Polar Terrain, Enceladus (centered at -84.53°N, 259.09°E). NW to SE trending sulci where most of the water vapor originates are labeled. NASA Cassini Imaging Science Subsystem-Narrow Angle camera image #N1500061253_1, resolution ~123.42 m/pix, credit: NASA/JPL-Caltech.

Concerning other speleogenic processes, Ceres appears to be highly fractured at both the local impact crater scale (Buczowski et al., 2019) and global scale (Scully et al., 2017). This implies that processes like subsurface fluid transport, mantle convection, and solid-state diapirism were likely active in the geologic past. Additionally, ice-related diapirism and extension may also be responsible for the Nar Sulcus features (Figure 5a) in the southern hemisphere, which are a set of large fractures that may be imbricated normal faults (Hughson, Russell, Schmidt, Travis, et al., 2019). Furthermore, ice sublimation, hydrologic, and cryovolcanic processes are hypothesized to govern the creation of large edifices (e.g., Ahuna Mons; Ruesch et al., 2016) and pitted terrains (Sizemore et al., 2019).

Subsurface fluid drainage and ice loss through sublimation in the near surface may also be effective methods of cavity formation. These processes may be analogous to permafrost degradation and lava tube development on Earth, especially if local concentrations of water ice remain from mixing due to large impacts (e.g., Prettyman et al., 2021). Future geophysical investigations of the geologic and gravitational structure of Ceres, both from orbital remote sensing and landed investigations, will be critical towards improving our understanding of speleogenic processes and products that may have formed in the ice-rich upper layer of Ceres.

Unlike other icy worlds in the solar system, such as Europa and Ganymede, water ice is not thermodynamically stable on the surface of Ceres and sublimates over geologic time leaving behind a lag layer of refractory compounds on its surface (Hayne & Aharonson, 2015; Landis et al., 2017; Prettyman et al., 2017; Schörghofer, 2016). Thus, determining natural regions of void formation will be important for future lander missions, as well as quantifying how local ice conditions and void spaces affect long-term volatile loss.

Finally, ample evidence of water-rock interactions and liquid brine activity on Ceres make it a priority target for future astrobiological investigations (Castillo-Rogez et al., 2020). Like other astrobiologically relevant worlds, potential biomarkers or prebiotic compounds are unlikely to be preserved due

to Ceres' hostile surface conditions. However, if these compounds still exist, they may be preserved in the shallow subsurface—thus further emphasizing the importance of identifying and characterizing speleogenic features on Ceres.

2.2.2.2. Europa

Europa, the most diminutive of the four Galilean moons, is covered with water ice, which is mixed with salts such as sulfates and chlorides (Ligier et al., 2016). Beneath the 20–50 km thick ice crust (Howell, 2021), Europa likely hosts an approximately 100 km deep global liquid water ocean (Anderson et al., 1998). The moon's interior and surface are periodically deformed by tidal forces due to Jupiter, resulting in intense geological activity. With an estimated age between 30 and 70 Ma (Zahnle et al., 2003), the surface is one of the youngest in the solar system and is covered with a variety of geological features (e.g., Greeley et al., 2000). Of these features, fractures may represent access to the subsurface. Figure 5b shows a fracture network imaged by the Galileo spacecraft in the 1990s.

Fracture initiation and propagation has been studied by several groups of researchers; their work is summarized by Craft et al. (2016). The development of fractures requires overcoming ice tensile strength, which could occur because of ice shell thickening (Nimmo, 2004) or tidal forces acting on the ice shell (Lee et al., 2005). These features could propagate from the surface toward the ocean (Lee et al., 2005), from the shell base toward the surface (Crawford & Stevenson, 1988), or be initiated within the ice shell and then propagate in both upward and downward directions (Manga & Wang, 2007).

We have no evidence to suggest that these fracture networks provide access to the deep subsurface. However, these landscapes do warrant further examination. Europa's surface is exposed to micrometeorite impacts, as well

as high energy electron radiation from Jupiter's magnetosphere. Thus, the upper 30 cm of the ice shell is exposed to surface radiation, which could destroy potential chemical biosignatures (Costello et al., 2021; Nordheim et al., 2018). Subsequently, deep fractures would represent high priority targets as these features may contain materials protected from the surface radiation.

Additionally, previous studies described a variety of geological features potentially indicative of partially melted subsurface lenses. These include the double ridges (Nimmo & Gaidos, 2002), pits and domes (Michaut & Manga, 2014), chaotic, disruptive terrains (Sotin et al., 2002), and smooth plains (Fagents, 2003; Lesage et al., 2021). As demonstrated by Kalousová et al. (2014, 2016), water drainage is highly efficient in locally heated ice such as diapirs or tidally activated faults, which might lead to the formation of cavities in Europa's upper ice shell.

The repeated detection of localized water vapor in Europa's atmosphere (Paganini et al., 2019; Roth et al., 2014, 2016; Sparks et al., 2016) may be caused by the eruption of water from the subsurface, but the source of these putative plumes cannot be precisely determined given the low resolution of available imagery and the large spatial extent of the water vapor plumes. For now, given the low number of high-resolution images from the Galileo imager (~100 images with resolution higher than 100 m/px), it is difficult to estimate the number of SAPs on Europa. This question could be addressed through a statistical examination of fracture density per terrain type (e.g., chaotic terrain, smooth plains, and bands) but this has yet to be attempted. Additionally, radar sounding data and high-resolution visible imagery should be acquired and examined in the future. These analyses will be critical for determining the types of speleogenic products formed within the upper ice layers, their extent, and their potential for exploration.

Because the subsurface ocean has been identified as a high-priority target in the search for the life in our solar system, this icy moon is the focus of the upcoming NASA Europa Clipper mission (Howell & Pappalardo, 2020) and the ESA JUICE mission (Grasset et al., 2013). With a planned launch in 2024 and arrival scheduled for 2030, Europa Clipper will have an array of cameras (visible and thermal), spectrometers, and radar. This platform could be used to confirm and potentially characterize currently identified SAPs, identify new SAPs, better constrain formation processes, and perhaps monitor active cryovolcanism. Ice penetrating radar could potentially differentiate between shallow SAPs versus fractures extending deep into the crust. The JUICE mission (with a planned launch date of August 2023 and orbital insertion scheduled for August 2031) will spend at least three years making detailed observations of Jupiter and three of its largest moons—Ganymede, Callisto, and Europa. Data acquired and analyzed from these two missions are expected to expand the number of SAPs for Europa (as well as other targeted bodies).

2.2.2.3. Titan

Saturn's moon Titan has a unique surface composition and chemistry that enables Earth-like processes such as karstic dissolution and subsequent speleogenesis (e.g., Soderblom et al., 2007), albeit dissolution is methane-based. Due to the potential for large-scale karstic processes on Titan's organic surface, in addition to the other "typical" processes found on icy worlds (cryovolcanism, diapirism, and fracture formation), Titan is perhaps one of the best places in the solar system for planetary cave exploration.

Observing constraints include a thick (1.5 bar) hazy atmosphere (Gupta et al., 1981; Israël et al., 2005; Sagan & Thompson, 1984), which constrains flyby/orbital visible spectrum/near infrared observations to a few narrow spectral windows (e.g., 0.637, 0.681, 0.754, 0.827, 0.937, and 1.046 μm ; Vixie et al., 2012). The best available data set for SAP identification is currently the Cassini Synthetic Aperture Radar (SAR) data set, which acquired multiple swaths at 200–500 m/px resolution (refer to Elachi et al., 2004; Lopes et al., 2019).

Global orbital imagery at higher resolutions could also potentially confirm the presence of additional karstic landscapes, as well as identify additional SAPs. For the Cassini data, only 46% of Titan's surface was captured with SAR at <1 km/px scale, with the highest resolution SAR data at 200 m/px resolution (Lopes et al., 2019). On Earth, typical karstic landscapes only become evident at 1–10 m resolution; it is a testament to the larger scale of Titan karst features that we were able to detect SAPs at >100 m/px scale. On Titan, labyrinth terrains are in higher southern mid-latitudes and polar regions—locations with the lowest coverage in the Cassini SAR data set (Malaska et al., 2020). Thus, it is likely that even full global coverage at the Cassini scale would enable more labyrinth terrain units to be discovered. Importantly, with an increasing resolution, more detailed and perhaps smaller isolated patches of these terrains could be revealed (Sotin et al., 2017). Visible or near-infrared imaging

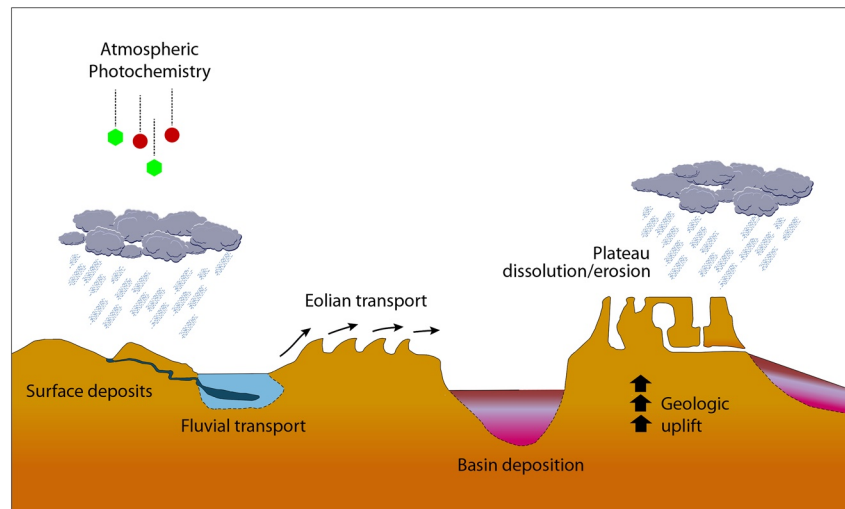


Figure 6. The putative Titan sediment and karst cycle. Atmospheric photochemistry delivers complex organic molecules to the surface. Basins are filled by fluvial activity from hydrocarbon rains and eolian transport. Then, uplift exposes basin sediments as uplifted plateaus. Hydrocarbon rainfall and fluvial activity dissolves soluble materials and creates subsurface conduits in the soluble substrate, leading to closed valleys and other karstic features. Dashed lines within the liquid-filled depression are used to infer wall and floor extent.

over multiple wavelengths could also provide spectral data that could distinguish compositional classes over these terrains (e.g., Solomonidou et al., 2020). While great achievements have been made to extract altimetry data from SAR swaths (Corlies et al., 2017; Stiles et al., 2009), acquisition of high-resolution elevation data inside many labyrinth terrains was not possible; this was largely due to limited availability of swaths that enabled the development of stereogrammetric imagery (Kirk et al., 2009).

Here we summarize the 1,270 SAPs identified in the organic sedimentary deposits of Titan (Table 2; refer to Malaska, Schoenfeld, et al., 2022). Like Earth, Titan has a rainfall and sediment cycle, but unlike Earth, Titan's weather cycle is driven by cryogenic hydrocarbon rains (methane with dissolved nitrogen) that carve through a landscape of organic materials. In Titan's upper atmosphere, photochemical processes convert atmospheric methane and nitrogen into complex organics that eventually become deposited onto the surface to create a landscape of organic materials superimposed on an icy crust (for some recent photochemical models see Hörst, 2017; Krasnopolsky, 2009, 2014; Lavvas et al., 2008; Willacy et al., 2016). Once on the surface, these organic materials are transported by wind and hydrocarbon-based fluvial processes downstream into basins, possibly creating layers of organic materials as basin deposits (Figure 6). After uplift, some of the soluble organics could be dissolved and allow physical breakdown or transport of insoluble grains just like the breakdown of calcite-cemented sandstone here on Earth. There is observational evidence for surface evaporites on Titan, which in turn suggests that dissolution, transport, and redeposition of organic materials can occur (Barnes et al., 2011; MacKenzie & Barnes, 2016; MacKenzie et al., 2014). Once these former deposits are uplifted, they would reveal a large block of exposed organic materials that may undergo resolubilization of the matrix and release of the grains to create a karstic landscape. Laboratory work and modeling have both confirmed that many Titan materials have saturation amounts and kinetics that would allow karstic processes to occur (Cornet et al., 2015; Malaska & Hodyss, 2014).

One of the more enigmatic terrain types on Titan is labyrinth terrains (Figures 7a and 7b). These areas are characterized by large plateaus up to 500 m thick and composed primarily of organic materials (Malaska et al., 2020). Labyrinth terrains account for about 1.5% of Titan's overall surface (Lopes et al., 2020; Malaska et al., 2020), but contain between 14% and 35% of Titan's solid organics by volume and thus represent a major reservoir of complex organic molecules (Malaska et al., 2020). Interestingly, many of the labyrinth terrains display morphologies like karstic terrains on Earth—including closed valleys, which are usually diagnostic for karst in mesic areas (EPA, 2002), as well as surrounding features with karst-like morphologies, such as structural poljes or depressions (Malaska et al., 2010). In addition, landscape evolution models that incorporate dissolution have reproduced the labyrinth terrain morphologies seen on Titan (Birch et al., 2019, 2020; Cornet et al., 2017; Umurhan et al., 2020). One of these labyrinth terrain types, the polygonal labyrinth terrain type (referred to as “lbp” in

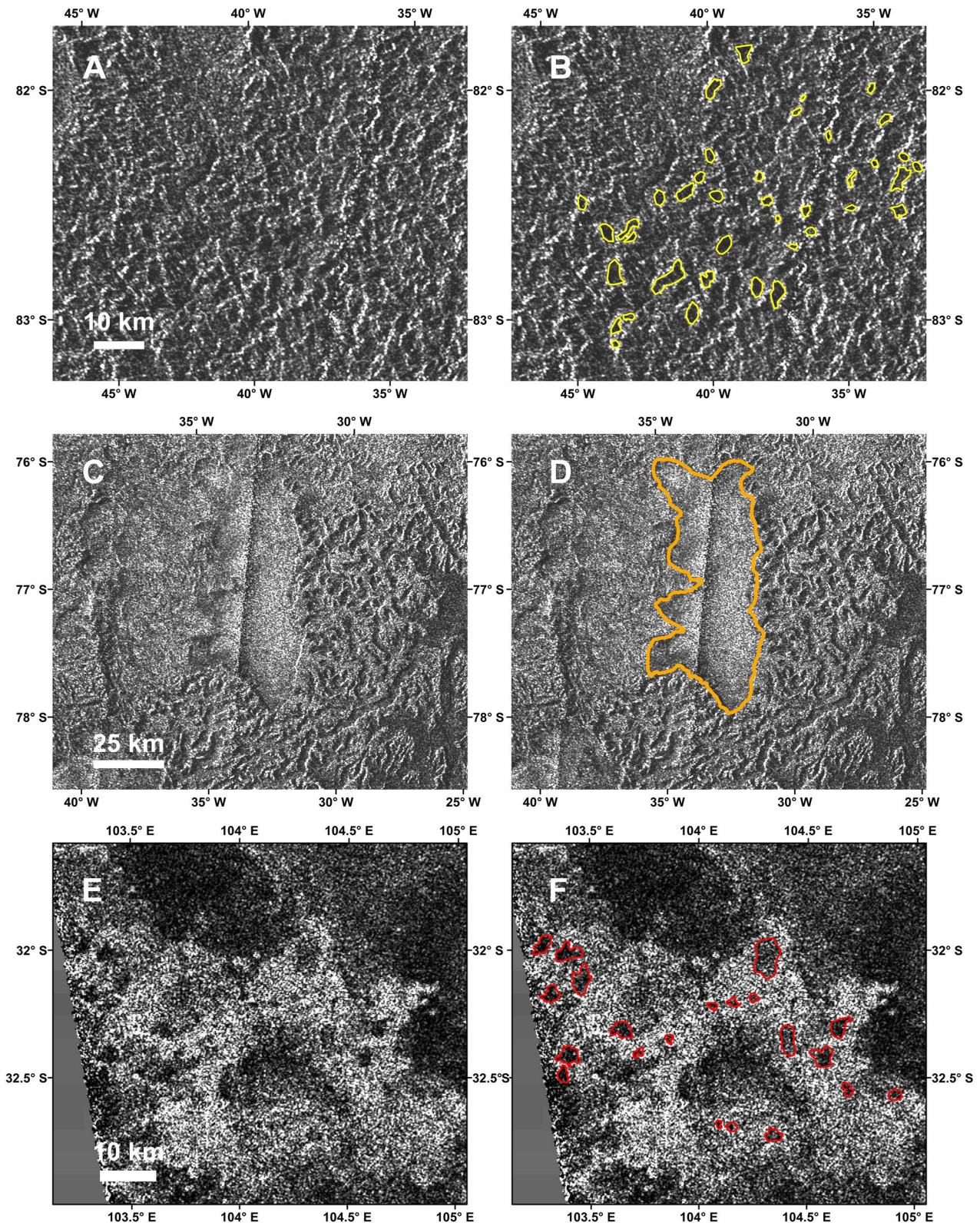


Figure 7.

Malaska et al. (2020)), is morphologically akin to polygonal karst terrain found on Earth. Both terrestrial and Titan terrains display a series of “closed valleys” containing valley networks with a low branching order separated by steep-sided walls that are polygonal in planform. The main difference between polygonal karst on Earth and polygonal labyrinth terrain on Titan is their relative size; the features on Titan are roughly 10 times larger than their Earthbound counterparts (Malaska et al., 2020; Williams, 1972). On Earth, these features are thought to form through competitive karstic dissolution of a pre-existing joint network in a soluble or partially soluble block (Fleurant et al., 2008; Williams, 1972), which can give rise to extensive maze cave networks (refer to Palmer, 2007). Analogous to Earth, the intersection of joints in Titan’s uplifted organic plateaus could provide an initial entry point for surface liquids that then plausibly created the observed closed valleys.

The number of closed valleys in polygonal labyrinth terrains (reaching up to 100%) and other types of labyrinth terrains can be used to estimate the number of SAPs. Each of these would be assumed to lead to a subsurface phreatic and vadose network like on Earth but constructed of organic materials and carrying hydrocarbon liquids. We estimated the total number of subsurface access points in labyrinth terrains by estimating the number of closed valleys in the observed labyrinth terrains from mapping presented in Malaska et al. (2020), where 30 closed valleys were identified in a section of Ecaz Labyrinthus. To extrapolate this estimate to other labyrinth terrains, we determined the total closed valley area in each labyrinth unit (based on percentage estimates), then calculated the number of closed valleys that could be contained in that area based on a “closed valley” dimension of 2 to 1 valley width plus intervening plateau width. Our extrapolated value was approximately 20,000 SAPs. Over 5,000 were estimated in the vast labyrinth region (“The Great Southern Labyrinth”) surrounding Titan’s south pole, with over 750 estimated SAPs in the entire Ecaz Labyrinthus. This number is likely an underestimate because (a) not all labyrinth terrains have been identified, as Cassini imaging was particularly poor in the southern middle to high latitudes (an area particularly rich in labyrinth terrains; see Malaska et al., 2020) and (b) many sub-resolution karstic conduit features are likely to exist.

Other Titan surface morphologies similar to terrestrial karst terrains include the steep-sided empty lakes found in the polar regions (Figures 7c and 7d). Formation processes for these features vary between putative caldera-like processes (Mitri et al., 2019; Wood & Radebaugh, 2020) and karstic dissolution in a highly porous regolith. Many of the lakes appear to be in closed depressions (consistent with both formation scenarios), but have the same hydrological elevation, which is consistent with porous regolith and connectivity between the depressions (Hayes, 2016; Hayes et al., 2008, 2017). The second largest lake in the south polar terrain, Crveno Lacus, is inset into a large labyrinth terrain unit with a steep scarp as observed by radar shadowing—this would be consistent with a karstic hypothesis, although it does not rule out a caldera blowout of a soluble organic overburden (Malaska et al., 2020). Elsewhere in Titan’s south polar terrain, Veliko Lacuna, an empty lake basin, is partially surrounded by Sikun Labyrinthus on its eastern and southern sides, with abrupt straight boundaries (Figures 7c and 7d).

Intriguingly, detailed examination of the drainage networks in Sikun Labyrinthus reveals that the networks integrate away from this basin, suggesting drainage conduits and transport leading from the lake through the labyrinth to topographically lower lying areas outside Sikun Labyrinthus (Malaska et al., 2010). These observations are consistent with Veliko Lacuna being a structural polje, fed from outside the lake, ponded temporarily, then later diffused through the labyrinth conduit network. There is evidence that transient ponding and subsequent drainage has been observed by the Cassini spacecraft’s ISS infrared mapping instrument. All the evidence is consistent with karstic drainage (polje-like) processes for at least this large empty lake basin, although sub-resolution channels cannot be ruled out. Our estimate assumed that each empty or filled steep-sided depression contains at least one subsurface access point. Considering the total number of empty and flooded steep-sided depressions, there are at least 869 mapped lake features (Hayes, 2016).

Figure 7. Examples of dissolution-driven subsurface access points on Titan. These include labyrinths, steep-sided lakes, and equatorial pits. (a) Cassini Synthetic Aperture Radar (SAR) image of a section of Ecaz Labyrinthus with a more cell-like structure of orthogonally connected plateau “walls.” Radar illumination from left. (b) Annotated image of Ecaz Labyrinthus with closed valleys featured and indicated by yellow shapes. Sinusoidal projection centered at 39°W. (c) SAR image of Veliko Lacuna (brighter area in center of image) is in close association with the highly dissected plateau of Sikun Labyrinthus to the east and south. Sinusoidal projection centered at 33°W. (d) Annotated version indicating contact of Veliko Lacuna with Sikun Labyrinthus. Near the east margin of Veliko Lacuna, bright edges suggest straight steep scarps. Careful examination shows that dissection increases away from Veliko Lacuna, ultimately overall towards the dark area at the middle of the eastern edge of the image. (e) Cassini SAR image of low backscatter (darker) equatorial pits in hummocky terrain in the south Belet region, Titan. (f) Annotated images with several pits outlined in red. For both (e and f), sinusoidal projection centered at 104°E longitude. North is at top in all images. Scale as shown.

Other potentially karstic features include the equatorial pits (Figures 7e and 7f) found in pitted hummocky terrain, which are small, low-radar backscatter areas usually between 1 and 6 km in diameter (Adams & Jurdy, 2012; Lopes et al., 2020; Schoenfeld et al., 2021) and located in an icy substrate. In a recent analysis of an area in the south Belet region of Titan, Schoenfeld et al. (2021) posited multiple formation scenarios for the equatorial pits, including processes such as cryovolcanic blowout and sinkhole formation and collapse following dissolution or volatile loss. While these features are small, when present they can be numerous. Since they are in Titan's equatorial sand seas, it is possible that there are many more features that have been buried by sand or were sub-resolution to Cassini radar (200 m/px scale) and thus were not detected. Currently, approximately 370 pits in Titan's equatorial regions have been identified (Adams & Jurdy, 2012; Schoenfeld et al., 2021) and at least one putative cryovolcanic pit has been observed (Lopes et al., 2013).

Overall, Titan is an example of a world with dissimilar materials to Earth, but with similar overall geological processes. The story of subsurface access points on Titan is dominated by dissolution geology and karstic processes in organic materials by cryogenic hydrocarbon materials—to the point where tens of thousands of subsurface access points may be present. Of these, each subsurface access point type may be a key to understanding both the hydrology (for simplicity this term is used for all liquids) and material transport on Titan. As an exploration target, the steep walls of the labyrinth terrains may provide access to uplifted and exposed layers that are testament to the detailed transport and chemical synthesis history of Titan. Further examining the likely phreatic and vadose conduits of these terrains could also lead to greater understanding of chemical, geological, hydrological, and speleological processes on a world with fundamentally different parameters. In many ways, due to the interplay between insoluble grains, multiple types of organic materials, and at least three different types of liquids (methane with dissolved nitrogen, ethane, and propane), Titan presents as an even more speleologically sophisticated system when compared to Earth.

Dragonfly, an astrobiological drone mission to Titan is scheduled to launch in 2027 (Barnes et al., 2021) with arrival planned for 2036. The proposed landing site, on the edge of the Shangri-La Sand Sea near Selk Crater, is not close to any known mapped karstic landscapes or SAPs (Malaska et al., 2016, 2022). However, with an operational range of several hundred kilometers, it is possible Dragonfly could identify SAPs and begin to characterize newly discovered features not resolved in the Cassini data set.

2.2.2.4. Enceladus

Enceladus is characterized by a deep subsurface global ocean of liquid water (Lobo et al., 2021; Patthoff & Kattenhorn, 2011), an active icy shell surface sculpted by impact cratering and tidal forces (Martin et al., 2017), and a fracture network providing communication between the subsurface ocean and icy shell (Helfenstein & Porco, 2015). Ice shell thickness ranges from ~30 km in the South Polar Terrain region (SPT) to ~70 km in the northern hemisphere (Lucchetti et al., 2017; references therein). SPT fractures extend up to ~130 km in length, are 0.5 km deep, and average ~2 km in width (Gioia et al., 2007; Porco et al., 2006).

The potential for subsurface cavities consists of the initial identification of water ice plumes in the SPT (Porco et al., 2006; Figure 5c) and the ultimate characterization of 100 associated jets (Porco et al., 2014); these jets are now considered potential SAPs. Tidal forces from Saturn produced these tensile fractures, as well as other major strike-slip structures (Běhounková et al., 2015; Hedman et al., 2013; Helfenstein & Porco, 2015; Nimmo et al., 2014; Porco et al., 2014). Additionally, the SPT fracture network is produced and maintained by the latent heat of upwelling water vapor and condensed water, while tensile stress is considered the primary process driving fracture expansion and contraction (Porco et al., 2014).

Other potential cave-bearing targets include ~2,000 “narrow troughs” (ranging in size from a few to tens of kilometers in length), which occur between 60°S and 55°N. These features have a nearly global longitudinal distribution (Crow-Willard & Pappalardo, 2015), appear indicative of recent tectonic activity, and dissect older geologic terrains. Formed in tensile conditions, these “narrow troughs” likely penetrate the icy shell for several kilometers but are probably not in direct communication with the subsurface ocean (Lucchetti et al., 2017). Fracture penetration depth and their probable interaction with the subsurface ocean has been analyzed in detail for several regions including the tiger stripes (refer to Lucchetti et al., 2017).

Moreover, the “narrow troughs” as potentially open structures were derived from observations of pit craters and pit crater chains in the Cratered Plains geologic unit (Martin et al., 2017). This region is characterized by a mantling of loose regolith formed by impacts and plume ejecta. Pit crater and pit crater chains are

intimately associated with these structures since they are either isolated or aligned along the length of the troughs. Furthermore, their morphology and distribution are consistent with extensional fractures or dilational faulting, where the surface regolith appears to have collapsed forming a sinkhole-like feature. Pit crater depth ranges from 90 to 290 m and width ranges from 450 to 700 m; inter-pit spacing is between 200 and 500 m along the chain extent (see Martin et al., 2017).

Finally, features potentially associated with cryovolcanism may provide access to the deep subsurface (Walker & Schmidt, 2015). These isolated depressions may have formed via the collapse of an ice lid that once covered a cavity. The underground void may have originated by the emptying of a shallow liquid pocket via sublimation, which could be caused by depressurization driven by tectonic activity (i.e., the icy shell fractures due to tidal forces facilitating sublimation of the material within the void) (Walker & Schmidt, 2015). A possible example is the SPT depression, which is ovate (240–310 km across) and characterized by a raised rim (Walker & Schmidt, 2015).

Overall, Enceladus is a tectonically active world characterized by numerous features that provide access to the deep subsurface. Barring the SPT fracture network (which is connected to a deep subsurface liquid water ocean), the depths to which other features, such as the narrow troughs and pit craters, penetrate the icy shell are unknown and will require further study (e.g., acquisition and examination of high-resolution visible spectrum imagery and radargrams in high priority regions). Whether cryovolcanic activity occurs on Enceladus, or if such features formed similarly to the proposed cryovolcanoes of Pluto (see below), will also require further examination.

2.2.2.5. *Ganymede*

At ~5,200 km in diameter, Jupiter's moon Ganymede is the largest in the solar system. Surface spectral characteristics indicate its composition is roughly equally composed of water ice and rocky material; concerning the latter, the rocky half is ostensibly composed of carbonaceous chondrite (Morrison, 1982). Based upon the Galileo SSI (Solid State Imaging) imagery from 1995 to 2003 (Carr et al., 1995), potential cave-bearing terrains are expected to occur within both material types; these include regions of a largely icy crust subjected to tidal forces, phase transitions, and cryovolcanic activity. To date, only one possible cryovolcanic caldera has been identified on Ganymede (Head et al., 2002; Schenk et al., 2001). Subsequently, this Jovian moon is early in the SAP identification stage. Due to limited availability of imaging assets, only potential speleogenic processes can be inferred at this time.

Ganymede has likely undergone at least five processes that would promote speleogenesis. These include tectonic activity, cryovolcanism, meteor impacts, phase transitions, and sublimation. Pit crater chains (i.e., linear assemblages of rimless pits) are common features on icy and rocky bodies (e.g., Cushing, 2017; Martin et al., 2017; Okubo & Martel, 1998). These features have been associated with caves on Earth (e.g., Ferrill et al., 2011; Okubo & Martel, 1998) and SAPs on other planetary bodies (e.g., refer to Section 2.2.1.3 The Moon and 2.2.1.4 Mars above). At least three unusual crater chains have been identified, which likely represent the impact scars of tidally disrupted comets that struck Ganymede (Schenk, 1993). Additionally, several pit crater chains, especially the four largest catenae (Enki (Figure 8b), Khnum, Nanshe, and Terah), may support tectonic caves.

Although Ganymede is no longer tectonically active, evidence of past cryovolcanism has been documented (Schenk & Moore, 1995; Squyres, 1980). For example, sources and vents for cryovolcanism (such as Sippar Sulcus; Figure 8a) have been identified in Galileo SSI images (Head et al., 2002; Schenk et al., 2001). Cryovolcanic activity has also been proposed to explain the resurfacing of the bright terrains on Ganymede (Pappalardo et al., 2004) whereby water-ice magmas pushed to the surface appear to have filled low lying areas. Similar to processes on Ceres, near-surface fluid drainage may give rise to cavity formation (e.g., Prettyman et al., 2021). Cryolava compositions on Ganymede include H₂O or a brine mix of H₂O, MgSO₄, and Na₂SO₄ (Kargel, 1995).

Fracture caves may also be present on Ganymede. These features may have formed or been enlarged by processes as simple as crumbling or non-fluid undercutting in faults, scarps, and other fractures (e.g., Cooper & Mylroie, 2015), as well as by meteor impacts (e.g., Scully et al., 2020). Subsequent cave enlargement may have occurred via the freezing expansion of ice (Boston, 2004). Ice fractures and cravasses have been confirmed on other icy bodies (refer to icy body sections herein). Additionally, because of the extremely low global temperatures on Ganymede (−183°C to −123°C) (Hanel et al., 1979; Pappalardo et al., 2004), SAPs formed within ice may represent more permanent features as opposed to their more transient nature of glacial caves and fractures on Earth (Boston, 2004).

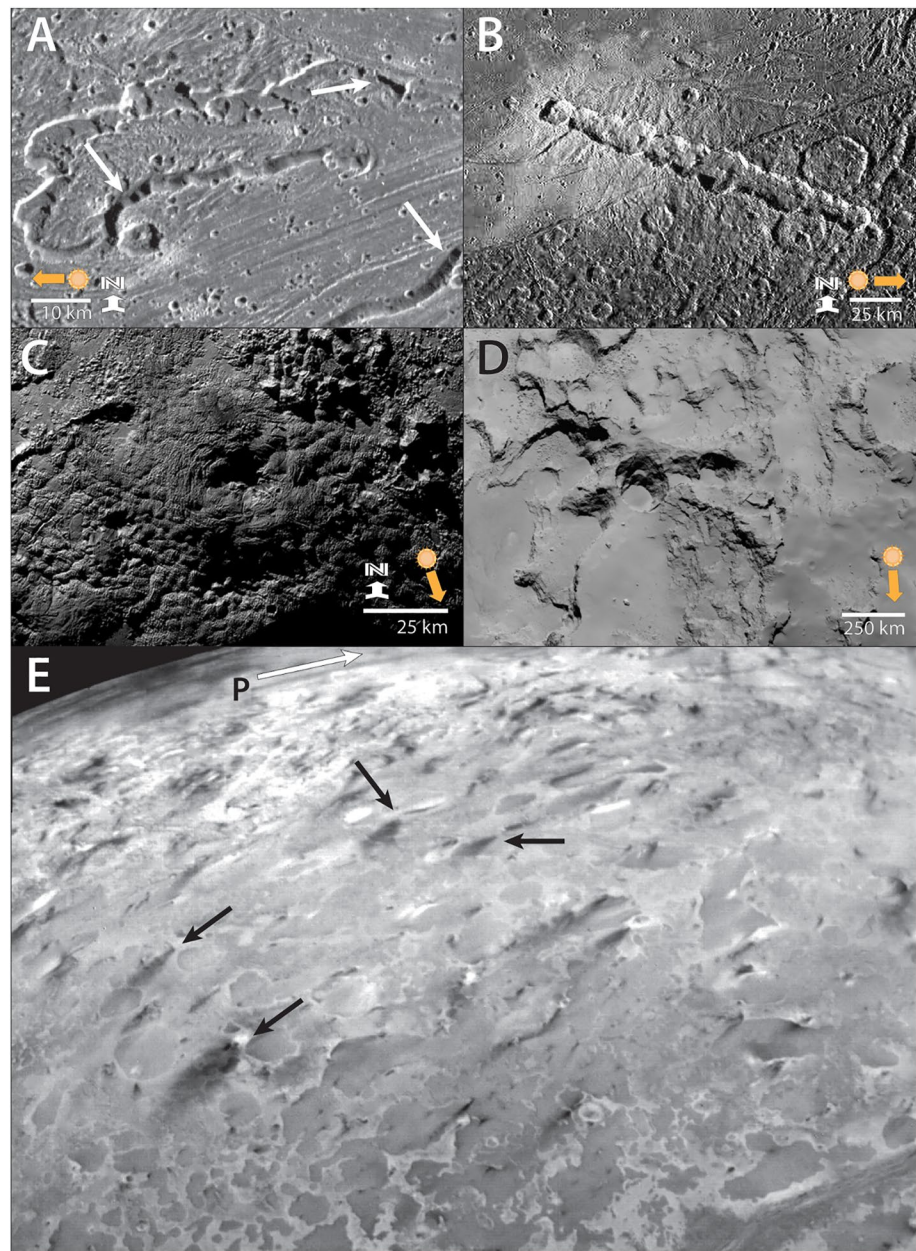


Figure 8. Products and processes for Ganymede, Pluto, Comet 67P, and Triton. (a) Sippar Sulcus region, Ganymede. White arrows represent candidate features indicative of cryovolcanism. NASA Galileo Solid State Imaging image # PIA01614, credit: NASA/Brown University. (b) Enki Canana, Ganymede. This crater chain formed by impact of cometary fragments. NASA Galileo Solid State Imaging image # PIA03217, credit: NASA/Brown University. (c) Wright Mons cryovolcanic caldera, Pluto. Wright Mons rises ~ 4 km above the surrounding terrain and has a central cavus (middle, in shadow) that is at least ~ 4 km deep. NASA New Horizons, enhanced Long Range Reconnaissance Imager image mosaic, credit: NASA/JHU-APL/SwRI. (d) Sublimation pits (center) in Seth region, northern hemisphere of the big lobe on Comet 67P. As this comet is bilobate with the rotational axes at the neck between the two lobes, cardinal directions are not useful. ESA Rosetta OSIRIS camera, image # NAC_2014-08-29T07.42.54.589Z_ID30_1397549800_F22, credit: ESA. (e) Mahilani plume (annotated with P with a white arrow above the feature) was observed erupting to ~ 8 km altitude, before turning due to interactions with winds. Numerous dark fans interpreted as plume deposits (with several identified by black arrows) in the South Polar Terrain on Triton. NASA Voyager 2 Imaging Science System, image #C1139503, credit NASA/JPL-Caltech.

Two additional processes are possible on Ganymede—phase transitions and sublimation. The icy permafrost crust can undergo ground ice sapping, subsequent collapse, and void formation. Additionally, the heat of an impact event releases volatiles in the ice, resulting in the formation of subsurface void spaces (Boston, 2004).

Additionally, Roth et al. (2021) confirmed the presence of water vapor in Ganymede's atmosphere—reinforcing the potential for sublimation-driven speleogenesis.

Overall, post-impact tectonic processes on Ganymede lend credence to the possibility of cave formation. Based on the ages of landscape features, caves, if they still exist, are likely ancient. These processes may be relevant to the formation of near-surface voids and creating access to the subsurface, which is of important consequence as Ganymede's subsurface ocean is of astrobiological interest. Future geophysical investigations (e.g., JUICE and Europa Clipper) on the geologic and gravitational structure of Ganymede will be critical toward improving our understanding of potential speleogenic processes. Importantly, future reconnaissance efforts should be focused on areas of known cryovolcanic activity (e.g., Sippar Sulcus and the bright terrain regions).

Refer to the Europa section above (Section 2.2.2.2) for an overview on the JUICE mission (with a planned launch date of August 2023 and orbital insertion scheduled for August 2031). Given that this mission will include detailed and high-resolution observations of Ganymede, it is likely SAPs will ultimately be identified on this Jovian moon.

2.2.2.6. Triton

The seventh largest moon in our solar system, Triton is an unusual world. It may have originated as a large Kuiper Belt object, similar to Pluto, before it was captured into orbit around Neptune and subjected to intense changes (e.g., McKinnon, 1984). The sole visit by a spacecraft, Voyager 2 in 1989, resulted in imaging of only one hemisphere (~40% of the surface) at resolutions sufficient for geological interpretation (~340–2,000 m/px resolution), leaving Triton with the most extensive unmapped surface area of any known moon in the solar system. Furthermore, because it is 30 AU from the Sun, it also has limited ground-based astronomy with whole-disk (or nearly so) spectroscopy (e.g., Grundy et al., 2010). Based upon interpretations of available imagery, while no specific interpretations of caves have been made due to remote sensing limitations, we speculate that three speleogenic processes are plausible on Triton; these include void space created through plume activity, cryovolcanism, and tidally-driven tectonic activity.

It is tempting to consider the possibility of karst-like geology and speleogenesis on Triton, due to its extensive methane- and electron-rich ionosphere (Tyler et al., 1989). Like Titan (see Section 3.2.2.3 above), these mechanisms drive photochemical production and precipitation of potentially soluble organic compounds (Krasnopolsky & Cruikshank, 1995). However, Triton's ~1–4 Pa neutral atmosphere is five orders of magnitude thinner than Titan's atmosphere and is more akin to the atmosphere of Pluto (Lellouch et al., 2011; references therein). Furthermore, based upon our observations to date, the surface appears to be mostly covered in refractory and volatile ices (Bertrand et al., 2022; Grundy et al., 2010) and lacks the massive dark surface deposits observed on Titan (Lorenz et al., 2008) or even the more limited dark deposits on Pluto (e.g., Fayolle et al., 2021; references therein). In the aggregate, these factors suggest relatively low levels of cumulative precipitation of potentially soluble organics, making the presence of karst highly unlikely.

Aside from karst-analog processes, however, there are other processes at work on Triton that offer some prospect for caves. Triton is subject to intense tides that likely sustain an internal ocean and drive endogenic geology (Nimmo & Spencer, 2015). The moon's young surface age (<10 Ma; Schenk & Zahnle, 2007) is almost certainly in part a result of extensive tectonics, convecting and/or cryovolcanic resurfacing, resulting in rare and unique geomorphologic landforms including walled plains, pit chains, guttae, extensive ridges, and cantaloupe terrain (e.g., Croft et al., 1995). While no caves have been identified, the apparent pervasiveness of cryovolcanism, which is thought to be the cause of several landforms including Leviathan Patera and Set Catena (Croft et al., 1995), implies that cryolava tubes and tectonic caves are plausible. A series of at least six regions involving a complex of pits, pit crater chains, and linear depressions (Croft et al., 1995), as well as three active plumes (Soderblom et al., 1990) are indicative of both cave-bearing terrains and potential SAPs.

Of Voyager 2's discoveries, Triton's towering plumes and possible plume deposit fans were among the most spectacular (Figure 8e). Thus far, three plumes (Mahilani, Hili, and Cipango) and more than 100 fans (i.e., dark surface features inferred to be cryovolcanic vents and/or phase change caves) have been identified in the Southern Hemisphere terrain (e.g., Hansen et al., 1990; Hofgartner et al., 2022). Although plume locations have been mapped with a high degree of confidence, the coordinate system used is now outmoded, and the current data base did not include a complete accounting of the caveats concerning lighting, resolution, and other considerations.

Efforts are underway to update this information and integrate these data into the next USGS Triton map. At which time, a more complete list of fans, their locations, and data interpretations will be published.

While several mechanisms for their formation have been suggested (refer to Kirk et al., 1995; Hofgartner et al., 2022) for plume and fan formation, the dominant paradigm is a solar-driven, solid-state greenhouse effect involving subsurface heating of condensable, nitrogen-rich volatile layers in the South Polar Terrain (SPT). This process would lead to a pressurized phase change from solid to vapor and explosive venting (Soderblom et al., 1990). This mechanism may also give rise to the formation of extensive subsurface void space, estimated at $\sim 0.2 \text{ km}^3$ per eruption (Soderblom et al., 1990). If accurate, this speleogenic process would result in the development of caves larger than any known cave systems on Earth (cf., Son Đoòng Cave, Vietnam, which is Earth's largest known cave; Osipova, 2015). Overall, the longevity of both the voids and the SPT remains unclear.

2.2.2.7. The Plutonian System

Pluto. The recent New Horizons mission provided the first flyby observations of bodies in the Kuiper Belt, unveiling the surfaces of Pluto and its moons in unprecedented detail (Stern et al., 2015). In particular, Pluto was revealed to be a surprisingly geologically active body characterized by mountains, glaciers, canyons, and a convectively overturning nitrogen ice sheet that covers about 5% of its surface (Moore et al., 2016). The uppermost surface ice layer is composed principally of nitrogen, with lesser contributions of CH_4 and CO ice and some exposures of water ice up to $\sim 100 \text{ km}$ thick (Protopapa et al., 2017); this ice shell overlies a subsurface liquid water ocean (Nimmo et al., 2016). Pluto's climate is controlled by vapor pressure equilibrium with its thin nitrogen atmosphere (Bertrand et al., 2020; Hansen & Paige, 1996), which supports a nitrogen sublimation-deposition cycle that actively drives nitrogen glacial flow (Umurhan et al., 2017), sculpts pits (Moore et al., 2017), and penitentes (Moore et al., 2018; Moores et al., 2017). This nitrogen sublimation-deposition cycle is thought to be responsible for other features unique to Pluto including various features associated with ponded nitrogen ice, and “washboard” and “fluted” terrain formed by ancient nitrogen ice glaciation (Howard et al., 2017; White et al., 2017, 2019).

The features with the most promise to yield access to the subsurface are related to potential H_2O cryovolcanic activity. The most prominent features interpreted to be related to cryovolcanism on Pluto are Piccard and Wright Montes (Figure 8c), located at the southern end of Sputnik Planitia (approximately 20°S , 170°E). Wright Mons reaches $\sim 4 \text{ km}$ above the surrounding topography, with a width of $\sim 150 \text{ km}$, while Piccard Mons reaches $\sim 6 \text{ km}$ and spans $\sim 225 \text{ km}$ (Moore et al., 2021; Schenk et al., 2018; Singer et al., 2016). West of Wright Mons is a region interpreted to be a cryovolcanic flow, which hosts depressions appearing to have formed via collapse and may represent additional subsurface access points. Another potential degraded cryovolcanic flow occurs to the north of Wright Mons (Singer et al., 2016). Each mons hosts a central, tens-of-kilometers-wide irregularly shaped steep-sided depression with a depth similar to the rise of the mons above the surrounding topography (i.e., $\sim 4\text{--}6 \text{ km}$; Singer et al., 2016). These may be analogous to calderas, and thus may indicate access to subsurface plumbing that sourced the putative flows (e.g., cryolava tubes or vents). The flanks of Wright Mons exhibit a distinctive pillow-like hummocky texture, which may be related to cryovolcanic flows (Singer et al., 2016) or perhaps convex surface-normal volatile accretion around nucleation points (Moore et al., 2021). Either of these processes could potentially produce subterranean features—flows by destruction (voids left behind after cryolavas drained) or accretion by construction (e.g., roofs formed between adjacent accreting mounds)—with potential subsurface access available within the complex interstices of the mounds.

Cryovolcanism appears to be widespread across Pluto, with potential cryovolcanic activity documented in the uplands north and east of Sputnik Planitia (Howard et al., 2017), and to the west in Virgil Fossae (Cruikshank et al., 2019) and Viking Terra (Cruikshank et al., 2021). Myriad upland features have prospective cryovolcanic origins with material emplaced through transport in the solid, liquid, or gas phase across a range of mechanisms from explosions to the slow emission of gasses (Howard et al., 2017). These inferred processes imply communication between the surface and subsurface and may signal locations with subsurface access. For example, swaths of pits east of Sputnik Planitia may be the result of collapses into subsurface voids (Howard et al., 2017) with potential subsurface access along their sides. Likewise, it appears that collapses following subsurface mass evacuation during cryovolcanic flows in Virgil Fossae led to the formation of pit craters, which may also represent SAPs (e.g., Cruikshank et al., 2019).

It is also interesting to consider the possibility of subsurface voids within the upper layers of more volatile (N_2 , CH_4 , and CO) ices. Pluto's sublimation-deposition cycle has led to the formation of hundreds of thousands of >100-m-scale closed contour depressions (i.e., sublimation pits; e.g., Buhler & Ingersoll, 2018; White et al., 2017). At the regional (tens to hundreds of kilometers) scale, the sublimation landscapes appear rough (White et al., 2017). However, observation shows most sublimation pits are smooth walled (Buhler & Ingersoll, 2018; Moore et al., 2017; White et al., 2017) in the highest resolution images (~ 80 m/px, mostly across Sputnik Planitia; Stern et al., 2015; Weaver et al., 2009). Most of the high relief terrain in the uplands north and east of Sputnik Planitia were imaged at several hundred meters per pixel or lower, but these landforms appear compatible with the formation of subsurface features via sublimation (Howard et al., 2017) and/or eolian (Moore et al., 2018; Moores et al., 2017) processes. Additionally, ice block calving at finer-than-observed scales may have produced talus caves along sublimation margins—analogueous to the calving of meter-scale blocks from CO_2 -ice sublimation processes documented on Mars (Buhler et al., 2017; Thomas et al., 2009).

There is substantial uncertainty about how long caves produced in N_2 and CH_4 ices may support themselves structurally or how large such structures could become. This is due to large (nine orders of magnitude) uncertainty in knowledge of the viscosity of N_2 and CH_4 ice under plutonian conditions (Eluszkiewicz & Stevenson, 1990; Moore et al., 2017; Yamashita et al., 2010). However, the viscosity of nitrogen ice in Sputnik Planitia is evidently high enough to support hundred-meter-scale pits for hundreds of thousands of (Earth) years (Buhler & Ingersoll, 2018).

Finally, the longevity of all potential plutonian subsurface voids should be considered. These features are shielded from the sun and therefore potential cold traps (e.g., Perşoiu & Onac, 2019; Tuttle & Stevenson, 1978). Over time, the deposition of volatile ices (e.g., N_2 and CH_4) may potentially seal some of these openings. However, without more detailed information about Pluto's speleogenic processes, it is not yet possible to rigorously assess how these features may be produced and/or the rate(s) and efficacy of entrance sealing.

Charon. In contrast to Pluto, the surface of Charon appears mostly quiescent, lacks an atmosphere, and is devoid of the richly varied volatile ice landscapes observed on Pluto (Beyer et al., 2017; Moore et al., 2016; Singer et al., 2019; Stern et al., 2017). The hemisphere of Charon documented by New Horizons can be divided into two general regions: the rugged, tectonically disrupted northern highlands and the smooth plain southern lowlands (Beyer et al., 2017, 2019; Robbins et al., 2019).

The northern highlands are rugged and comprise at least ten steep-sided plateaus that are hundreds of kilometers wide and separated by troughs tens of kilometers across (Robbins et al., 2019), while the southern lowlands are generally smooth and were likely emplaced by extensive cryovolcanic resurfacing early in Charon's history (Beyer et al., 2019; Robbins et al., 2019). Both the northern and southern terrains are incised by widespread tectonic features, including dozens of grabens and myriad grooves. These structures are likely the result of an ancient episode of extensional tectonic activity driven by the freezing (and thus volumetric expansion) of a subsurface ocean ~ 4 Ga (Beyer et al., 2017; Robbins et al., 2019). However, except for one catena (chain of pits), none of these features seem speleogenic in origin. The catena of potential interest is in the northern highlands ($30^\circ N$, $10^\circ E$) and consists of a series of linearly aligned, conjoined pits; the currently favored interpretation is that it formed due to an endogenous collapse either following the evacuation of a cryolava tube sourced from an unresolved cryovolcanic construct or a collapse over a tectonic fracture (Robbins et al., 2019).

Finally, 13 lobate debris aprons have been identified on Charon, mostly along the steep topographic boundary between the northern highlands and southern lowlands (Beddingfield et al., 2020; Robbins et al., 2019). These lobate debris aprons are interpreted as the result of mass wasting landslides, with four likely triggered by nearby impacts (Robbins et al., 2019). It is probable that talus caves formed within some of these landslides.

2.2.2.8. Comet 67P/Churyumov-Gerasimenko

Comets are considered one of the most primitive remnants of the primordial solar system. The physical properties, composition, and inner structure of their nuclei are thought to unravel the processes at play within the proto-planetary disk (Davidsson et al., 2016; Mandt et al., 2015; Weissman et al., 2020). Flyby missions including Giotto (Keller et al., 1988), Stardust (Brownlee, 2014), Deep Space 1 (Soderblom et al., 2002), Deep Impact (A'Hearn et al., 2005), and the more intensive Rosetta mission, which orbited 67P/Churyumov-Gerasimenko (hereafter 67P) have revealed the complex geomorphological features of cometary nuclei, including circular depressions or pits, extended fractures, and landslides (Birch et al., 2017; Massironi et al., 2015; Thomas

et al., 2015; Thomas, A'Hearn, Belton, et al., 2013; Thomas, A'Hearn, Veverka, et al., 2013). Although no SAPs have been identified within these terrains, thermal and gravitational effects exerted on comets shape their nuclei (Zhang & Michel, 2021) and give rise to three potential speleogenic processes. These include the formation of pits and sinkholes driven by sublimation (refer to Vincent, Bodewits, et al., 2015; Figure 8d), fracturing generated by thermal and mechanical stresses (El-Maarry et al., 2015), and the potential formation of talus caves associated with mass wasting deposits.

Sublimation is perhaps the most difficult process to study due to the lack of appropriate Earth analogs, and our inability to observe and document this behavior because of limited observational windows. We speculate that long-term sublimation continuously erodes the nucleus and replenishes the coma with particles and volatiles, whereas sudden explosive events (outburst) could, at least in principle, produce instant morphological changes to the body. Over the 2-year observational window of the Rosetta mission, only minor morphological changes were observed on 67P (El-Maarry et al., 2017; Pajola et al., 2017); this suggests most surface processes may have occurred prior to the Rosetta mission.

Sublimation-driven pits may represent the most common cave-like features on comets. To date, these features have been examined on 67P (Vincent, Bodewits, et al., 2015), and observed on comets 9P/Tempel 1 (Thomas, A'Hearn, Belton, et al., 2013) and 81P/Wild 2 (Brownlee et al., 2004). The circular cliffs bounding these depressions are often completely intact with some features surprisingly cylindrical. The lack of features typical of impact craters (i.e., ejecta blankets, a bowl-shaped morphology, and raised rims), and their specific size/frequency distribution, preclude an impact scenario (Belton et al., 2013; Ip et al., 2016; Vincent, Oklay, et al., 2015).

The origin of cometary pits seems to be intimately connected with the sublimation of ices, although the exact mechanism remains unclear (Ip et al., 2016). A violent release of dust and volatiles from an explosive outburst could produce localized mass wasting, leaving behind circular depressions with vertical walls (Belton et al., 2013). Alternatively, these depressions might be the result of the collapse of thin-roofed subsurface cavities, in a process similar to the formation of sinkholes on Earth and other rocky planets (Vincent, Bodewits, et al., 2015). Whatever the formation process, the sudden exposure of fresh ice along the cavity walls would produce a release of dust and volatiles, which have been observed within some of the 67P pits (Vincent, Bodewits, et al., 2015), and can cause walls to retreat and collapse resulting in circular-shaped terraces (Pajola et al., 2016).

Both pit formation mechanisms imply the presence of shallow subsurface cavities. Being that the inner structure of the comet is often homogeneous (Ciarletti et al., 2017; Pätzold et al., 2016), the primary subsurface cavities produced during the comet's formation must be excluded, and ice sublimation appears to be the only process that could create suitable subsurface voids (Vincent, Bodewits, et al., 2015).

Nevertheless, if cometary pits are formed by the violent release of volatiles, subsurface cavities might even not be needed since a porosity between 60% and 80% (Herique et al., 2019; Pätzold et al., 2016) would provide adequate pore space to accumulate over-pressurized volatiles that are then released in an explosive event. In this case, voids would be formed upon the outburst opening of the pit, and a network of subsurface cavities should be excluded, given that ejecta would fall back into the pit and other subsequent infilling may obscure possible lateral passages.

To date, at least 18 pits have been indentified on Comet 67P (refer to Vincent, Bodewits, et al., 2015). All were circular pits, wider than deep, range from 50 to 310 m in diameter, and 10–210 m deep (Vincent, Bodewits, et al., 2015). Pit size may be a measure of the intensity of the exhalation episode. However, considering that erosion by sublimation must have reworked these features after their opening to the surface, and possibly increasing their diameters, an average size for subsurface pockets could have been much smaller—on the order of several tens of meters. Of the 18 identified pits, two pits (Seth 1 and 3; refer to Vincent, Bodewits, et al., 2015) warrant further examination as they were largely intact and cylindrical in shape—albeit neither appears to provide access to the deeper subsurface. Overall, the speleogenic nature of all 18 sublimation pits remain speculative; further investigations will be required to more cogently constrain the formation process(es) of these features, as well as the potential sublimation pits observed on other cometary bodies.

On comet 67P, additional shallow rounded depressions were observed. These features bounded by steep scarps and with a raised wide central bulge were observed growing from a few to several hundred meters (the latter potentially represent the development of an explosive exhalation event) over about a 1-month observational period close to perihelium (Groussin et al., 2015). Whether these features represent the genesis of pit formation is unknown—as pit formation has not been directly observed.

Hence, the presence of subsurface cavities on comets, as well as their size, extent, and potential accessibility remains unresolved. Their existence has been hypothesized in relation to the observed circular pits, which are common on several resolved nuclei. However, their relation to subsurface cavities is still uncertain.

Fractures have also been observed on comets. These features may function to drive surficial heat deeper into the nucleus, which could contribute to fracture development (Höfner et al., 2017) or produce short-lived outbursts (Skorov et al., 2016). On comet 67P, fractures were more than 200 m in length (El-Maarry et al., 2015; Franceschi et al., 2020; Thomas et al., 2015)—however, estimating the depth of these features was not possible.

Additionally, thermal stress and ice sublimation can occur when the comet approaches the Sun and then progressively diminish when solar heating drops during the outward orbital trajectory. Diurnal temperature changes, exceeding more than 200 K during perihelium, are thought to be responsible for most of the fractures visible in 67P (Attree et al., 2018; Auger et al., 2017; El-Maarry et al., 2015) and may act as a major predisposing factor for gravitational instability phenomena (e.g., Pajola et al., 2017).

Interestingly, cometary gravity plays an important role in mass wasting events (Lucchetti et al., 2019; Pajola et al., 2017). For example, on 67P, the observed landslide deposits are surprisingly like those found on Earth and other rocky planets (Lucchetti et al., 2019). Although this behavior has not been directly observed, it is likely that the resultant aggregations of ice blocks may also form talus caves.

The existence of large subsurface cavities within cometary nuclei is highly relevant to a more cogent comprehension of planetary processes. Importantly, understanding speleogenic processes can refine our understanding related to the formation and evolution of comets, the wide range of processes observed on their surface, and the thermophysical properties of these small but incredibly complex objects. Moreover, examining the effects of sublimation processes on highly porous materials will require laboratory experiments and numerical modeling (Haghighipour et al., 2018; Hu et al., 2019; Kreuzig et al., 2021). Future cometary missions should acquire imagery within pits, fractures, and gravitational taluses, as well as data of the inner structure of the cometary body (Eyraud et al., 2020; Sava & Asphaug, 2018).

3. Conclusions: Caves Are Out There

Caves are expected to be ubiquitous across the solar system, occurring on most, if not all, rocky or icy bodies of sufficient size to have had speleogenic processes active during at least part of their evolution. To date, 3,545 SAPs are known to occur on 11 planetary bodies. Speleogenic processes (and thus the potential for SAPs) have occurred on Mercury and Vesta, are occurring on Venus and Io, and have been observed on at least three comets. Speleogenic processes cataloged across the solar system thus far include volcanic (cryo- and magmatic), fracturing (tectonic and impact melt), sublimation, suffusion, dissolution, and landslides.

As we have shown from other planetary bodies with confirmed SAPs, their detection will require the acquisition and subsequent analysis of high-resolution imagery. For the Moon, Mars, and to a lesser degree Titan, this has permitted both potential cave-bearing terrains and SAPs to be cataloged (e.g., Cushing, 2017; Malaska, Schoenfeld, et al., 2022; Wagner & Robinson, 2021). Subsequently, the number of SAPs across the solar system will continue to increase as more missions with high resolution instrumentation are flown.

For planetary bodies closer to home, namely the Moon and Mars, robotic exploration is achievable within the next one to two decades. However, for the more-distant ocean worlds, potentially confirming SAPs as caves and characterizing their entrances and/or subsurface extents will require rover and/or drone missions equipped with the appropriate suite of instrumentation. Over the next few decades, additional assets capable of identifying, characterizing, and ultimately exploring caves will be sent to planetary bodies across the solar system.

Conflict of Interest

The authors declare no conflicts of interest relevant to this study.

Data Availability Statement

All supporting information is available via the Harvard Dataverse online repository (<https://doi.org/10.7910/DVN/IOLNC4>).

Acknowledgments

We thank Kaj Williams, Tenielle Gaither, and two anonymous reviewers for providing erudite comments leading to the improvement of this paper. Contract #80NM0018D0004 between the Jet Propulsion Laboratory, California Institute of Technology and the National Aeronautics and Space Administration supported AGD, LK, EL, EJL, MJM, KLM, CBP, AL and RP were supported by the Italian Space Agency (ASI) under the ASI-INAF contract 2018-25-HH.0. PBB was supported by NASA Grant 80NSSC21K0212.

References

- Adams, K. A., & Jurdy, D. M. (2012). Pit distribution in the equatorial region of Titan. *Planetary and Space Science*, 65(1), 58–66. <https://doi.org/10.1016/j.pss.2012.01.007>
- Agha-Mohammadi, A., Otsu, K., Morrell, B., Fan, D. D., Thakker, R., Santamaria-Navarro, A., et al. (2021). NeBula: Quest for robotic autonomy in challenging environments; TEAM CoSTAR at the DARPA subterranean Challenge. *Journal of Field Robotics*.
- A'Hearn, M. F., Belton, M. J. S., Delamere, W. A., Kissel, J., Klaasen, K. P., McFadden, L. A., et al. (2005). Deep impact: Excavating comet Tempel 1. *Science*, 310(5746), 258–264. <https://doi.org/10.1126/science.1118923>
- Anderson, J. D., Schubert, G., Jacobson, R. A., Lau, E. L., Moore, W. B., & Sjogren, W. L. (1998). Europa's differentiated internal structure: Inferences from four Galileo encounters. *Science*, 281(5385), 2019–2022. <https://doi.org/10.1126/science.281.5385.2019>
- Andrews-Hanna, J. C., & Lewis, K. W. (2011). Early Mars hydrology: 2. Hydrological evolution in the Noachian and Hesperian epochs. *Journal of Geophysical Research*, 116(E2), E02007. <https://doi.org/10.1029/2010je003709>
- Ashley, J. W., Robinson, M. S., Hawke, B. R., van der Bogert, C. H., Hiesinger, H., Sato, H., et al. (2012). Geology of the King crater region: New insights into impact melt dynamics on the Moon. *Journal of Geophysical Research*, 117(E12), E00H29. <https://doi.org/10.1029/2011je003990>
- Attree, N., Groussin, O., Jorda, L., Rodionov, S., Auger, A.-T., Thomas, N., et al. (2018). Thermal fracturing on comets: Applications to 67P/Churyumov-Gerasimenko. *Astronomy & Astrophysics*, 610, A76. <https://doi.org/10.1051/0004-6361/201731937>
- Auger, A.-T., Groussin, O., Jorda, L., El-Maarry, M. R., Bouley, S., Séjourné, A., et al. (2017). Meter-scale thermal contraction crack polygons on the nucleus of comet 67P/Churyumov-Gerasimenko. *Icarus*, 301, 173–188. <https://doi.org/10.1016/j.icarus.2017.09.037>
- Baioni, D. (2018). Karst landforms as markers of recent climate change on Mars: An example from a Late Amazonian Epoch evaporate-karst within a trough in western Noctis Labyrinthus. In R. Soare, S. Conway, & S. M. Clifford (Eds.), *Dynamic Mars: Recent and current landscape evolution of the Red Planet* (pp. 411–429). Elsevier.
- Baioni, D., Murana, A., & Hajna, N. Z. (2014). Karstic morphology in northern Sinus Meridiani, Mars. *Geosciences Journal*, 18(3), 261–268. <https://doi.org/10.1007/s12303-014-0003-0>
- Baioni, D., & Sgavetti, M. (2013). Karst terrains as possible lithologic and stratigraphic markers in northern Sinus Meridiani, Mars. *Planetary and Space Science*, 75, 173–181. <https://doi.org/10.1016/j.pss.2012.08.011>
- Baioni, D., Zupan-Hajna, N., & Wezel, F. C. (2009). Karst landforms in a Martian evaporitic dome. *Acta Carsologica*, 38(1), 9–18. <https://doi.org/10.3986/ac.v38i1.132>
- Barnes, J. W., Bow, J., Schwartz, J., Brown, R. H., Soderblom, J. M., Hayes, A. G., et al. (2011). Organic sedimentary deposits in Titan's dry lakebeds: Probable evaporite. *Icarus*, 216(1), 136–140. <https://doi.org/10.1016/j.icarus.2011.08.022>
- Barnes, J. W., Turtle, E. P., Trainer, M. G., Lorenz, R. D., MacKenzie, S. M., Brinckerhoff, W. B., et al. (2021). Science goals and objectives for the Dragonfly Titan rotorcraft relocatable lander. *The Planetary Science Journal*, 2(4), 130. <https://doi.org/10.3847/PSJ/abfdcf>
- Barnes, S. J. (1985). The petrography and geochemistry of komatiite flows from the Abitibi Greenstone Belt and a model for their formation. *Lithos*, 18, 241–270. [https://doi.org/10.1016/0024-4937\(85\)90030-1](https://doi.org/10.1016/0024-4937(85)90030-1)
- Basilevsky, A. T., Kuzmin, R. O., Nikolaeva, O. V., Pronin, A. A., Ronca, L. B., Avdukevsky, V. S., et al. (1985). The surface of Venus as revealed by the Venera landings: Part II. *Geological Society of America Bulletin*, 96(1), 137–144. [https://doi.org/10.1130/0016-7606\(1985\)96<137:tsov ar>2.0.co;2](https://doi.org/10.1130/0016-7606(1985)96<137:tsov ar>2.0.co;2)
- Beddingfield, C. B., Beyer, R. A., Singer, K., Nimmo, F., McKinnon, W. B., Moore, J. M., et al. (2018). Landslides in the Serenity Chasma region, Charon. In *Lunar and Planetary Science Conference*. Abstract #2378.
- Beddingfield, C. B., Beyer, R. A., Singer, K. N., McKinnon, W. B., Runyon, K., Grundy, W., et al. (2020). Landslides on Charon. *Icarus*, 335, 113383. <https://doi.org/10.1016/j.icarus.2019.07.017>
- Běhouňková, M., Tobie, G., Čadek, O., Choblet, G., Porco, C., & Nimmo, F. (2015). Timing of water plume eruptions on Enceladus explained by interior viscosity structure. *Nature Geoscience*, 8, 601–604. <https://doi.org/10.1038/ngeo2475>
- Belton, M. J. S., Thomas, P., Carcich, B., Quick, A., Veverka, J., Melosh, H. J., et al. (2013). The origin of pits on 9P/Tempel 1 and the geologic signature of outbursts in Stardust-NExT images. *Icarus*, 222(2), 477–486. <https://doi.org/10.1016/j.icarus.2012.03.007>
- Bertrand, T., Forget, F., White, O., Schmitt, B., Stern, S. A., Weaver, H. A., et al. (2020). Pluto's beating heart regulates the atmospheric circulation: Results from high-resolution and multiyear numerical climate simulations. *Journal of Geophysical Research: Planets*, 125(2), e2019JE006120. <https://doi.org/10.1029/2019JE006120>
- Bertrand, T., Lellouch, E., Holler, B. J., Young, L. A., Schmitt, B., Oliveira, J. M., et al. (2022). Volatile transport modeling on Triton with new observational constraints. *Icarus*, 373, 114764. <https://doi.org/10.1016/j.icarus.2021.114764>
- Beyer, R. A., Nimmo, F., McKinnon, W. B., Moore, J. M., Binzel, R. P., Conrad, J. W., et al. (2017). Charon tectonics. *Icarus*, 287, 161–174. <https://doi.org/10.1016/j.icarus.2016.12.018>
- Beyer, R. A., Spencer, J. R., McKinnon, W. B., Nimmo, F., Beddingfield, C., Grundy, W. M., et al. (2019). The nature and origin of Charon's smooth plains. *Icarus*, 323, 16–32. <https://doi.org/10.1016/j.icarus.2018.12.036>
- Bierson, C. J., Tulaczyk, S., Courville, S. W., & Putzig, N. E. (2021). Strong MARSIS radar reflections from the base of Martian south polar cap may be due to conductive ice or minerals. *Geophysical Research Letters*, 48(13), e2021GL093880. <https://doi.org/10.1029/2021GL093880>
- Birch, S. P. D., Hayes, A. G., Poggiali, V., Hofgartner, J. D., Lunine, J. I., Malaska, M. J., et al. (2019). Raised rims around Titan's sharp-edged depressions. *Geophysical Research Letters*, 46(11), 5846–5854. <https://doi.org/10.1029/2018gl078099>
- Birch, S. P. D., Tang, Y., Hayes, A. G., Kirk, R. L., Bodewits, D., Campins, H., et al. (2017). Geomorphology of comet 67P/Churyumov-Gerasimenko. *Monthly Notices of the Royal Astronomical Society*, 469(Suppl 2), S50–S67. <https://doi.org/10.1093/mnras/stx1096>
- Birch, S. P. D., Umurhan, O. M., Hayes, A. G., & Malaska, M. J. (2020). Simulating the evolution of Titan's surface through fluvial and dissolution erosion. II. The details. In *Lunar and Planetary Science Conference*. Abstract #1979.
- Bleacher, J. E., Orr, T. R., Andrew, P., Zimbleman, J. R., Hamilton, C. W., Garry, W. B., et al. (2017). Plateaus and sinuous ridges as the fingerprints of lava flow inflation in the Eastern Tharsis Plains of Mars. *Journal of Volcanology and Geothermal Research*, 342, 29–46. <https://doi.org/10.1016/j.jvolgeores.2017.03.025>
- Blewett, D. T., Chabot, N. L., Denevi, B. W., Ernst, C. M., Head, J. W., Izenberg, N. R., et al. (2011). Hollows on Mercury: MESSENGER evidence for geologically recent volatile-related activity. *Science*, 333(6051), 1856–1859. <https://doi.org/10.1126/science.1211681>

- Boston, P. J. (2004). Extraterrestrial caves. In J. Gunn (Ed.), *Encyclopedia of Caves and Karst Science* (pp. 355–358). Fitzroy Dearborn.
- Boston, P. J., Hose, L. D., Northup, D. E., & Spilde, M. N. (2006). The microbial communities in sulfur caves: A newly appreciated geologically driven system on Earth and potential model for Mars. In R. S. Harmon & C. M. Wicks (Eds.), *Perspectives in Karst Geomorphology, Hydrology, and Geochemistry* (pp. 331–344). GSA Special Paper, 404.
- Bridges, J. C., Hicks, L. J., & Treiman, A. H. (2019). Carbonates on Mars. In J. Filiberto & S. P. Schwenzer (Eds.), *Volatiles in the Martian crust* (pp. 89–118). Elsevier.
- Brownlee, D. (2014). The Stardust mission: Analyzing samples from the edge of the solar system. *Annual Review of Earth and Planetary Sciences*, 42(1), 179–205. <https://doi.org/10.1146/annurev-earth-050212-124203>
- Brownlee, D. E., Horz, F., Newburn, R. L., Zolensky, M., Duxbury, T. C., Sandford, S., et al. (2004). Surface of young Jupiter family comet 81P/Wild 2: View from the Stardust spacecraft. *Science*, 304(5678), 1764–1769. <https://doi.org/10.1126/science.1097899>
- Buczowski, D. L., Scully, J. E. C., Quick, L., Castillo-Rogez, J., Schenk, P. M., Park, R. S., et al. (2019). Tectonic analysis of fracturing associated with Occator crater. *Icarus*, 320, 49–59. <https://doi.org/10.1016/j.icarus.2018.05.012>
- Buczowski, D. L., Wyrick, D. Y., Iyer, K. A., Kahn, E. G., Scully, J. E. C., Nathues, A., et al. (2012). Large-scale troughs on Vesta: A signature of planetary tectonics. *Geophysical Research Letters*, 39(18), L18205. <https://doi.org/10.1029/2012GL052959>
- Buczowski, D. L., Wyrick, D. Y., Toplis, M., Yingst, R. A., Williams, D. A., Garry, W. B., et al. (2014). The unique geomorphology and physical properties of the Vestalia Terra plateau. *Icarus*, 244, 89–103. <https://doi.org/10.1016/j.icarus.2014.03.035>
- Buhler, P. B., & Ingersoll, A. P. (2018). Sublimation pit distribution indicates convection cell surface velocities of ~10 cm per year in Sputnik Planitia, Pluto. *Icarus*, 300, 327–340. <https://doi.org/10.1016/j.icarus.2017.09.018>
- Buhler, P. B., Ingersoll, A. P., Ehlmann, B. L., Fassett, C. I., & Head, J. W. (2017). How the Martian residual south polar cap develops quasi-circular and heart-shaped pits, troughs, and moats. *Icarus*, 286, 69–93. <https://doi.org/10.1016/j.icarus.2017.01.012>
- Byrne, P. K., Klimczak, C., Williams, D. A., Hurwitz, D. M., Solomon, S. C., Head, J. W., et al. (2013). An assemblage of lava flow features on Mercury. *Journal of Geophysical Research: Planets*, 118(6), 1303–1322. <https://doi.org/10.1002/jgre.20052>
- Byrne, P. K., Ostrach, L. R., Fassett, C. I., Chapman, C. R., Denevi, B. W., Evans, A. J., et al. (2016). Widespread effusive volcanism on Mercury likely ended by about 3.5 Ga. *Geophysical Research Letters*, 43(14), 7408–7416. <https://doi.org/10.1002/2016gl069412>
- Byrne, P. K., Whitten, J. L., Klimczak, C., McCubbin, F. M., & Ostrach, L. R. (2018). The volcanic character of Mercury. In S. C. Solomon (Ed.), *Mercury: The view after MESSENGER* (pp. 287–323). Cambridge University Press.
- Cantrall, C., de Kleer, K., de Pater, I., Williams, D. A., Davies, A. G., & Nelson, D. (2018). Variability and geologic associations of volcanic activity on Io in 2001–2016. *Icarus*, 312, 267–294. <https://doi.org/10.1016/j.icarus.2018.04.007>
- Carr, M. H., Belton, M. J. S., Bender, K., Breneman, H., Greeley, R., Head, J. W., et al. (1995). The Galileo imaging team plan for observing the satellites of Jupiter. *Journal of Geophysical Research*, 100(E9), 18935–18955. <https://doi.org/10.1029/95je00971>
- Carr, M. H., Greeley, R., Blasius, K. R., Guest, J. E., & Murray, J. B. (1977). Some Martian volcanic features as viewed from the Viking orbiters. *Journal of Geophysical Research*, 82(28), 3985–4015. <https://doi.org/10.1029/jf082i028p03985>
- Castillo-Rogez, J. C., Neveu, M., Scully, J. E. C., House, C. H., Quick, L. C., Bouquet, A., et al. (2020). Ceres: Astrobiological target and possible ocean world. *Astrobiology*, 20(2), 269–291. <https://doi.org/10.1089/ast.2018.1999>
- Chabot, N. L., Ernst, C. M., Paige, D. A., Nair, H., Denevi, B. W., Blewett, D. T., et al. (2016). Imaging Mercury's polar deposits during MESSENGER's low-altitude campaign. *Geophysical Research Letters*, 43(18), 9461–9468. <https://doi.org/10.1002/2016gl070403>
- Chabot, N. L., Murchie, S. L., Hawkins, S. E., Hayes, J. R., Boldt, J. D., Barnouin, O. S., et al. (2012). Compact imagers based on MESSENGER's Mercury Dual Imaging System. In *International Workshop on Instrumentation for Planetary Missions*. Abstract # 1062, LPI Contribution No. 1683.
- Chappaz, L., Sood, R., Melosh, H. J., Howell, K. C., Blair, D. M., Milbury, C., & Zuber, M. T. (2017). Evidence of large empty lava tubes on the Moon using GRAIL gravity. *Geophysical Research Letters*, 44(1), 105–112. <https://doi.org/10.1002/2016gl071588>
- Ciarletti, V., Herique, A., Lasue, J., Levasseur-Regourd, A.-C., Plettemeier, D., Lemmonier, F., et al. (2017). CONSERT constrains the internal structure of 67P at a few metres size scale. *Monthly Notices of the Royal Astronomical Society*, 469(Suppl 2), S805–S817. <https://doi.org/10.1093/mnras/stx3132>
- Combe, J.-P., Raponi, A., Tosi, F., De Sanctis, M. C., Carrozzo, F. G., Zambon, F., et al. (2019). Exposed H₂O-rich areas detected on Ceres with the dawn visible and infrared mapping spectrometer. *Icarus*, 318, 22–41. <https://doi.org/10.1016/j.icarus.2017.12.008>
- Coombs, C. R., & Hawke, B. R. (1992). A search for intact lava tubes on the Moon: Possible lunar base habitats. In *Paper presented at 2nd Conference on Lunar Bases and Space Activities of the 21st Century* (pp. 219–229). NASA CP-3166.
- Cooper, M. P., & Mylroie, J. E. (2015). *Glaciation and speleogenesis: Interpretations from the northeastern United States*. Springer.
- Corlies, P., Hayes, A. G., Birch, S. P. D., Lorenze, R., Stiles, B. W., Kirk, R., et al. (2017). Titan's topography and shape at the end of the Cassini mission. *Geophysical Research Letters*, 44(23), 11754–11761. <https://doi.org/10.1002/2017gl075518>
- Cornet, T., Cordier, D., Le Bahers, T., Bourgeois, O., Fleurant, C., Le Mouélic, S., & Altobelli, N. (2015). Dissolution on Titan and on Earth: Towards the age of Titan's karstic landscapes. *Journal of Geophysical Research: Planets*, 120(6), 1044–1074. <https://doi.org/10.1002/2014je004738>
- Cornet, T., Fleurant, C., Seignovert, B., Cordier, D., Bourgeois, O., Le Mouélic, S., et al. (2017). Landscape formation through dissolution on Titan: A 3D landscape evolution model. In *Lunar and Planetary Science Conference*. Abstract #1835.
- Costello, E. S., Phillips, C. B., Lucey, P. G., & Ghent, R. R. (2021). Impact gardening on Europa and repercussions for possible biosignatures. *Nature Astronomy*, 5(9), 951–956. <https://doi.org/10.1038/s41550-021-01393-1>
- Craft, K. L., Patterson, G. W., Lowell, R. P., & Germanovich, L. (2016). Fracturing and flow: Investigations on the formation of shallow water sills on Europa. *Icarus*, 274, 297–313. <https://doi.org/10.1016/j.icarus.2016.01.023>
- Crawford, G. D., & Stevenson, D. J. (1988). Gas-driven water volcanism and the resurfacing of Europa. *Icarus*, 73(1), 66–79. [https://doi.org/10.1016/0019-1035\(88\)90085-1](https://doi.org/10.1016/0019-1035(88)90085-1)
- Cremonese, G., Fantinel, D., Giro, E., Capria, M. T., da Deppo, V., Naletto, G., et al. (2009). The stereo camera on the BepiColombo ESA/JAXA mission: A novel approach. *Advances in Geosciences: Planetary Science*, 15, 305–322.
- Croft, S. K., Kargel, J. S., Kirk, R. L., Moore, J. M., Schenk, P. M., & Strom, R. G. (1995). The geology of Triton. In D. P. Cruikshank (Ed.), *Neptune and Triton* (pp. 879–947). University of Arizona Press.
- Crown, D. A., Sizemore, H. G., Yingst, R. A., Mest, S. C., Platz, T., Berman, D. C., et al. (2018). Geologic mapping of the Urvara and Yalode Quadrangles of Ceres. *Icarus*, 316, 167–190. <https://doi.org/10.1016/j.icarus.2017.08.004>
- Crow-Willard, E. N., & Pappalardo, R. T. (2015). Structural mapping of Enceladus and implications for formation of tectonized regions. *Journal of Geophysical Research: Planets*, 120(5), 928–950. <https://doi.org/10.1002/2015JE004818>
- Cruikshank, D. P., Dalle Ore, C. M., Scipioni, F., Beyer, R. A., White, O. L., Moore, J. M., et al. (2021). Cryovolcanic flooding in Viking Terra on Pluto. *Icarus*, 356, 113786. <https://doi.org/10.1016/j.icarus.2020.113786>

- Cruikshank, D. P., Umurhan, O. M., Beyer, R. A., Schmitt, B., Keane, J. T., Runyon, K. D., et al. (2019). Recent cryovolcanism in Virgil Fossae on Pluto. *Icarus*, 330, 155–168. <https://doi.org/10.1016/j.icarus.2019.04.023>
- Curl, R. L. (1964). On the definition of a cave. *Bulletin of National Speleological Society*, 26, 1–6.
- Cushing, G. E. (2012). Candidate cave entrances on Mars. *Journal of Cave and Karst Studies*, 74(1), 33–47. <https://doi.org/10.4311/2010ex0167r>
- Cushing, G. E. (2017). *Mars global cave candidate catalog archive bundle*. U.S. Geological Survey. Retrieved from https://astrogeology.usgs.gov/search/map/Mars/MarsCaveCatalog/mars_cave_catalog.zip
- Cushing, G. E., Okubo, C. H., & Titus, T. N. (2015). Atypical pit craters on Mars: New insights from THEMIS, CTX, and HiRISE observations. *Journal of Geophysical Research: Planets*, 120(6), 1023–1043. <https://doi.org/10.1002/2014je004735>
- Cushing, G. E., Titus, T. N., Wynne, J. J., & Christensen, P. (2007). THEMIS observes possible cave skylights on Mars. *Geophysical Research Letters*, 34(17), L17201. <https://doi.org/10.1029/2007gl030709>
- Daga, A., Schneider Puente, I., Uzman, Z., de Leon, P., & Harris, G. (2010). Habitat architecture concept definition for “integrated strategies for the human exploration of the Moon and Mars” (a NASA-funded study): Interim status report. In *Paper presented at 40th International Conference on Environmental Systems AIAA* (pp. 2010–6072).
- Davidsson, B. J. R., Sierks, H., Güttler, C., Marzari, F., Pajola, M., Rickman, H., et al. (2016). The primordial nucleus of comet 67P/Churyumov-Gerasimenko. *Astronomy & Astrophysics*, 592, A63. <https://doi.org/10.1051/0004-6361/201526968>
- Davies, A. G. (1996). Io’s volcanism: Thermo-physical models of silicate lava compared with observations of thermal emission. *Icarus*, 124(1), 45–61. <https://doi.org/10.1006/icar.1996.0189>
- Davies, A. G. (2003). Volcanism on Io: Estimation of eruption parameters from Galileo NIMS data. *Journal of Geophysical Research*, 108(E9), 5106–5120. <https://doi.org/10.1029/2001je001509>
- Davies, A. G. (2007). *Volcanism on Io: A comparison with Earth*. Cambridge University Press.
- Davies, A. G., Keszthelyi, L., & McEwen, A. S. (2016). Determination of eruption temperature of Io’s lavas using lava tube skylights. *Icarus*, 278, 266–278. <https://doi.org/10.1016/j.icarus.2016.06.003>
- Davies, A. G., Lopes-Gautier, R., Smyth, W. D., & Carlson, R. W. (2000). Silicate cooling model fits to Galileo NIMS data of volcanism on Io. *Icarus*, 148(1), 212–225. <https://doi.org/10.1006/icar.2000.6486>
- Davies, A. G., Veeder, G. J., Hill, S. L., Matson, D. L., & Johnson, T. V. (2014). Charting thermal emission variability at Amirani with the Galileo NIMS Io Thermal Emission Database (NITED). *Icarus*, 241, 190–199. <https://doi.org/10.1016/j.icarus.2014.06.034>
- Davies, A. G., Wilson, L., Matson, D., Leone, G., Keszthelyi, L., & Jaeger, W. (2006). The heartbeat of the volcano: The discovery of episodic activity at Prometheus on Io. *Icarus*, 184(2), 460–477. <https://doi.org/10.1016/j.icarus.2006.05.012>
- de Kleer, K., de Pater, I., Molter, E. M., Banks, E., Davies, A. G., Alvarez, C., et al. (2019). Io’s volcanic activity from time-domain adaptive optics observations: 2013–2018. *Astronomical Journal*, 158, 1–29.
- Denevi, B. W., Ernst, C. M., Meyer, H. M., Robinson, M. S., Murchie, S. L., Whitten, J. L., et al. (2013). The distribution and origin of smooth plains on Mercury. *Journal of Geophysical Research: Planets*, 118(5), 891–907. <https://doi.org/10.1002/jgre.20075>
- de Pater, I., Davies, A. G., & Marchis, F. (2016). Keck observations of eruptions on Io in 2003–2005. *Icarus*, 274, 284–296. <https://doi.org/10.1016/j.icarus.2015.12.054>
- Deutsch, A. N., Head, J. W., Chabot, N. L., & Neumann, G. A. (2018). Constraining the thickness of polar ice deposits on Mercury using the Mercury Laser Altimeter and small craters in permanently shadowed regions. *Icarus*, 305, 139–148. <https://doi.org/10.1016/j.icarus.2018.01.013>
- Elachi, C., Allison, M. D., Borgarelli, L., Encrenaz, P., Im, E., Janssen, M. A., et al. (2004). Radar: The Cassini Titan radar mapper. In C. T. Russell (Ed.), *The Cassini-Huygens Mission: Orbital Remote Sensing Investigations* (pp. 71–110). Springer.
- El-Maarry, M. R., Groussin, O., Thomas, N., Pajola, M., Auger, A.-T., Davidsson, B., et al. (2017). Surface changes on comet 67P/Churyumov-Gerasimenko suggest a more active past. *Science*, 6332, 1392–1395. <https://doi.org/10.1126/science.aak9384>
- El-Maarry, M. R., Thomas, N., Gracia-Berná, A., Marschall, R., Auger, A.-T., Groussin, O., et al. (2015). Fractures on comet 67P/Churyumov-Gerasimenko observed by Rosetta/OSIRIS. *Geophysical Research Letters*, 42(13), 5170–5178. <https://doi.org/10.1002/2015GL064500>
- Eluzkiewicz, J., & Stevenson, D. J. (1990). Rheology of solid methane and nitrogen: Applications to Triton. *Geophysical Research Letters*, 17(10), 1753–1756. <https://doi.org/10.1029/g1017i010p01753>
- Environmental Protection Agency [EPA]. (2002). *A lexicon of cave and karst terminology with special reference to environmental karst hydrology* EPA/600/R-02/003. U.S. Environmental Protection Agency. Retrieved from <https://hinko.org/hinko/Downloads/11/2/XI-2-09.pdf>
- Ermakov, A. I., Fu, R. R., Castillo-Rogez, J. C., Raymond, C. A., Park, R. S., Preusker, F., et al. (2017). Constraints on Ceres’ internal structure and evolution from its shape and gravity measured by the Dawn spacecraft. *Journal of Geophysical Research: Planets*, 122(11), 2267–2293. <https://doi.org/10.1002/2017JE005302>
- Estes, N. M., Robinson, M. S., & the LROC team. (2019). LROC: Ten years exploring the Moon. In *Planetary Data Workshop*. Abstract #7082, LPI Contribution No. 2151. Retrieved from <https://www.hou.usra.edu/meetings/planetdata2019/pdf/7082.pdf>
- Eyraud, C., Sorsa, L.-I., Herique, A., Geffrin, J.-M., Pursiainen, S., & Kofman, W. (2020). Towards asteroid tomography: Modellings and measurements using an analogue model. In *Paper Presented at 14th European Conference on Antennas and Propagation (EuCAP)* (pp. 1–4). IEEE. <https://doi.org/10.23919/EuCAP48036.2020.9136060>
- Fagents, S. A. (2003). Considerations for effusive cryovolcanism on Europa: The post-Galileo perspective. *Journal of Geophysical Research*, 108(E12), 5139. <https://doi.org/10.1029/2003je002128>
- Fayolle, M., Quirico, E., Schmitt, B., Jovanovic, L., Gautier, T., Carrasco, N., et al. (2021). Testing tholins as analogues of the dark reddish material covering Pluto’s Cthulhu region. *Icarus*, 367, 114574. <https://doi.org/10.1016/j.icarus.2021.114574>
- Ferrill, D. A., Wyrick, D. Y., & Smart, K. J. (2011). Coseismic, dilational-fault and extension-fracture related pit chain formation in Iceland: Analog for pit chains on Mars. *Lithosphere*, 3(2), 133–142. <https://doi.org/10.1130/L123.1>
- Fielder, G. (1965). *Lunar geology*. Lutterworth Press.
- Fleurant, C., Tucker, G. E., & Viles, H. A. (2008). A model of cockpit karst landscape, Jamaica. *Géomorphologie: Relief, Processus, Environnement*, 14(1), 3–14. <https://doi.org/10.4000/geomorphologie.5653>
- Ford, D. C., & Williams, P. (2007). *Karst hydrology and geomorphology*. Wiley.
- Franceschi, M., Penasa, L., Massironi, M., Naletto, G., Ferrari, S., Fondriest, M., et al. (2020). Global-scale brittle plastic rheology at the comets merging of comet 67P/Churyumov-Gerasimenko. *Proceedings of the National Academy of Sciences*, 117(19), 10181–10817. <https://doi.org/10.1073/pnas.1914552117>
- Freeman, A., Smrekar, S. E., Hensley, S., Wallace, M., Sotin, C., Darrach, M., et al. (2016). VERITAS: A discovery-class Venus surface geology and geophysics mission (pp. 1–11). IEEE.
- Frumkin, A., & Naor, R. (2019). Formation and modification of pit craters—example from the Golan volcanic plateau, southern Levant. *Zeitschrift für Geomorphologie*, 62(3), 163–181. <https://doi.org/10.1127/zfg/2019/0614>

- Ghail, R. C., Hall, D., Mason, P. J., Herrick, R. R., Carter, L. M., & Williams, E. (2018). VenSAR on EnVision: Taking Earth observation radar to Venus. *International Journal of Applied Earth Observation and Geoinformation*, *64*, 365–376. <https://doi.org/10.1016/j.jag.2017.02.008>
- Gillis-Davis, J. J., Blewett, D. T., Gaskell, R. W., Denevi, B. W., Robinson, M. S., Strom, R. G., et al. (2009). Pit-floor craters on Mercury: Evidence of near-surface igneous activity. *Earth and Planetary Science Letters*, *285*(3–4), 243–250. <https://doi.org/10.1016/j.epsl.2009.05.023>
- Gioia, G., Chakraborty, P., Marshak, S., & Kieffer, S. W. (2007). Unified model of tectonics and heat transport in a frigid Enceladus. *Proceedings of the National Academy of Sciences*, *104*(34), 13578–13581. <https://doi.org/10.1073/pnas.0706018104>
- Gràcia, E., Bideau, D., Hekinian, R., Lagabrielle, Y., & Parson, L. M. (1997). Along-axis magmatic oscillations and exposure of ultramafic rocks in a second-order segment of the Mid-Atlantic Ridge (33° 43'N to 34° 07'N). *Geology*, *25*(12), 1059–1062. [https://doi.org/10.1130/0091-7613\(1997\)025<1059:aamoae>2.3.co;2](https://doi.org/10.1130/0091-7613(1997)025<1059:aamoae>2.3.co;2)
- Grasset, O., Dougherty, M. K., Coustenis, A., Bunce, E. J., Erd, C., Titov, D., et al. (2013). JUPITER ICy moons Explorer (JUICE): An ESA mission to orbit Ganymede and to characterise the Jupiter system. *Planetary and Space Science*, *78*, 1–21. <https://doi.org/10.1016/j.pss.2012.12.002>
- Greeley, R. (1971). Lava tubes and channels in the lunar Marius Hills. *The Moon*, *3*, 289–314. <https://doi.org/10.1007/bf00561842>
- Greeley, R., Figueredo, P. H., Williams, D. A., Chuang, F. C., Klemaszewski, J. E., Kadel, S. D., et al. (2000). Geologic mapping of Europa. *Journal of Geophysical Research*, *105*(E9), 22559–22578. <https://doi.org/10.1029/1999je001173>
- Greeley, R., & Spudis, P. D. (1981). Volcanism on Mars. *Reviews of Geophysics*, *19*(1), 13–41. <https://doi.org/10.1029/rg019i001p00013>
- Green, W. E., & Oh, P. Y. (2005). A MAV that flies like an airplane and hovers like a helicopter. In *IEEE/ASME International Conference on Advanced Intelligent Mechatronics* (Vol. TBI-02, pp. 693–698).
- Groussin, O., Sierks, H., Barbieri, C., Lamy, P., Rodrigo, R., Koschny, D., et al. (2015). Temporal morphological changes in the Imhotep region of comet 67P/Churyumov-Gerasimenko. *Astronomy & Astrophysics*, *583*, A36. <https://doi.org/10.1051/0004-6361/201527020>
- Grundy, W. M., Young, L. A., Stansberry, J. A., Buie, M. W., Olkin, C. B., & Young, E. F. (2010). Near-infrared spectral monitoring of Triton with IRTF/Spex II: Spatial distribution and evolution of ices. *Icarus*, *205*(2), 594–604. <https://doi.org/10.1016/j.icarus.2009.08.005>
- Gupta, S., Ochiai, E., & Ponnampuruma, C. (1981). Organic-synthesis in the atmosphere of Titan. *Nature*, *293*(5835), 725–727. <https://doi.org/10.1038/293725a0>
- Haghighipour, N., Maindl, T. I., Schäfer, C. M., & Wandel, O. J. (2018). Triggering the activation of main-belt comets: The effect of porosity. *The Astrophysical Journal*, *855*(1), 60. <https://doi.org/10.3847/1538-4357/aaa7f3>
- Halliday, W. R. (1966). Terrestrial pseudokarst and the lunar topography. *National Speleological Society Bulletin*, *28*, 167–170.
- Halliday, W. R. (2004). Pseudokarst. In J. Gunn (Ed.), *Encyclopedia of Caves and Karst Science* (pp. 604–608). Fitzroy Dearborn.
- Hanel, R., Conrath, B., Flasar, M., Kunde, V., Lowman, P., Maguire, W., et al. (1979). Infrared observations of the Jovian system from Voyager 1. *Science*, *204*(4396), 972–976. <https://doi.org/10.1126/science.204.4396.972>
- Hansen, C. J., McEwen, A. S., Ingersoll, A. P., & Terrile, R. J. (1990). Surface and airborne evidence for plumes and fans on Triton. *Science*, *250*(4979), 421–424. <https://doi.org/10.1126/science.250.4979.421>
- Hansen, C. J., & Paige, D. A. (1996). Seasonal nitrogen cycles on Pluto. *Icarus*, *120*(2), 247–265. <https://doi.org/10.1006/icar.1996.0049>
- Harmon, J. K., & Slade, M. A. (1992). Radar mapping of Mercury: Full-disk images and polar anomalies. *Science*, *258*(5082), 640–643. <https://doi.org/10.1126/science.258.5082.640>
- Harris, A. J. L., & Rowland, S. K. (2009). Effusion rate controls on lava flow length and the role of heat loss: A review. *Studies in Volcanology: The Legacy of George Walker: Special Publications of IAVCEI* (Vol. 2, pp. 33–51).
- Haruyama, J., Hioki, K., Shirao, M., Morota, T., Hiesinger, H., van der Bogert, C. H., et al. (2009). Possible lunar lava tube skylight observed by SELENE cameras. *Geophysical Research Letters*, *36*(21), L21206. <https://doi.org/10.1029/2009gl040635>
- Hawkins, S. E., Boldt, J. D., Darlington, E. H., Espiritu, R., Gold, R. E., Gotwols, B., et al. (2007). The Mercury dual imaging system on the MESSENGER spacecraft. *Space Science Reviews*, *131*(1–4), 247–338. <https://doi.org/10.1007/s11214-007-9266-3>
- Hayes, A. G. (2016). The lakes and seas of Titan. *Annual Reviews of Earth and Planetary Science*, *44*(1), 57–83. <https://doi.org/10.1146/annurev-earth-060115-012247>
- Hayes, A. G., Aharonson, O., Callahan, P., Elachi, C., Gim, Y., Kirk, R., et al. (2008). Hydrocarbon lakes on Titan: Distribution and interaction with a porous regolith. *Geophysical Research Letters*, *35*(9), L09204. <https://doi.org/10.1029/2008gl033409>
- Hayes, A. G., Birch, S. P. D., Dietrich, W. E., Howard, A. D., Kirk, R. L., Poggiali, V., et al. (2017). Topographic constraints on the evolution and connectivity of Titan's lacustrine basins. *Geophysical Research Letters*, *44*(23), 11745–11753. <https://doi.org/10.1002/2017gl075468>
- Hayne, P. O., & Aharonson, O. (2015). Thermal stability of ice on Ceres with rough topography. *Journal of Geophysical Research: Planets*, *120*(9), 1567–1584. <https://doi.org/10.1002/2015je004887>
- Heacock, R. L., Kuiper, G. P., Shoemaker, E. M., Urey, H. C., & Whitaker, E. A. (1966). *Ranger VII and IX: Part II. Experimenters' analyses and interpretations*. JPL Technical Report 32-700 (p. 382). California Institute of Technology, Jet Propulsion Laboratory.
- Head, J. W., Chapman, C. R., Strom, R. G., Fassett, C. I., Denevi, B. W., Blewett, D. T., et al. (2011). Flood volcanism in the northern high latitudes of Mercury revealed by MESSENGER. *Science*, *333*(6051), 1853–1856. <https://doi.org/10.1126/science.1211997>
- Head, J. W., Murchie, S. L., Prockter, L. M., Robinson, M. S., Solomon, S. C., Strom, R. G., et al. (2008). Volcanism on Mercury: Evidence from the first MESSENGER flyby. *Science*, *321*(5885), 69–72. <https://doi.org/10.1126/science.1159256>
- Head, J. W., Murchie, S. L., Prockter, L. M., Solomon, S. C., Chapman, C. R., Strom, R. G., et al. (2009). Volcanism on Mercury: Evidence from the first MESSENGER flyby for extrusive and explosive activity and the volcanic origin of plains. *Earth and Planetary Science Letters*, *285*(3–4), 227–242. <https://doi.org/10.1016/j.epsl.2009.03.007>
- Head, J. W., Pappalardo, R., Collins, G., Belton, M. J. S., Giese, B., Wagner, R., et al. (2002). Evidence for Europa-like tectonic resurfacing styles on Ganymede. *Geophysical Research Letters*, *29*(24), 4–1. <https://doi.org/10.1029/2002gl015961>
- Hedman, M. M., Gosmeyer, C. M., Nicholson, P. D., Sotin, C., Brown, R. H., Clark, R. N., et al. (2013). An observed correlation between plume activity and tidal stresses on Enceladus. *Nature*, *500*(7461), 182–184. <https://doi.org/10.1038/nature12371>
- Helfenstein, P., & Porco, C. C. (2015). Enceladus' Geysers: Relation to Geological features. *The Astronomical Journal*, *150*(3), 96. <https://doi.org/10.1088/0004-6256/150/3/96>
- Herique, A., Kofman, W., Zine, S., Blum, J., Vincent, J.-B., & Ciarletti, V. (2019). Homogeneity of 67P/Churyumov-Gerasimenko as seen by CONSERT: Implication on composition and formation. *Astronomy & Astrophysics*, *630*, A6. <https://doi.org/10.1051/0004-6361/201834865>
- Hiesinger, H., Head, J. W., Wolf, U., Jaumann, R., & Neukum, G. (2011). Ages and stratigraphy of lunar mare basalts: A synthesis. *Recent Advances and Current Research Issues in Lunar Stratigraphy*, *477*, 1–51. [https://doi.org/10.1130/2011.2477\(01\)](https://doi.org/10.1130/2011.2477(01))
- Hill, R. E. T., Barnes, S. J., Gole, M. J., & Dowling, S. E. (1995). The volcanology of komatites as deduced from field relationships in the Norseman-Wiluna greenstone belt, Western Australia. *Lithos*, *34*(1–3), 159–188. [https://doi.org/10.1016/0024-4937\(95\)90019-5](https://doi.org/10.1016/0024-4937(95)90019-5)
- Hobley, D. E., Moore, J. M., Howard, A. D., & Umurhan, O. M. (2020). Reply to: Penitente formation is unlikely on Europa. *Nature Geoscience*, *13*(1), 20–21. <https://doi.org/10.1038/s41561-019-0497-1>

- Hofgartner, J. D., Birch, S. P., Castillo, J., Grundy, W. M., Hansen, C. J., Hayes, A. G., et al. (2022). Hypotheses for Triton's plumes: New analyses and future remote sensing tests. *Icarus*, 375, 114835. <https://doi.org/10.1016/j.icarus.2021.114835>
- Höfner, S., Vincent, J.-B., Blum, J., Davidsson, B. J. R., Sierks, H., El-Maarry, M. R., et al. (2017). Thermophysics of fractures on comet 67P/Churyumov-Gerasimenko. *Astronomy & Astrophysics*, 608, A121. <https://doi.org/10.1051/0004-6361/20162872>
- Hong, I. S., Cho, E., Yi, Y., Yu, J., & Haruyama, J. (2015). 3D Printed structure of Lacus Mortis Pit Crater with Assumption of cave underneath. In *Paper presented at 2nd International Planetary Caves Conference*. Abstract #9015, LPI Contributions No. 1883.
- Hörst, S. M. (2017). Titan's atmosphere and climate. *Journal of Geophysical Research: Planets*, 122(3), 432–482. <https://doi.org/10.1002/2016je005240>
- Hörz, F. (1985). Lava tubes: Potential shelters for habitats. In *Lunar Bases and Space Activities of the 21st Century (A86-30113 13-14)* (pp. 405–412). Lunar and Planetary Science Institute.
- Howard, A. D., Moore, J. M., White, O. L., Umurhan, O. M., Schenk, P. M., Grundy, W. M., et al. (2017). Pluto: Pits and mantles on uplands north and east of Sputnik Planitia. *Icarus*, 293, 218–230. <https://doi.org/10.1016/j.icarus.2017.02.027>
- Howell, S. M. (2021). The likely thickness of Europa's icy shell. *The Planetary Science Journal*, 2(4), 129. <https://doi.org/10.3847/psj/abfe10>
- Howell, S. M., & Pappalardo, R. T. (2020). NASA's Europa Clipper—A mission to a potentially habitable ocean world. *Nature Communications*, 11, 1–4. <https://doi.org/10.1038/s41467-020-15160-9>
- Hu, X., Gundlach, B., von Borstel, I., Blum, J., & Shi, X. (2019). Effect of radiative heat transfer in porous comet nuclei: Case study of 67P/Churyumov-Gerasimenko. *Astronomy & Astrophysics*, 630, A5. <https://doi.org/10.1051/0004-6361/201834631>
- Hughson, K. H. G., Russell, C. T., Schmidt, B. E., Chilton, H. T., Sizemore, H., Schenk, P. M., & Raymond, C. A. (2019). Fluidized appearing ejecta on Ceres: Implications for the mechanical properties, frictional properties, and composition of its shallow subsurface. *Journal of Geophysical Research: Planets*, 124(7), 1819–1839. <https://doi.org/10.1029/2018JE005666>
- Hughson, K. H. G., Russell, C. T., Schmidt, B. E., Travis, B., Preusker, F., Neesemann, A., et al. (2019). Normal faults on Ceres: Insights into the mechanical properties and thermal history of Nar Sulcus. *Geophysical Research Letters*, 46(1), 80–88. <https://doi.org/10.1029/2018GL080258>
- Hughson, K. H. G., Russell, C. T., Williams, D. A., Buczkowski, D. L., Mest, S. C., Pasckert, J. H., et al. (2018). The Ac-5 (Fejokoo) quadrangle of Ceres: Geologic map and geomorphological evidence for ground ice mediated surface processes. *Icarus*, 316, 63–83. <https://doi.org/10.1016/j.icarus.2017.09.035>
- Ianson, E., Davis, R., Meyer, M., & Haltigin, T. (2021). *International Mars Ice Mapper Mission*. Mars Exploration Program Analysis Group, NASA-JPL. Retrieved from https://mepag.jpl.nasa.gov/meeting/2021-06/03_MIM_MEPAG_Presentation_%2021_JUN_2021.pdf
- Ip, W.-H., Lai, I.-L., Lee, J.-C., Cheng, Y.-C., Li, Y., Lin, Z.-Y., et al. (2016). Physical properties and dynamical relation of the circular depressions on comet 67P/Churyumov-Gerasimenko. *Astronomy & Astrophysics*, 591, A132. <https://doi.org/10.1051/0004-6361/201628156>
- Israël, G., Szopa, C., Raulin, F., Cabane, M., Niemann, H. B., Atreya, S. K., et al. (2005). Complex organic matter in Titan's atmospheric aerosols from in situ pyrolysis and analysis. *Nature*, 438(7069), 796–799. <https://doi.org/10.1038/nature04349>
- Ivanov, M. A., & Head, J. W. (2013). The history of volcanism on Venus. *Planetary and Space Science*, 84, 66–92. <https://doi.org/10.1016/j.pss.2013.04.018>
- Jaumann, R., Williams, D. A., Buczkowski, D. L., Yingst, R. A., Preusker, F., Hiesinger, H., et al. (2012). Vesta's shape and morphology. *Science*, 336(6082), 687–690. <https://doi.org/10.1126/science.1219122>
- Kaku, T., Haruyama, J., Miyake, W., Kumamoto, A., Ishiyama, K., Nishibori, T., et al. (2017). Detection of intact lava tubes at Marius Hills on the Moon by SELENE (Kaguya) lunar radar sounder. *Geophysical Research Letters*, 44(20), 10155–10161. <https://doi.org/10.1002/2017gl074998>
- Kalita, H., Nallapu, R. T., Warren, A., & Thangavelautham, J. (2017). Guidance, navigation and control of multirobot systems in cooperative cliff climbing. *Advances in the Astronautical Sciences Guidance, Navigation and Control*, 159, 1–14.
- Kalousová, K., Souček, O., Tobie, G., Choblet, G., & Čadek, O. (2014). Ice melting and downward transport of meltwater by two-phase flow in Europa's ice shell. *Journal of Geophysical Research: Planets*, 119(3), 532–549. <https://doi.org/10.1002/2013je004563>
- Kalousová, K., Souček, O., Tobie, G., Choblet, G., & Čadek, O. (2016). Water generation and transport below Europa's strike-slip faults. *Journal of Geophysical Research: Planets*, 121(12), 2444–2462. <https://doi.org/10.1002/2016je005188>
- Kargel, J. S. (1995). Cryovolcanism on the icy satellites. *Earth, Moon and Planets*, 67(1–3), 101–113. <https://doi.org/10.1007/bf00613296>
- Keller, H. U., Kramm, R., & Thomas, N. (1988). Surface features on the nucleus of comet Halley. *Nature*, 331(6153), 227–231. <https://doi.org/10.1038/331227a0>
- Kempe, S. (2019). Volcanic rock caves. In W. B. White & D. C. Culver (Eds.), *Encyclopedia of Caves* (3rd ed., pp. 1118–1127). Academic Press.
- Kerber, L., Denevi, B. W., Nesnas, I., Keszthelyi, L., Head, J. W., Pieters, C., et al. (2019). Moon Diver: A discovery mission concept for understanding secondary crust formation through the exploration of a lunar mare pit cross-section. In *Lunar and Planetary Science Conference*. Abstract #1163, LPI Contribution No. 2132. Retrieved from <https://www.hou.usra.edu/meetings/lpsc2019/pdf/1163.pdf>
- Kesner, S., Plante, J. S., Dubowsky, S., & Boston, P. J. (2007). A hopping mobility concept for a rough terrain search and rescue robot. *Advances in Climbing and Walking Robots, 2007*, 271–280.
- Keszthelyi, L., Jaeger, W., Milazzo, M., Radebaugh, J., Davies, A. G., & Mitchell, K. L. (2007). New estimates for Io eruption temperatures: Implications for the interior. *Icarus*, 192(2), 491–502. <https://doi.org/10.1016/j.icarus.2007.07.008>
- Keszthelyi, L., McEwen, A. S., Phillips, C. B., Milazzo, M., Geissler, P., Turtle, E. P., et al. (2001). Imaging of volcanic activity on Jupiter's Moon Io by Galileo during the Galileo Europa Mission and the Galileo Millennium Mission. *Journal of Geophysical Research*, 106(E12), 33025–33052. <https://doi.org/10.1029/2000je001383>
- Keszthelyi, L., & Self, S. (1998). Some physical requirements for the emplacement of long basaltic lava flows. *Journal of Geophysical Research*, 103(B11), 27447–27464. <https://doi.org/10.1029/98jb00606>
- Kim, S. K., Bouman, A., Salhotra, G., Fan, D. D., Otsu, K., Burdick, J., et al. (2021). PLGRIM: Hierarchical value learning for large-scale exploration in unknown environments. In *Proceedings of the International Conference on Automated Planning and Scheduling (Vol. 31)*. Retrieved from <https://arxiv.org/pdf/2102.05633.pdf>
- Kirk, R. L., Howington-Kraus, E., Redding, B. L., Becker, T. L., Lee, E. M., Stiles, B. W., et al. (2009). Three-dimensional views of Titan's diverse surface features from Cassini radar stereogrammetry. In *Lunar and Planetary Science Conference*. Abstract #1413.
- Kirk, R. L., Soderblom, L. A., Brown, R. H., Kieffer, S. W., & Kargel, J. S. (1995). Triton's plumes: Discovery, characteristics, and models. In D. P. Cruikshank (Ed.), *Neptune and Triton* (pp. 949–989). University of Arizona Press.
- Klimchouk, A. (2009). Morphogenesis of hypogenic caves. *Geomorphology*, 106(1–2), 100–117. <https://doi.org/10.1016/j.geomorph.2008.09.013>
- Komatsu, G., Kargel, J. S., & Baker, V. R. (1992). Canali-type channels on Venus: Some genetic constraints. *Geophysical Research Letters*, 19(13), 1415–1418. <https://doi.org/10.1029/92gl010147>
- Krasnopolsky, V. A. (2009). A photochemical model of Titan's atmosphere and ionosphere. *Icarus*, 201(1), 226–256. <https://doi.org/10.1016/j.icarus.2008.12.038>

- Krasnopolsky, V. A. (2014). Chemical composition of Titan's atmosphere and ionosphere: Observations and the photochemical model. *Icarus*, 236, 83–91. <https://doi.org/10.1016/j.icarus.2014.03.041>
- Krasnopolsky, V. A., & Cruikshank, D. P. (1995). Photochemistry of Triton's atmosphere and ionosphere. *Journal of Geophysical Research*, 100(E10), 21271–21286. <https://doi.org/10.1029/95je01904>
- Kreuzig, C., Kargl, G., Pommerol, A., Knollenberg, J., Lethuillier, A., Molinski, N. S., et al. (2021). The CoPhyLab comet-simulation chamber. *Review of Scientific Instruments*, 92(11), 115102. <https://doi.org/10.1063/5.0057030>
- Krishnan, S. (2021). A polyhedral approach for design of inflatable lunar habitats. In *Paper presented at 17th Biennial International Conference on Engineering, Science, Construction, and Operations in Challenging Environments* (pp. 1004–1011).
- Landis, M. E., Byrne, S., Combe, J. P., Marchi, S., Castillo-Rogez, J., Sizemore, H. G., et al. (2019). Water vapor contribution to Ceres' exosphere from observed surface ice and postulated ice-exposing impacts. *Journal of Geophysical Research: Planets*, 124(1), 61–75. <https://doi.org/10.1029/2018je005780>
- Landis, M. E., Byrne, S., Schörghofer, N., Schmidt, B. E., Hayne, P. O., Castillo-Rogez, J., et al. (2017). Conditions for sublimating water ice to supply Ceres' exosphere. *Journal of Geophysical Research: Planets*, 122(10), 1984–1995. <https://doi.org/10.1002/2017je005335>
- Lauro, S., Pettinelli, E., Caprarelli, G., Guallini, L., Rossi, A. P., Mattei, E., et al. (2021). Multiple subglacial water bodies below the south pole of Mars unveiled by new MARSIS data. *Nature Astronomy*, 5(1), 63–70. <https://doi.org/10.1038/s41550-020-1200-6>
- Lavvas, P. P., Coustenis, A., & Vardavas, I. M. (2008). Coupling photochemistry with haze formation in Titan's atmosphere, Part II: Results and validation with Cassini/Huygens data. *Planetary and Space Science*, 56(1), 67–99. <https://doi.org/10.1016/j.pss.2007.05.027>
- Lee, P., Kommedal, E., Horchler, A., Amoroso, E., Synder, K., & Birgisson, A. F. (2019). Lofthellir Lava Tube Ice Cave, Iceland: Subsurface micro-glaciers, rockfalls, drone lidar 3D-mapping, and implications for the exploration of potential ice-rich lava tubes on the Moon and Mars. In *Lunar and Planetary Science Conference*. Abstract #3118, LPI Contributions No. 2132. Retrieved from <https://www.hou.usra.edu/meetings/lpsc2019/pdf/3118>
- Lee, S., Pappalardo, R. T., & Makris, N. C. (2005). Mechanics of tidally driven fractures in Europa's ice shell. *Icarus*, 177(2), 367–379. <https://doi.org/10.1016/j.icarus.2005.07.003>
- Le Feuvre, M., & Wieczorek, M. A. (2011). Nonuniform cratering of the Moon and a revised crater chronology of the inner solar system. *Icarus*, 214, 1–20. <https://doi.org/10.1016/j.icarus.2011.03.010>
- Lellouch, E., de Bergh, C., Sicardy, B., Käufel, H. U., Smette, A., & Diderot, F. (2011). The tenuous atmospheres of Pluto and Triton explored by CRRES on the VLT. *The Messenger*, 145, 20–23.
- Leone, G., Davies, A. G., Wilson, L., Williams, D. A., Keszthelyi, L. P., Jaeger, W. L., & Turtle, E. P. (2009). Volcanic history, geologic analysis and map of the Prometheus Patera region on Io. *Icarus*, 187(1–2), 93–105. <https://doi.org/10.1016/j.jvolgeoes.2009.07.019>
- Lesage, E., Schmidt, F., Andrieu, F., & Massol, H. (2021). Constraints on effusive cryovolcanic eruptions on Europa using topography obtained from Galileo images. *Icarus*, 361, 114373. <https://doi.org/10.1016/j.icarus.2021.114373>
- Léveillé, R. J., & Datta, S. (2010). Lava tubes and basaltic caves as astrobiological targets on Earth and Mars: A review. *Planetary and Space Science*, 58(4), 592–598. <https://doi.org/10.1016/j.pss.2009.06.004>
- Ligier, N., Poulet, F., Carter, J., Brunetto, R., & Gourgeot, F. (2016). VLT/SINFONI observations of Europa: New insights into the surface composition. *The Astronomical Journal*, 151(6), 163. <https://doi.org/10.3847/0004-6256/151/6/163>
- Linne, D. L., Sanders, G. B., Starr, S. O., Eisenman, D. J., Suzuki, N. H., Anderson, M. S., et al. (2017). Overview of NASA technology development for in-situ resource utilization (ISRU). In *Paper presented at 68th International Astronautical Congress, Adelaide, Australia, 25–29 September 2017. IAC-17-D3.3.1*. Retrieved from <https://ntrs.nasa.gov/api/citations/2018000407/downloads/2018000407.pdf>
- Liteken, D. A. (2019). Inflatable technology: Using flexible materials to make large structures. In *Electroactive Polymer Actuators and Devices (EPAD) XXI* (Vol. 10966, p. 1096603). SPIE.
- Lobo, A. H., Thompson, A. F., Vance, S. D., & Tharimena, S. (2021). A pole-to-equator ocean overturning circulation on Enceladus. *Nature Geoscience*, 14(4), 185–189. <https://doi.org/10.1038/s41561-021-00706-3>
- Lopes, R. M., Kirk, R. L., Mitchell, K. L., LeGall, A., Barnes, J. W., Hayes, A., et al. (2013). Cryovolcanism on Titan: New results from Cassini RADAR and VIMS. *Journal of Geophysical Research: Planets*, 118(3), 416–435. <https://doi.org/10.1002/jgre.20062>
- Lopes, R. M. C., Wall, S. D., Elachi, C., Birch, S. P., Corlies, P., Coustenis, A., et al. (2019). Titan as revealed by the Cassini radar. *Space Science Reviews*, 215, 1–50.
- Lopes, R. M. L., Malaska, M. J., Schoenfeld, A. M., Solomonidou, A., Birch, S. P. D., Florence, M., et al. (2020). A global geomorphological map of Saturn's Moon Titan. *Nature Astronomy*, 4(3), 228–233. <https://doi.org/10.1038/s41550-019-0917-6>
- Lorenz, R. D., Mitchell, K. L., Kirk, R. L., Hayes, A. G., Aharonson, O., Zebker, H. A., et al. (2008). Titan's inventory of organic surface materials. *Geophysical Research Letters*, 35(2), L02206. <https://doi.org/10.1029/2007gl032118>
- Lucchetti, A., Penasa, L., Pajola, M., Massironi, M., Brunetti, M. T., Cremonese, G., et al. (2019). The rocky-like behavior of cometary landslides on 67P/Churyumov-Gerasimenko. *Geophysical Research Letters*, 46(24), 14336–14346. <https://doi.org/10.1029/2019GL085132>
- Lucchetti, A., Pozzobon, R., Mazzarini, F., Cremonese, G., & Massironi, M. (2017). Brittle ice shell thickness of Enceladus from fracture distribution analysis. *Icarus*, 297, 252–264. <https://doi.org/10.1016/j.icarus.2017.07.009>
- MacKenzie, S. M., & Barnes, J. W. (2016). Compositional distinctions and similarities between Titan's evaporitic terrains. *The Astrophysical Journal*, 821(1), 17. <https://doi.org/10.3847/0004-637x/821/1/17>
- MacKenzie, S. M., Barnes, J. W., Sotin, C., Soderblom, J. M., Le Mouelic, S., Rodriguez, S., et al. (2014). Evidence of Titan's climate history from evaporite distribution. *Icarus*, 243, 191–207. <https://doi.org/10.1016/j.icarus.2014.08.022>
- Malaska, M. J., & Hodyss, R. (2014). Dissolution of benzene, naphthalene, and biphenyl in a simulated Titan lake. *Icarus*, 242, 74–81. <https://doi.org/10.1016/j.icarus.2014.07.022>
- Malaska, M. J., Lopes, R. M. C., Williams, D. A., Neish, C. D., Solominidou, A., Soderblom, J. M., et al. (2016). Geomorphological map of the Afekan crater region, Titan: Terrain relationships in the equatorial and mid-latitude regions. *Icarus*, 270, 130–161. <https://doi.org/10.1016/j.icarus.2016.02.021>
- Malaska, M. J., Radebaugh, J., Lopes, R. M., Mitchell, K. L., Verlander, T., Schoenfeld, A. M., et al. (2020). Labyrinth terrain on Titan. *Icarus*, 344, 113764. <https://doi.org/10.1016/j.icarus.2020.113764>
- Malaska, M. J., Radebaugh, J., Lorenz, R., Mitchell, K., Farr, T., & Stofan, E. (2010). Identification of karst-like terrain on Titan from valley analysis. In *Lunar and Planetary Science Conference*. Abstract #1544.
- Malaska, M. J., Schoenfeld, A. M., Wynne, J. J., Mitchell, K. L., White, O., Howard, A., et al. (2022). Cave candidates on Titan. *Journal of Geophysical Research: Planets (This Issue)*. <https://doi.org/10.1029/2022JE007512>
- Mandt, K. E., Mousis, O., Bockelée-Morvan, D., & Russell, C. T. (2015). Comets as tracers of solar system formation and evolution. *Space Science Reviews*, 197(1–4), 5–7. <https://doi.org/10.1007/s11214-015-0215-2>

- Manga, M., & Wang, C.-Y. (2007). Pressurized oceans and the eruption of liquid water on Europa and Enceladus. *Geophysical Research Letters*, 34(7), L07202. <https://doi.org/10.1029/2007gl029297>
- Martin, E. S., Kattenhorn, S. A., Collins, G. C., Michaud, R. L., Pappalardo, R. T., & Wyrick, D. Y. (2017). Pit chains on Enceladus signal the recent tectonic dissection of the ancient cratered terrains. *Icarus*, 294, 209–217. <https://doi.org/10.1016/j.icarus.2017.03.014>
- Massironi, M., Simioni, E., Marzari, F., Cremonese, G., Giacomini, L., Pajola, M., et al. (2015). Two independent and primitive envelopes of the bilobate nucleus of comet 67P. *Nature*, 526(7573), 402–405. <https://doi.org/10.1038/nature15511>
- McEwen, A. S., Belton, M. J. S., Breneman, H. H., Fagents, S. A., Geissler, P., Greeley, R., et al. (2000). Galileo at Io: Results from high-resolution imaging. *Science*, 288(5469), 1193–1198. <https://doi.org/10.1126/science.288.5469.1193>
- McEwen, A. S., Turtle, E., Kestay, L., Khurana, K., Westlake, J. H., Wurz, P., et al. (2019). The Io Volcano Observer (IVO): Follow the heat. In *Lunar and Planetary Science Conference*. Abstract #1316.
- McKinnon, W. B. (1984). On the origin of Triton and Pluto. *Nature*, 311(5984), 355–358. <https://doi.org/10.1038/311355a0>
- Melosh, H. J. (1989). Impact cratering: A geologic process. *Oxford Monographs on Geology and Geophysics*, 11, 245.
- Michaut, C., & Manga, M. (2014). Domes, pits, and small chaos on Europa produced by water sills. *Journal of Geophysical Research: Planets*, 119(3), 550–573. <https://doi.org/10.1002/2013je004558>
- Mitri, G., Lunine, J. I., Mastrogiuseppe, M., & Poggiali, V. (2019). Possible explosion crater origin of small lake basins with raised rims on Titan. *Nature Geoscience*, 12(10), 791–796. <https://doi.org/10.1038/s41561-019-0429-0>
- Moore, J. M., Howard, A. D., Umurhan, O. M., White, O. L., Schenk, P. M., Beyer, R. A., et al. (2017). Sublimation as a landform-shaping process on Pluto. *Icarus*, 287, 320–333. <https://doi.org/10.1016/j.icarus.2016.08.025>
- Moore, J. M., Howard, A. D., Umurhan, O. M., White, O. L., Schenk, P. M., Beyer, R. A., et al. (2018). Bladed terrain on Pluto: Possible origins and evolution. *Icarus*, 300, 129–144. <https://doi.org/10.1016/j.icarus.2017.08.031>
- Moore, J. M., Howard, A. D., White, O. L., Umurhan, O. M., Singer, K. N., & Schenk, P. M. (2021). Are the surface textures of Pluto's Wright Mons and its surroundings exogenic. In *Lunar and Planetary Science Conference*. Abstract #1693, LPI Contributions No. 2548.
- Moore, J. M., McKinnon, W. B., Spencer, J. R., Howard, A. D., Schenk, P. M., Beyer, R. A., et al. (2016). The geology of Pluto and Charon through the eyes of New Horizons. *Science*, 351(6279), 1284–1293. <https://doi.org/10.1126/science.aad7055>
- Moore, J. E., Smith, C. L., Toigo, A. D., & Guzewich, S. D. (2017). Penitentes as the origin of the bladed terrain of Tartarus Dorsa on Pluto. *Nature*, 541(7636), 188–190. <https://doi.org/10.1038/nature20779>
- Morad, S. D., Dailey, T., Vance, L. D., & Thangavelautham, J. (2019). A spring propelled extreme environment robot for off-world cave exploration. In *IEEE Aerospace Conference* (pp. 1–9).
- Morrison, D. (1982). Introduction. In D. Morrison (Ed.), *Satellites of Jupiter* (pp. 3–43). University of Arizona Press.
- Mouginis-Mark, P. J. (2016). Geomorphology and volcanology of Maat Mons, Venus. *Icarus*, 277, 433–441. <https://doi.org/10.1016/j.icarus.2016.05.022>
- Murchie, S. L., Watters, T. R., Robinson, M. S., Head, J. W., Strom, R. G., Chapman, C. R., et al. (2008). Geology of the Caloris basin, Mercury: A view from MESSENGER. *Science*, 321(5885), 73–76. <https://doi.org/10.1126/science.1159261>
- Mylroie, J. E. (1984). Hydrologic classification of karst landforms. In R. LaFleur (Ed.), *Groundwater as a geomorphic agent* (pp. 157–172). Allen and Unwin.
- Mylroie, J. E. (2019). Caves in space. *Journal of Cave and Karst Studies*, 81(1), 25–32. <https://doi.org/10.4311/2018es0102>
- Nathues, A., Schmedemann, N., Thangjam, G., Pasckert, J. H., Mengel, K., Castillo-Rogez, J., et al. (2020). Recent cryovolcanic activity at Occator crater on Ceres. *Nature Astronomy*, 4(8), 794–801. <https://doi.org/10.1038/s41550-020-1146-8>
- National Academies of Sciences, Engineering, and Medicine [NASEM]. (2022). *Origins, worlds, and life: A decadal strategy for planetary science and astrobiology 2023–2032*. The National Academies Press. <https://doi.org/10.17726/26522>
- Nesnas, I. A., Matthews, J. B., Abad-Manterola, P., Burdick, J. W., Edlund, J. A., Morrison, J. C., et al. (2012). Axel and DuAxel rovers for the sustainable exploration of extreme terrains. *Journal of Field Robotics*, 29(4), 663–685. <https://doi.org/10.1002/rob.21407>
- Nimmo, F. (2004). Stresses generated in cooling viscoelastic ice shells: Application to Europa. *Journal of Geophysical Research*, 109(E12), E12001. <https://doi.org/10.1029/2004je002347>
- Nimmo, F., & Gaidos, E. (2002). Strike-slip motion and double ridge formation on Europa. *Journal of Geophysical Research*, 107(E4), 5-1–5-8. <https://doi.org/10.1029/2000je001476>
- Nimmo, F., Hamilton, D. P., McKinnon, W. B., Schenk, P. M., Binzel, R. P., Bierson, C. J., et al. (2016). Reorientation of Sputnik Planitia implies a subsurface ocean on Pluto. *Nature*, 540(7631), 94–96. <https://doi.org/10.1038/nature20148>
- Nimmo, F., Porco, C., & Mitchell, C. (2014). Tidally modulated eruptions on Enceladus: Cassini ISS observations and models. *The Astronomical Journal*, 148(3), 46. <https://doi.org/10.1088/0004-6256/148/3/46>
- Nimmo, F., & Spencer, J. R. (2015). Powering Triton's recent geological activity by obliquity tides: Implications for Pluto geology. *Icarus*, 245, 2–10. <https://doi.org/10.1016/j.icarus.2014.01.044>
- Nordheim, T. A., Hand, K. P., & Paranicas, C. (2018). Preservation of potential biosignatures in the shallow subsurface of Europa. *Nature Astronomy*, 2(8), 673–679. <https://doi.org/10.1038/s41550-018-0499-8>
- Oberbeck, V. R., Quaide, W. L., & Greeley, R. (1969). On the origin of lunar sinuous rilles. *Modern Geology*, 1, 75–80.
- Okubo, C. H., & Martel, S. J. (1998). Pit crater formation on Kilauea volcano, Hawaii. *Journal of Volcanology and Geothermal Research*, 86(1–4), 1–18. [https://doi.org/10.1016/s0377-0273\(98\)00070-5](https://doi.org/10.1016/s0377-0273(98)00070-5)
- Okubo, C. H., & Schultz, R. A. (2005). Evidence of normal faulting and dike intrusion at Valles Marineris from pit crater topography. In *Lunar and Planetary Science Conference*. Abstract #1008.
- Orosei, R., Lauro, S. E., Pettinelli, E., Cicchetti, A. N. D. R. E. A., Coradini, M., Cosciotti, B., et al. (2018). Radar evidence of subglacial liquid water on Mars. *Science*, 361(6401), 490–493. <https://doi.org/10.1126/science.aar7268>
- Osipova, N. A. (2015). Son Doong—the world's largest cave in Vietnam. In *Проблемы геологии и освоения недр: Труды XIX Международного симпозиума имени академика М.А. Усова студентов и молодых ученых, посвященного 70-летию юбилею Победы советского народа над фашистской Германией, Томск, 6-10 апреля 2015 г. Т. 2.—Томск* (Vol. 2, pp. 792–794). Retrieved from http://archive.tpu.ru/bitstream/11683/23040/1/conference_tpu-2015-C11-V2-357.pdf
- Owen, A. M. (2013). Tafoni development in the Bahamas. In M. J. Lacey & J. E. Mylroie (Eds.), *Coastal Karst Landforms*, *Coastal Research Library* (Vol. 5, pp. 177–205). Springer. <https://doi.org/10.1007/978-94-007-5016-68>
- Paganini, L., Villanueva, G. L., Roth, L., Mandell, A. M., Hurford, T. A., Retherford, K. D., & Mumma, M. J. (2019). A measurement of water vapour amid a largely quiescent environment on Europa. *Nature Astronomy*, 4(3), 266–272. <https://doi.org/10.1038/s41550-019-0933-6>
- Pajola, M., Höfner, S., Vincent, J. B., Oklay, N., Scholten, F., Preusker, F., et al. (2017). The pristine interior of comet 67P revealed by the combined Aswan outburst and cliff collapse. *Nature Astronomy*, 1(5), 0092. <https://doi.org/10.1038/s41550-017-0092>

- Pajola, M., Oklay, N., La Forgia, F., Giacomini, L., Massironi, M., Bertini, I., et al. (2016). Aswan site on comet 67P/Churyumov-Gerasimenko: Morphology, boulder evolution, and spectrophotometry. *Astronomy & Astrophysics*, 592, A69. <https://doi.org/10.1051/0004-6361/201527865>
- Palmer, A. N. (2007). *Cave geology*. Cave Books.
- Pappalardo, R. T., Collins, G. C., Head, J. W., Helfenstein, P., McCord, T. B., Moore, J. M., et al. (2004). Geology of Ganymede. In F. Bagenal, T. E. Dowling, & W. B. McKinnon (Eds.), *Jupiter: The planet, satellites, and magnetosphere* (pp. 363–396). Cambridge University Press.
- Parenti, C., Gutiérrez, F., Baioni, D., García-Arny, Á., Sevil, J., & Luzzi, E. (2020). Closed depressions in Kotido crater, Arabia Terra, Mars. Possible evidence of evaporite dissolution-induced subsidence. *Icarus*, 341, 113680. <https://doi.org/10.1016/j.icarus.2020.113680>
- Parness, A., Abcouwer, N., Fuller, C., Wiltis, N., Nash, J., & Kennedy, B. (2017). Lemur 3: A limbed climbing robot for extreme terrain mobility in space. In *IEEE International Conference on Robotics and Automation (ICRA)* (pp. 5467–5473). IEEE.
- Patrick, E. L., Mandt, K. E., Mitchell, E. J., Mitchell, J. N., Younkin, K. N., Seifert, C. M., & Williams, G. C. (2012). A prototype mass spectrometer for in situ analysis of cave atmospheres. *Review of Scientific Instruments*, 83(10), 105116. <https://doi.org/10.1063/1.4761927>
- Pathoff, D. A., & Kattenhorn, S. A. (2011). A fracture history on Enceladus provides evidence for a global ocean. *Geophysical Research Letters*, 38(18), L18201. <https://doi.org/10.1029/2011gl048387>
- Pätzold, M., Andert, T., Hahn, M., Asmar, S. W., Barriot, J.-P., Bird, M. K., et al. (2016). A homogeneous nucleus for comet 67P/Churyumov-Gerasimenko from its gravity field. *Nature*, 530(7588), 63–65. <https://doi.org/10.1038/nature16535>
- Peale, S. J., Cassen, P., & Reynolds, R. T. (1979). Melting of Io by tidal dissipation. *Science*, 203(4383), 892–894. <https://doi.org/10.1126/science.203.4383.892>
- Perşoiu, A., & Onac, B. P. (2019). Ice in caves. In W. B. White, D. C. Culver, & T. Pipan (Eds.), *Encyclopedia of Caves* (3rd ed., pp. 553–558). Academic Press.
- Peters, S. I., Christensen, P. R., & Clarke, A. B. (2021). Lava flow eruption conditions in the Tharsis volcanic province on Mars. *Journal of Geophysical Research: Planets*, 126(7), e2020JE006791. <https://doi.org/10.1029/2020je006791>
- Phillips-Lander, C. M., Agha-Mohamadi, A., Wynne, J. J., Titus, T. N., Chanover, N., Demirel-Floyd, C., et al. (2020). Mars astrobiological cave and Internal habitability Explorer (MACIE): A New Frontiers mission concept. *Bulletin of the American Astronomical Society*, 53(4). <https://doi.org/10.3847/25c2efeb.cf124da3>
- Pisani, L., & De Waele, J. (2021). Candidate cave entrances in a planetary analogue evaporite karst (Cordillera de la Sal, Chile): A remote sensing approach and ground-truth reconnaissance. *Geomorphology*, 389, 107851. <https://doi.org/10.1016/j.geomorph.2021.107851>
- Porco, C. C., DiNino, D., & Nimmo, F. (2014). How the geysers, tidal stresses, and thermal emission across the south polar terrain of Enceladus are related. *The Astronomical Journal*, 148(3), 45. <https://doi.org/10.1088/0004-6256/148/3/45>
- Porco, C. C., Helfenstein, P., Thomas, P. C., Ingersoll, A. P., Wisdom, J., West, R., et al. (2006). Cassini observes the active south pole of Enceladus. *Science*, 311(5766), 1393–1401. <https://doi.org/10.1126/science.1123013>
- Preston, L. J., Melim, L. A., Polyak, V. J., Asmerom, Y., & Southam, G. (2014). Infrared spectroscopic biosignatures from Hidden cave, New Mexico: Possible applications for remote life detection. *Geomicrobiology Journal*, 31(10), 929–941. <https://doi.org/10.1080/01490451.2014.913096>
- Prettyman, T. H., Yamashita, N., Landis, M. E., Castillo-Rogez, J. C., Schörghofer, N., Pieters, C. M., et al. (2021). Replenishment of near-surface water ice by impacts into Ceres' volatile-rich crust: Observations by Dawn's gamma ray and neutron detector. *Geophysical Research Letters*, 48(15), e2021GL094223. <https://doi.org/10.1029/2021gl094223>
- Prettyman, T. H., Yamashita, N., Toplis, M. J., McSween, H. Y., Schörghofer, N., Marchi, S., et al. (2017). Extensive water ice within Ceres' aqueously altered regolith: Evidence from nuclear spectroscopy. *Science*, 355(6320), 55–59. <https://doi.org/10.1126/science.aah6765>
- Prockter, L. M., Ernst, C. M., Denevi, B. W., Chapman, C. R., Head, J. W., Fassett, C. I., et al. (2010). Evidence for young volcanism on Mercury from the third MESSENGER flyby. *Science*, 329(5992), 668–671. <https://doi.org/10.1126/science.1188186>
- Protospapa, S., Grundy, W. M., Reuter, D. C., Hamilton, D. P., Dalle Ore, C. M., Cook, J. C., et al. (2017). Pluto's global surface composition through pixel-by-pixel Hapke modeling of New Horizons Ralph/LEISA data. *Icarus*, 287, 218–228. <https://doi.org/10.1016/j.icarus.2016.11.028>
- Radebaugh, J., McEwen, A. S., Milazzo, M. P., Kesztelyi, L. P., Davies, A. G., Turtle, E. P., & Dawson, D. D. (2004). Observations and temperatures of Io's Pele Patera from Cassini and Galileo spacecraft images. *Icarus*, 169(1), 65–79. <https://doi.org/10.1016/j.icarus.2003.10.019>
- Raponi, A., De Sanctis, M. C., Carozzo, F. G., Ciarniello, M., Castillo-Rogez, J. C., Ammannito, E., et al. (2019). Mineralogy of Occator crater on Ceres and insights into its evolution from the properties of carbonates, phyllosilicates, and chlorides. *Icarus*, 320, 83–96. <https://doi.org/10.1016/j.icarus.2018.02.001>
- Roatsch, T. E., Kersten, K.-D., Matz, F., Preusker, F., Scholten, S., Elgner, S. E., et al. (2016). Dawn FC2 derived Ceres Mosaics V1.0. DAWN-A-FC2-5-CERESMOSAIC-V1.0. NASA Planetary Data System. Retrieved from <https://sbn.psi.edu/pds/resource/dawn/dwncfmosaics.html>
- Robbins, S. J., Beyer, R. A., Spencer, J. R., Grundy, W. M., White, O. L., Singer, K. N., et al. (2019). Geologic landforms and chronostratigraphic history of Charon as revealed by a hemispheric geologic map. *Journal of Geophysical Research: Planets*, 124(1), 155–174. <https://doi.org/10.1029/2018JE005684>
- Robinson, M. S., Brylow, S. M., Tschimmel, M., Humm, D., Lawrence, S. J., Thomas, P. C., et al. (2010). Lunar Reconnaissance Orbiter Camera (LROC) instrument overview. *Space Science Reviews*, 150(1–4), 81–124. <https://doi.org/10.1007/s11214-010-9634-2>
- Rogers, P. G., & Zuber, M. T. (1998). Tectonic evolution of Bell Regio, Venus: Regional stress, lithospheric flexure, and edifice stresses. *Journal of Geophysical Research*, 103(E7), 16841–16853. <https://doi.org/10.1029/98je00585>
- Röling, W. F., Aerts, J. W., Patty, C. H., ten Kate, I. L., Ehrenfreund, P., & Direito, S. O. (2015). The significance of microbe-mineral-biomarker interactions in the detection of life on Mars and beyond. *Astrobiology*, 15(6), 492–507. <https://doi.org/10.1089/ast.2014.1276>
- Roth, L., Ivchenko, N., Gladstone, G. R., Saur, J., Grodent, D., Bonfond, B., et al. (2021). A sublimated water atmosphere on Ganymede detected from Hubble space telescope observations. *Nature Astronomy*, 5(10), 1043–1051. <https://doi.org/10.1038/s41550-021-01426-9>
- Roth, L., Saur, J., Retherford, K. D., Strobel, D. F., Feldman, P. D., McGrath, M. A., & Nimmo, F. (2014). Transient water vapor at Europa's South Pole. *Science*, 343(6167), 171–174. <https://doi.org/10.1126/science.1247051>
- Roth, L., Saur, J., Retherford, K. D., Strobel, D. F., Feldman, P. D., McGrath, M. A., et al. (2016). Europa's far ultraviolet oxygen aurora from a comprehensive set of HST observations. *Journal of Geophysical Research: Space Physics*, 121(3), 2143–2170. <https://doi.org/10.1002/2015ja022073>
- Rothery, D. A., Thomas, R. J., & Kerber, L. (2014). Prolonged eruptive history of a compound volcano on Mercury: Volcanic and tectonic implications. *Earth and Planetary Science Letters*, 385, 59–67. <https://doi.org/10.1016/j.epsl.2013.10.023>
- Ruesch, O., Platz, T., Schenk, P., McFadden, L. A., Castillo-Rogez, J. C., Byrne, S., et al. (2016). Cryovolcanism on Ceres. *Science*, 353, 6303. <https://doi.org/10.1126/science.aaf4286>

- Rummel, J. D., Beaty, D. W., Jones, M. A., Bakermans, C., Barlow, N. G., Boston, P. J., et al. (2014). A new analysis of Mars "special regions": Findings of the second MEPAG Special Regions Science Analysis Group (SR-SAG2). *Astrobiology*, *11*, 888–868. <https://doi.org/10.1089/ast.2014.1227>
- Russell, C. T., & Raymond, C. A. (2011). The Dawn mission to Vesta and Ceres. *Space Science Reviews*, *163*(1–4), 3–23. <https://doi.org/10.1007/s11214-011-9836-2>
- Russell, C. T., Raymond, C. A., Ammannito, E., Buczkowski, D. L., De Sanctis, M. C., Hiesinger, H., et al. (2016). Dawn arrives at Ceres: Exploration of a small, volatile-rich world. *Science*, *353*(6303), 1008–1010. <https://doi.org/10.1126/science.aaf4219>
- Russell, C. T., Raymond, C. A., Coradini, A., McSween, H. Y., Zuber, M. T., Nathues, A., et al. (2012). Dawn at Vesta: Testing the protoplanetary paradigm. *Science*, *336*(6082), 684–686. <https://doi.org/10.1126/science.1219381>
- Sagan, C., & Thompson, W. R. (1984). Production and condensation of organic gases in the atmosphere of Titan. *Icarus*, *59*(2), 133–161. [https://doi.org/10.1016/0019-1035\(84\)90018-6](https://doi.org/10.1016/0019-1035(84)90018-6)
- Santamaria-Navarro, A., Thakker, R., Fan, D. D., Morrell, B., & Agha-Mohammadi, A. (2019). Towards resilient autonomous navigation of drones. In *International Symposium on Robotics Research* (pp. 1–16).
- Sauro, F., Pozzobon, R., Massironi, M., De Berardinis, P., Santagata, T., & De Waele, J. (2020). Lava tubes on Earth, Moon and Mars: A review on their size and morphology revealed by comparative planetology. *Earth-Science Reviews*, *209*, 103288. <https://doi.org/10.1016/j.earscirev.2020.103288>
- Sava, P., & Asphaug, E. (2018). 3D radar wavefield tomography of comet interiors. *Advances in Space Research*, *61*(8), 2198–2213. <https://doi.org/10.1016/j.asr.2018.01.040>
- Schenk, P. M. (1993). Central pit and dome craters: Exposing the interiors of Ganymede and Callisto. *Journal of Geophysical Research*, *98*(E4), 7475–7498. <https://doi.org/10.1029/93je00176>
- Schenk, P. M., Beyer, R. A., McKinnon, W. B., Moore, J. M., Spencer, J. R., White, O. L., et al. (2018). Basins, fractures and volcanoes: Global cartography and topography of Pluto from New Horizons. *Icarus*, *314*, 400–433. <https://doi.org/10.1016/j.icarus.2018.06.008>
- Schenk, P. M., McKinnon, W. B., Gwynn, D., & Moore, J. M. (2001). Flooding of Ganymede's bright terrains by low-viscosity water-ice lavas. *Nature*, *410*(6824), 57–60. <https://doi.org/10.1038/35065027>
- Schenk, P. M., & Moore, J. M. (1995). Volcanic constructs on Ganymede and Enceladus: Topographic evidence from stereo images and photogrammetry. *Journal of Geophysical Research*, *100*(E9), 19009–19022. <https://doi.org/10.1029/95je01854>
- Schenk, P. M., & Zahnle, K. (2007). On the negligible surface age of Triton. *Icarus*, *192*(1), 135–149. <https://doi.org/10.1016/j.icarus.2007.07.004>
- Schmedermann, N., Kneissl, T., Ivanov, B. A., Michael, G. G., Wagner, R. J., Neukum, G., et al. (2014). The cratering record, chronology and surface ages of (4) Vesta in comparison to smaller asteroids and the ages of HED meteorites. *Planetary and Space Science*, *103*, 104–130. <https://doi.org/10.1016/j.pss.2014.04.004>
- Schmidt, B. E., Hughson, K. H. G., Chilton, H. T., Scully, J. E. C., Platz, T., Nathues, A., et al. (2017). Geomorphological evidence for ground ice on dwarf planet Ceres. *Nature Geoscience*, *10*(5), 338–343. <https://doi.org/10.1038/ngeo2936>
- Schmidt, B. E., Sizemore, H. G., Hughson, K. H. G., Duarte, K. D., Romero, V. N., Scully, J. E. C., et al. (2020). Post-impact cryo-hydrologic formation of small mounds and hills in Ceres's Occator crater. *Nature Geoscience*, *13*(9), 605–610. <https://doi.org/10.1038/s41561-020-0581-6>
- Schoenfeld, A. M., Lopes, R. M. C., Malaska, M. J., Solomonidou, A., Williams, D. A., Birch, S. P. D., et al. (2021). Geomorphological map of the South Belet Region of Titan. *Icarus*, *366*, 114516. <https://doi.org/10.1016/j.icarus.2021.114516>
- Schörghofer, N. (2016). Predictions of depth-to-ice on asteroids based on an asynchronous model of temperature, impact stirring, and ice loss. *Icarus*, *276*, 88–95. <https://doi.org/10.1016/j.icarus.2016.04.037>
- Schörghofer, N. (2021). Ice caves on Mars: Hoarfrost and microclimates. *Icarus*, *357*, 114271. <https://doi.org/10.1016/j.icarus.2020.114271>
- Schörghofer, N., Businger, S., & Leopold, M. (2018). The coldest places in Hawaii: The ice-preserving microclimates of high-altitude craters and caves on tropical island volcanoes. *Bulletin of the American Meteorological Society*, *99*(11), 2313–2324. <https://doi.org/10.1175/bams-d-17-0238.1>
- Scully, J. E. C., Buczkowski, D. L., Schmedermann, N., Raymond, C. A., Castillo-Rogez, J. C., King, S. D., et al. (2017). Evidence for the interior evolution of Ceres from geologic analysis of fractures. *Geophysical Research Letters*, *44*(19), 9564–9572. <https://doi.org/10.1002/2017GL075086>
- Scully, J. E. C., Schenk, P. M., Castillo-Rogez, J. C., Buczkowski, D. L., Williams, D. A., Pasckert, J. H., et al. (2020). The varied sources of faculae-forming brines in Ceres' Occator crater emplaced via hydrothermal brine effusion. *Nature Communications*, *11*, 1–11. <https://doi.org/10.1038/s41467-020-15973-8>
- Selensky, M. J., Masterson, A. L., Blank, J. G., Lee, S. C., & Osburn, M. R. (2021). Stable carbon isotope depletions in lipid biomarkers suggest subsurface carbon fixation in lava caves. *Journal of Geophysical Research: Biogeosciences*, *126*(7), e2021JG006430. <https://doi.org/10.1029/2021jg006430>
- Senske, D. A., Schaber, G. G., & Stefan, E. R. (1992). Regional topographic rises on Venus: Geology of western Eistla Regio and comparison to Beta Regio and Atla Regio. *Journal of Geophysical Research*, *97*(E8), 13395–13420. <https://doi.org/10.1029/92je01167>
- Sierks, H., Keller, H. U., Jaumann, R., Michalik, H., Behnke, T., Bubenhausen, F., et al. (2011). The Dawn framing camera. *Space Science Reviews*, *163*(1–4), 263–327. <https://doi.org/10.1007/s11214-011-9745-4>
- Singer, K. N., McKinnon, W. B., Gladman, B., Greenstreet, S., Bierhaus, E. B., Stern, S. A., et al. (2019). Impact craters on Pluto and Charon indicate a deficit of small Kuiper belt objects. *Science*, *363*(6430), 955–959. <https://doi.org/10.1126/science.aap8628>
- Singer, K. N., White, O. L., Schenk, P. M., Moore, J. M., Spencer, J. R., McKinnon, W. B., et al. (2016). Pluto's putative cryovolcanic constructs. *Annual Planetary Geologic Mappers Meeting, 1920*, 7017.
- Sizemore, H. G., Schmidt, B. E., Buczkowski, D. A., Sori, M. M., Castillo-Rogez, J. C., Berman, D. C., et al. (2019). A global inventory of ice-related morphological features on dwarf planet Ceres: Implications for the evolution and current state of the cryosphere. *Journal of Geophysical Research: Planets*, *123*(7), 1650–1689. <https://doi.org/10.1029/2018JE005699>
- Skorov, Y. V., Rezac, L., Hartogh, P., Bazilevsky, A. T., & Keller, H. U. (2016). A model of short-lived outbursts on the 67P from fractured terrains. *Astronomy & Astrophysics*, *593*, A76. <https://doi.org/10.1051/0004-6361/201628365>
- Smith, I. B., Lalich, D. E., Rezza, C., Horgan, B. H. N., Whitten, J. L., Nerozzi, S., & Holt, J. W. (2021). A solid interpretation of bright radar reflectors under the Mars south polar ice. *Geophysical Research Letters*, *48*(15), e2021GL093618. <https://doi.org/10.1029/2021GL093618>
- Soderblom, L. A., Becker, T. L., Bennett, G., Boice, D. C., Britt, D. T., Brown, R. H., et al. (2002). Observations of Comet 19P/Borrelly by the miniature integrated camera and spectrometer aboard Deep Space 1. *Science*, *296*(5570), 1087–1091. <https://doi.org/10.1126/science.1069527>
- Soderblom, L. A., Kieffer, S. W., Becker, T. L., Brown, R. H., Cook, A. F., Hansen, C. J., et al. (1990). Triton's geyser-like plumes: Discovery and basic characterization. *Science*, *250*(4979), 410–415. <https://doi.org/10.1126/science.250.4979.410>

- Soderblom, L. A., Kirk, R. L., Lunine, J. I., Anderson, J. A., Baines, K. H., Barnes, J. W., et al. (2007). Correlations between Cassini VIMS spectra and RADAR SAR images: Implications for Titan's surface composition and the character of the Huygens Probe Landing site. *Planetary and Space Science*, 55(13), 2025–2036. <https://doi.org/10.1016/j.pss.2007.04.014>
- Solomonidou, A., Neish, C., Coustenis, A., Malaska, M., Le Gall, A., Lopes, R. M. C., et al. (2020). The chemical composition of impact craters on Titan. I. Implications for exogenic processing. *Astronomy and Astrophysics*, 641, A16. <https://doi.org/10.1051/0004-6361/202037866>
- Sotin, C., Hayes, A., Malaska, M., Nimmo, F., Trainer, M., Mastrogiuseppe, M., et al. (2017). OCEANUS: A new frontiers orbiter to study Titan's potential habitability. *EGU General Assembly*. Abstract #10958.
- Sotin, C., Head, J. W., & Tobie, G. (2002). Europa: Tidal heating of upwelling thermal plumes and the origin of lenticulae and chaos melting. *Geophysical Research Letters*, 29(8), 74-1–74-4. <https://doi.org/10.1029/2001gl013844>
- Sparks, W. B., Hand, K. P., McGrath, M. A., Bergeron, E., Cracraft, M., & Deustua, S. E. (2016). Probing for evidence of plumes on Europa with HST/STIS. *The Astrophysical Journal*, 829(2), 121. <https://doi.org/10.3847/0004-637x/829/2/121>
- Squyres, S. W. (1980). Topographic domes on Ganymede: Ice volcanism or isostatic upwarping. *Icarus*, 44(2), 472–480. [https://doi.org/10.1016/0019-1035\(80\)90038-x](https://doi.org/10.1016/0019-1035(80)90038-x)
- Stern, S. A., Bagenal, F., Ennico, K., Gladstone, G. R., Grundy, W. M., McKinnon, W. B., et al. (2015). The Pluto system: Initial results from its exploration by New Horizons. *Science*, 350, 6258. <https://doi.org/10.1126/science.aad1815>
- Stern, S. A., Kammer, J. A., Gladstone, G. R., Steffl, A. J., Cheng, A. F., Young, L. A., et al. (2017). New Horizons constraints on Charon's present day atmosphere. *Icarus*, 287, 124–130. <https://doi.org/10.1016/j.icarus.2016.09.019>
- Stiles, B. W., Hensley, S., Gim, Y., Bates, D. M., Kirk, R. L., Hayes, A., et al. (2009). Determining Titan surface topography from Cassini SAR data. *Icarus*, 202(2), 584–598. <https://doi.org/10.1016/j.icarus.2009.03.032>
- Storrie-Lombardi, M. C., Hall, A. P., Hang, S., Lyzenga, G. A., Clark, C. M., Sattler, B. I., et al. (2011). Spectral profiling and imaging (SPI): Extending LIFE technology for the remote exploration of life in ice caves (RELIC) on Earth and Mars. *SPIE: Instruments, Methods, and Missions for Astrobiology XIV*, 8152, 355–366.
- Thakker, R., Alatur, N., Fan, D., Tordesillas, J., Paton, M., Otsu, K., et al. (2021). Autonomous off-road navigation over extreme terrains with perceptually-challenging conditions. In *Experimental Robotics: 17th International Symposium* (pp. 161–171).
- Theinat, A. K., Modiriasari, A., Bobet, A., Melosh, H. J., Dyke, S. J., Ramirez, J., et al. (2020). Lunar lava tubes: Morphology to structural stability. *Icarus*, 338, 113442. <https://doi.org/10.1016/j.icarus.2019.113442>
- Thomas, N., Sierks, H., Barbieri, C., Lamy, P. L., Rodrigo, R., Rickman, H., et al. (2015). The morphological diversity of comet 67P/Churyumov-Gerasimenko. *Science*, 347(6220), aaa0440. <https://doi.org/10.1126/science.aaa0440>
- Thomas, P. C., A'Hearn, M., Belton, M. J. S., Brownlee, D., Carcich, B., Hermalyn, B., et al. (2013). The nucleus of Comet 9P/Tempel 1: Shape and geology from two flybys. *Icarus*, 222(2), 453–466. <https://doi.org/10.1016/j.icarus.2012.02.037>
- Thomas, P. C., A'Hearn, M. F., Veverka, J., Belton, M. J. S., Kissel, J., Klaasen, K. P., et al. (2013). Shape, density, and geology of the nucleus of Comet 103P/Hartley 2. *Icarus*, 222, 550–558. <https://doi.org/10.1016/j.icarus.2012.05.034>
- Thomas, P. C., James, P. B., Calvin, W. M., Haberle, R., & Malin, M. C. (2009). Residual south polar cap of Mars: Stratigraphy, history, and implications of recent changes. *Icarus*, 203(2), 352–375. <https://doi.org/10.1016/j.icarus.2009.05.014>
- Titus, T. N., Wynne, J. J., Boston, P. J., de Leon, P., Demirel-Floyd, C., Jones, H., et al. (2021). Science and technology requirements to explore caves in our solar system. *Bulletin of the American Astronomical Society*, 53(4), 167. <https://doi.org/10.3847/25c2feb.a68ba8cb>
- Titus, T. N., Wynne, J. J., Malaska, M. J., Agha-Mohammadi, A., Buhler, P. B., Alexander, E. C., et al. (2021). A roadmap for planetary caves science and exploration. *Nature Astronomy*, 5(6), 524–525. <https://doi.org/10.1038/s41550-021-01385-1>
- Titus, T. N., Wynne, J. J., Ruby, D., & Cabrol, N. A. (2010). The Atacama Desert Cave Shredder: A case for conduction thermodynamics. In *Paper presented at 41st Lunar and Planetary Science Conference. LPI Contributions No. 1096*.
- Tuttle, M. D., & Stevenson, D. E. (1978). Variation in the cave environment and its biological implications. In R. Zuber, J. Chester, S. Gilbert, & D. Rhodes (Eds.), *1977 National Cave Management Symposium Proceedings* (pp. 108–121). Adobe Press.
- Tyler, G. L., Sweetnam, D. N., Anderson, J. D., Borutzki, S. E., Campbell, J. K., Eshleman, V. R., et al. (1989). Voyager radio science observations of Neptune and Triton. *Science*, 246(4936), 1466–1473. <https://doi.org/10.1126/science.246.4936.1466>
- Uckert, K., Parness, A., Chanover, N., Eshelman, E. J., Abcouwer, N., Nash, J., et al. (2020). Investigating habitability with an integrated rock-climbing robot and astrobiology instrument suite. *Astrobiology*, 20(12), 1427–1449. <https://doi.org/10.1089/ast.2019.2177>
- Umurhan, O. M., Birch, S. P. D., Hayes, A. G., & Malaska, M. J. (2020). Simulating the evolution of Titan's surface through fluvial dissolution erosion: I. The big picture. In *Lunar and Planetary Science Conference*. Abstract #1552.
- Umurhan, O. M., Howard, A. D., Moore, J. M., Earle, A. M., White, O. L., Schenk, P. M., et al. (2017). Modeling glacial flow on and onto Pluto's Sputnik Planitia. *Icarus*, 287, 301–319. <https://doi.org/10.1016/j.icarus.2017.01.017>
- Veeder, G. J., Davies, A. G., Matson, D. L., & Johnson, T. V. (2009). Io: Heat flow from dark volcanic fields. *Icarus*, 204(1), 239–253. <https://doi.org/10.1016/j.icarus.2009.06.027>
- Veeder, G. J., Davies, A. G., Matson, D. L., Johnson, T. V., Williams, D. A., & Radebaugh, J. (2015). Io: Heat flow from small volcanic features. *Icarus*, 245, 379–410. <https://doi.org/10.1016/j.icarus.2014.07.028>
- Vijayan, S. (2020). Craters in the vicinity of Valles Marineris region, Mars: Chronological implications to the graben and pits activities. *Icarus*, 343, 113704. <https://doi.org/10.1016/j.icarus.2020.113704>
- Vincent, J.-B., Bodewits, D., Besse, S., Sierks, H., Barbieri, C., Lamy, P., et al. (2015). Large heterogeneities in comet 67P as revealed by active pits from sinkhole collapse. *Nature*, 523(7558), 63–66. <https://doi.org/10.1038/nature14564>
- Vincent, J.-B., Oklay, N., Marchi, S., Höfner, S., & Sierks, H. (2015). Craters on comets. *Planetary and Space Science*, 107, 53–63. <https://doi.org/10.1016/j.pss.2014.06.008>
- Vixie, G., Barnes, J. W., Bow, J., Le Mouélic, S., Rodriguez, S., Brown, R. H., et al. (2012). Mapping Titan's surface features within the visible spectrum via Cassini VIMS. *Planetary and Space Science*, 60(1), 52–61. <https://doi.org/10.1016/j.pss.2011.03.021>
- Wagner, R. V., & Robinson, M. S. (2014). Distribution, formation mechanisms, and significance of lunar pits. *Icarus*, 237, 52–60. <https://doi.org/10.1016/j.icarus.2014.04.002>
- Wagner, R. V., & Robinson, M. S. (2021). Occurrence and origin of lunar pits: Observations from a new catalog. In *Lunar and Planetary Science Conference*. Abstract #2530, LPI Contributions No. 2548.
- Wagner, R. V., Robinson, M. S., Speyerer, E. J., & Plescia, J. B. (2014). Locations of anthropogenic sites on the Moon. In *Lunar and Planetary Science Conference*. Abstract #2259.
- Walker, C. C., & Schmidt, B. E. (2015). Ice collapse over trapped water bodies on Enceladus and Europa. *Geophysical Research Letters*, 42(3), 712–719. <https://doi.org/10.1002/2014gl062405>
- Weaver, H. A., Gibson, W. C., Tapley, M. B., Young, L. A., & Stern, S. A. (2009). Overview of the New Horizons science payload. In C. T. Russell (Ed.), *New Horizons*. Springer. https://doi.org/10.1007/978-0-387-89518-5_5

- Weissman, P., Morbidelli, A., Davidsson, B., & Blum, J. (2020). Origin and evolution of cometary nuclei. *Space Science Reviews*, 216, 1–40. <https://doi.org/10.1007/s11214-019-0625-7>
- Westall, F., Foucher, F., Bost, N., Bertrand, M., Loizeau, D., Vago, J. L., et al. (2015). Biosignatures on Mars: What, where, and how? Implications for the search for Martian life. *Astrobiology*, 15(11), 998–1029. <https://doi.org/10.1089/ast.2015.1374>
- White, O. L., Moore, J. M., Howard, A. D., McKinnon, W. B., Keane, J. T., Singer, K. N., et al. (2019). Washboard and fluted terrains on Pluto as evidence for ancient glaciation. *Nature Astronomy*, 3(1), 62–68. <https://doi.org/10.1038/s41550-018-0592-z>
- White, O. L., Moore, J. M., McKinnon, W. B., Spencer, J. R., Howard, A. D., Schenk, P. M., et al. (2017). Geological mapping of Sputnik Planum on Pluto. *Icarus*, 287, 261–286. <https://doi.org/10.1016/j.icarus.2017.01.011>
- White, W. B. (1988). *Geomorphology and hydrology of limestone terrains*. Oxford.
- Whittaker, W. L., Jones, H. L., Ford, J. S., Sharif, K., & Wong, U. Y. (2021). Skylight: A mission concept for in-situ investigation of the morphology, geology and mineralogy of lunar pits. In *Lunar and Planetary Science Conference*, LPI Contributions No. 2644.
- Wiens, P., Misra, A., Matthies, L. H., Johnson, W., Young, L. A., Clegg, S., et al. (2019). Airborne reconnaissance mission concept for organics in a Martian cave. In *Paper presented at 3rd International Planetary Cave Conference*. Abstract # 1063, LPI Contributions # 2197.
- Willacy, K., Allen, M., & Yung, Y. (2016). A new astrobiological model of the atmosphere of Titan. *The Astrophysical Journal*, 829(2), 1–11. <https://doi.org/10.3847/0004-637x/829/2/79>
- Williams, D. A., Davies, A. G., Keszthelyi, L. P., & Greeley, R. (2001). The summer 1997 eruption at Pillan Patera on Io: Implications for ultrabasic lava flow emplacement. *Journal of Geophysical Research*, 106(E12), 33105–33119. <https://doi.org/10.1029/2000je001339>
- Williams, K. E., & McKay, C. P. (2015). Comparing flow-through and static ice cave models for Shoshone Ice Cave. *International Journal of Speleology*, 44(2), 115–123. <https://doi.org/10.5038/1827-806x.44.2.2>
- Williams, K. E., McKay, C. P., Toon, O. B., & Head, J. W. (2010). Do ice caves exist on Mars? *Icarus*, 209(2), 358–368. <https://doi.org/10.1016/j.icarus.2010.03.039>
- Williams, P. W. (1972). Morphometric analysis of polygonal karst in New Guinea. *Geological Society of America Bulletin*, 83(3), 761–796. [https://doi.org/10.1130/0016-7606\(1972\)83\[761:maopki\]2.0.co;2](https://doi.org/10.1130/0016-7606(1972)83[761:maopki]2.0.co;2)
- Wilson, L., Hawke, B. R., Giguere, T. A., & Petrycki, E. R. (2011). An igneous origin for Rima Hyginus and Hyginus crater on the Moon. *Icarus*, 215(2), 584–595. <https://doi.org/10.1016/j.icarus.2011.07.003>
- Wood, C. A., & Radebaugh, J. (2020). Morphologic evidence for volcanic craters near Titan's north polar region. *Journal of Geophysical Research: Planets*, 125(8), e2019JE006036. <https://doi.org/10.1029/2019je006036>
- Wynne, J. J., Ashley, J. W., Boston, P. J., Cushing, G. E., & Parness, A. (2014). Target selection and evaluation criteria for caves on the Moon and Mars. In *Paper presented at 2014 NASA/JPL Planetary Cave Workshop* (p. 2).
- Wynne, J. J., Jenness, J., Sonderegger, D. L., Titus, T. N., Jhabvala, M. D., & Cabrol, N. A. (2021). Advancing cave detection with terrain analysis and thermal imagery. *Remote Sensing*, 13, 3578. <https://doi.org/10.3390/rs13183578>
- Wynne, J. J., Malaska, M. J., Cushing, G. E., Wagner, R. V., Lesage, E., Hughson, K., et al. (2022). Supporting information for: Planetary caves: A solar system view of processes and products. *Harvard Dataverse*. <https://doi.org/10.7910/DVN/1OLNC4>
- Wynne, J. J., Titus, T. N., Agha-Mohammadi, A.-A., Azua-Bustos, A., Boston, P. J., de León, P., et al. (2022). Fundamental science and engineering questions in planetary cave exploration. *Journal of Geophysical Research: Planets*, 127, e2022JE007194. <https://doi.org/10.1029/2022JE007194>
- Wynne, J. J., Titus, T. N., & Chong Diaz, G. (2008). On developing thermal cave detection techniques for Earth, the Moon and Mars. *Earth and Planetary Science Letters*, 272(1–2), 240–250. <https://doi.org/10.1016/j.epsl.2008.04.037>
- Wyrick, D., Ferrill, D. A., Morris, A. P., Colton, S. L., & Sims, D. W. (2004). Distribution, morphology, and origins of Martian pit crater chains. *Journal of Geophysical Research*, 109, E6. <https://doi.org/10.1029/2004je002240>
- Ximenes, S. W., Elliott, J. O., & Bannova, O. (2012). Defining a mission architecture and technologies for lunar lava tube reconnaissance. In *Earth and Space 2012: Engineering, Science, Construction, and Operations in Challenging Environments* (pp. 344–354).
- Yamashita, Y., Kato, M., & Arakawa, M. (2010). Experimental study on the rheological properties of polycrystalline solid nitrogen and methane: Implications for tectonic processes on Triton. *Icarus*, 207(2), 972–977. <https://doi.org/10.1016/j.icarus.2009.11.032>
- Yingst, R. A., Mest, S. C., Berman, D. C., Garry, W. B., Williams, D. A., Buczkowski, D., et al. (2014). Geologic mapping of Vesta. *Planetary and Space Science*, 103, 2–23. <https://doi.org/10.1016/j.pss.2013.12.014>
- Yokota, Y., Haruyama, J., Yamamoto, S., Kaku, T., Matsunaga, T., Ohtake, M., et al. (2018). Formation scenario of continuous slopes associated with lunar mare pit/hole structures. In *Lunar and Planetary Science Conference*. Abstract #1907, LPI Contributions No. 1907.
- Zahnle, K., Schenk, P., Levison, H., & Dones, L. (2003). Cratering rates in the outer solar system. *Icarus*, 163(2), 263–289. [https://doi.org/10.1016/s0019-1035\(03\)00048-4](https://doi.org/10.1016/s0019-1035(03)00048-4)
- Zhang, Y., & Michel, P. (2021). Shapes, structures, and evolution of small bodies. *Astrodynamics*, 5(4), 293–329. <https://doi.org/10.1007/s42064-021-0128-7>
- Zhao, J., Huang, J., Kraft, M. D., Xiao, L., & Jiang, Y. (2017). Ridge-like lava tube systems in southeast Tharsis, Mars. *Geomorphology*, 295, 831–839. <https://doi.org/10.1016/j.geomorph.2017.08.023>